Western Washington University
Western CEDAR

WWU Graduate School Collection | WWU Graduate and Undergraduate Scholarship

Fall 2018

Improved Thermal and Mechanical Properties and Increased Miscibility of Polybenzoxazine in Blends with Functionalized Thermoplastics and Particles

Emily A. Brown
Western Washington University, eannbrown94@gmail.com

Follow this and additional works at: https://cedar.wwu.edu/wwuet

Part of the Chemistry Commons

Recommended Citation

Brown, Emily A., "Improved Thermal and Mechanical Properties and Increased Miscibility of Polybenzoxazine in Blends with Functionalized Thermoplastics and Particles" (2018). *WWU Graduate School Collection*. 764.
https://cedar.wwu.edu/wwuet/764

This Masters Thesis is brought to you for free and open access by the WWU Graduate and Undergraduate Scholarship at Western CEDAR. It has been accepted for inclusion in WWU Graduate School Collection by an authorized administrator of Western CEDAR. For more information, please contact westerncedar@wwu.edu.

Improved Thermal and Mechanical Properties and Increased Miscibility of Polybenzoxazine in Blends with Functionalized Thermoplastics and Particles

By

Emily A. Brown

Accepted in Partial Completion
of the Requirements for the Degree
Master of Chemistry

ADVISORY COMMITTEE

Dr. David A. Rider

Dr. Gregory W. O'Neil

Dr. John M. Misasi

GRADUATE SCHOOL

Dr. Gautam Pillay, Dean

Master's Thesis

In presenting this thesis in partial fulfillment of the requirements for a master's degree at Western Washington University, I grant to Western Washington University the non-exclusive royalty-free right to archive, reproduce, distribute, and display the thesis in any and all forms, including electronic format, via any digital library mechanisms maintained by WWU.

I represent and warrant this is my original work, and does not infringe or violate any rights of others. I warrant that I have obtained written permissions from the owner of any third party copyrighted material included in these files.

I acknowledge that I retain ownership rights to the copyright of this work, including but not limited to the right to use all or part of this work in future works, such as articles or books.

Library users are granted permission for individual, research and non-commercial reproduction of this work for educational purposes only. Any further digital posting of this document requires specific permission from the author.

Any copying or publication of this thesis for commercial purposes, or for financial gain, is not allowed without my written permission.

Emily A. Brown

September 7, 2018

Polybenzoxazine Networks with Polymer for Increased Thermal Stability and Modulus and Benzoxazine Surfactant Stabilized Monomer and Aqueous Solutions

A Thesis
Presented to
The Faculty of
Western Washington University

In Partial Fulfillment
Of the Requirements for the Degree
Master of Science

by
Emily A. Brown
September, 2018

Abstract

The solubility, polymerization, and the macromolecular characterization of cured blends of BPA-based benzoxazine (BA-a) in end group tosylated poly(ethylene glycol) (mPEGOTs), polysulfone (PSUOTs), and poly(D,L-lactic acid) (PDLLAOTs) are studied and compared to their hydroxyl terminated analogues. The cure temperature for BA-a blends with tosylated polymers was reduced by ~60 °C compared to that of the pure BA-a. This confirms that the tosylated polymer is an accelerant for BA-a ring opening polymerization (ROP). There are two proposed mechanism for the production of free tosylate and cationic BA-a based initiators as a cure catalyst for BA-a ROP – where the former was detected by TGA-FTIR and TGA-MS. SEM confirmed a grafted polymer network from BA-a and mPEGOTs, P(BA-a)-graft-mPEGOTs, this homogenous microstructure was also found in PBA-a/PSUOTs blends. The glass transition temperature and the thermal stability of the P(BA-a)-graft-mPEGOTs can be tuned based on the composition of the BA-a/mPEGOTs resin. The potential applications of such grafted polymers may lead to novel materials for the biomedical plastics, electronics, membranes, and aerospace industries. Further blends were prepared with microparticles of silica (SiOH) and the tosylate- (SiOTs) and phenyl- (SiPh) functionalized analogues. Increased modulus of PBA-a was found in all silica blends, the reduction in cure temperature was found only in blends of BA-a and SiOTs. By SEM, PBA-a/SiOTs blends were determined to have a unique morphology. Three benzoxazine-based surfactants were synthesized from the coupling of p-hydroxy methylbenzoxazine with mPEGOTs. All three surfactants had good monomer loading, up to 4.72 monomer to surfactant by mass.

Acknowledgements

The completion of this work would not be possible without the guidance and support of many mentors, colleagues, and friends. I would like to thank my committee, Dr. Gregory O'Neil and Dr. John Misasi, for their patience and assistance during my time at Western Washington University. I would also like to thank our collaborators, Zodiac Aerospace, for the many opportunities they have provided me both as an undergraduate and graduate student.

I extend my gratitude to the current and past members of the Rider group and to the researchers of CB 420 for their continuous help and motivation. Foremost, I would especially like to thank Ayesha Nadeem for her contributions and assistance as well as her limitless patience and knowledge. Her perseverance and dedication is deeply appreciated.

Finally, I would also like to thank my mentor, Dr. David Rider, for his advice, encouragement, and the countless opportunities he has afforded me. Under his leadership I have been able to flourish and explore many avenues of interest. His unending support and motivation has been the foundation of my research. Thank you for your guidance.

Table of Contents

Abstract iv

Acknowledgements v

List of Figures viii

List of Tables xv

List of Schemes xvi

Chapter 1: Introduction 1

Chapter 2: Pegylated polybenzoxazine from miscible blends of poly(ethylene glycol) and benzoxazine monomer 20

2.1 Introduction 20

2.2 Experimental 22

2.3 Results and discussion 24

2.4 Conclusions 44

Chapter 3: Alternative blends of bisphenol A benzoxazine with polymers and particles 46

3.1 Introduction 46

3.2 Experimental 48

3.3 Results and discussion 52

3.4 Conclusions 76

Chapter 4: Benzoxazine based surfactants for monomer processing 78

4.1 Introduction 78

4.2 Experimental 81

4.3 Results and discussion 84

4.4 Conclusions 98

Chapter 5: Conclusions 99

Works Cited 103

Appendix A 118

Appendix B 128

Appendix C 135

List of Abbreviations 137

List of Figures

Figure 1.1. Synthesis of benzoxazine monomer from a phenol, an amine, and formaldehyde. R^1-R^3 can be a variety of substituents to target different functionalities. 2

Figure 1.2. Nomenclature of benzoxazine and the oxazine substructure. 3

Figure 1.3. Synthesis of mono-functional benzoxazine, 3,4-Dihydro-2H-3-phenyl-1,3-benzoxazine. 4

Figure 1.4. The thermal polymerization of benzoxazine monomer into the phenoxy and phenolic form of polybenzoxazine. 4

Figure 1.5. Tosylate initiators for the ROP polymerization of benzoxazine studied by Endo et al. listed with their induced cure temperature when loaded at 1 mol %. 5

Figure 1.6. Mechanisms proposed by Endo et al. responsible for the accelerated ROP of benzoxazine. 6

Figure 1.7. Effect of (a) heat rates and (b) sample size on thermal events in the DSC heat curve. 7

Figure 1.8. The polymerization of (a) mono-, (b) bis-, and (c) tri- functional benzoxazine into linear or densely cross-linked polybenzoxazine networks. 9

Figure 1.9. Novel benzoxazine molecules functionalized by alternative starting materials, the benzoxazine functional group is colored in orange. 10

Figure 1.10. Synthesized polymers from literature containing benzoxazine in the main or side chain which possess the ability to further polymerize upon thermal activation to yield a densely crosslinked material. The benzoxazine functional group is colored in orange. 11

Figure 1.11. Example of Gordon-Taylor relationship between two arbitrary glass transition temperatures of 130 and 50 °C with the fitting constant of (a) 0.10, (b) 0.50, and (c) 0.90. 14

Figure 2.1. DSC curves from the first heat cycle after quenching (exothermic direction is up) of BA-a blends with either (a) $mPEGOH_{2000}$ or (b) $mPEGOTs_{2000}$. Curves have been offset for clarity. Plots for the percent crystallinity of (c) $mPEGOH_{2000}$, (d) $mPEGOTs_{2000}$, and (e) $mPEGOTs_{900}$. The dash line in (c-d) represents the theoretical crystallinity of PEG assuming no interaction with non-crystallizable BA-a. 26

Figure 2.2. DSC cure study of quenched blends of benzoxazine with (a) $mPEGOH_{2000}$, (b) $mPEGOTs_{2000}$, and (c) $mPEGOTs_{900}$. Plots for the percent cure of blends with (d) $mPEGOH_{2000}$, (e) $mPEGOTs_{2000}$ (●) and $mPEGOTs_{900}$ (▲). The dash line represents the theoretical cure of benzoxazine assuming no interaction with PEG. (f) Plot for the T_g of the PBA-a for cured samples from the $mPEGOTs_{900}$ series. The theoretical curve superimposed over the data points is the result of fitting a Gordon–Taylor relation. 29

Figure 2.3. FTIR spectra (C-H and O-H stretch region) for cured blends of BA-a with (a) $mPEGOH_{2000}$ and (b) $mPEGOTs_{2000}$. The minima for the OH stretch signal for selected samples are connected by dotted and dashed lines in each figure. The dotted line at 3372 cm^{-1} in (a) tracks the wavenumber corresponding the highest signal for the hydroxyl-region and indicates that the phenolic residues in the mPEGOH series are largely free of H-bonding. The dashed line at 3245 cm^{-1} in (b) tracks the wavenumber corresponding the highest signal for the hydroxyl-region and indicates that the phenolic residues in the mPEGOTs series have significant H-bonding. 33

Figure 2.4. FTIR tracer plots for S-OH stretch at 885 cm^{-1} of the effluent from PBA-a blends with (a) $mPEGOH_{900}$ and (b) $mPEGOTs_{900}$ from thermogravimetric analysis. The generation of the *p*-TSA fragment with increasing temperature (c) as determined with (i) TGA thermogram (ii) Tracer plot of the signal at 885 cm^{-1} (iii) TGA-MS spectrum scan for m/z 91 and (iv) a DSC thermogram of the 1:1 BA-a:$mPEGOTs_{900}$ blend. 38

Figure 2.5. SEM images for chloroform extracted PBA-a blends with decreasing $mPEGOH_{2000}$ (a-g) and $mPEGOTs_{2000}$ (h-n) content. In (a-g) the original $mPEGOH_{2000}$ content was 90, 80, 70, 60, 50, 40 and 20

wt %, respectively. In (h-n) the original $mPEGOTs_{2000}$ content was 90, 80, 70, 60, 50, 40 and 20 wt %, respectively. The scale bar in (h) applies to all SEM images. 40

Figure 3.1. X-ray diffraction patterns of blends of BA-a at 40 wt % PEG with (a,b) $mPEGOH_{2000}$ and (c,d) $mPEGOTs_{2000}$. The plots in the right column are the baseline corrected versions of those in the left column. 55

Figure 3.2. (a) The percent crystallinity of BA-a blends with $mPEGOH_{2000}$ from the spectra in Figures 1 and 2. The dotted and solid lines are the linear fits of the $mPEGOH_{2000}$ and $mPEGOTs_{2000}$ blends respectively. The fit for the $mPEGOTs_{2000}$ blends ignores the data point at 70 wt %. (b) A sketch of predicted crystallinity behavior dependent on PEG/PBA-a miscibility. 56

Figure 3.3. Tan delta from the DMA of benzoxazine blends with either (a) $mPEGOH_{500}$, (b) $mPEGOTs_{900}$, or (c) $mPEGOTs_{2000}$ at various weight loading. (d) The glass transition temperatures their respective Gordon-Taylor fits determined from the peak tan delta signals in b-c for blends with $mPEGOTs_{900}$ (triangles, dashed fit, k = 0.95) and $mPEGOTs_{2000}$ (empty squares, dotted fit, k=1.25) overlaid with the glass transition temperatures and their fit for $mPEGOTs_{900}$ (circles, solid line, k = 0.41) as determined from the DSC data in chapter 2. 57

Figure 3.4. DSC heat curves from the first scan of blends of BA-a with (a) PSUOH and (b) PSUOTs. (c) The onset of cure and (d) the peak cure temperature of the blends with PSUOH and PSUOTs with linear fits in the dotted and solid lines respectively. (e) The percent cure was determined by the enthalpy of the exotherm from the scans in (a) and (b). 59

Figure 3.5. SEM images of PBA-a blends with either PSUOTs at 80, 50, and 20 PSUOH wt % (a-c) or PSUOH at 80, 50, and 20 PSUOTs wt % (d-f) after a rinse in chloroform. 61

Figure 3.6. (a) Tensile modulus of PSU blends with PBA-a determined from stress-strain curves and (b) the error in the tensile modulus measurements plotted against PSU content. (c) An image of a representative film of 50:50 PSUOTs and PBA-a. 63

Figure 3.7. FTIR of the cured PBA-a and its blends with either PSUOH (blue, dotted line) or PSUOTs (solid, orange) from 1200 to 700 cm^{-1}. 64

Figure 3.8. First heat scan from the DSC of blends of BA-a with (a) non-functionalized silica, (b) tosylated silica, and (c) phenyl functionalized silica. (d) The enthalpy values of the exothermic peaks from the polymerization of BA-a of all blends. 66

Figure 3.9. (a) The onset of cure and (b) the max curing temperature of PBA-a blends with silica as determined from DSC. 67

Figure 3.10. (a-c) The storage modulus, (d-f) loss modulus, and (g-i) the tan delta for blends of PBA-a with SiOH, SiPh, and SiOTs respectively at varying loading. 69

Figure 3.11. (a) The storage modulus at 30 °C, (b) glass transition temperature determined from the max signal of the tan delta, (c) the max loss modulus signal, (d) the temperature at max loss modulus, and (e) the loss modulus at 100 °C of pure benzoxazine and its blends with SiOH, SiOTs, and SiPh particles. ... 70

Figure 3.12. SEM images of (a) SiOTs and blends of PBA-a with (b) SiOTs and (c) SiOH at 50 wt % silica content. 71

Figure 3.13. The first heat scans from DSC of blends of BA-a with (a) PDLLAOH and (b) PDLLAOTs. 72

Figure 3.14. The (a) DSC curve of 50:50 PLGA blended at 50 wt % with BA-a and (b) the TGA curve of 50:50 PLGA. 73

Figure 3.15. (a) The stacked ^{1}H NMR of the degradation of PLLDAOH in acetonitrile-3 and D_2O (9:1), with DMAP, acquired over several days. The integrated area of the signals corresponding to methine of the internal polymer (5.15 ppm), the D- and L-methine end groups (4.84 and 4.24 ppm), and the methine of the lactic acid (3.86 ppm) of (b) PDLLAOH, (c) 50:50 PDLLAOTs/PBA-a, and (d) 50:50 PDLLAOH/PBA-a. 74

Figure 4.1. Examples of benzoxazine-based surfactants from literature. 80

Figure 4.2. The ^{1}H NMR spectra (500 MHz) of *p*HBA-a in (a) DCM-d2 to provide characterization of the aromatic region and in (b) $CDCl_3$ to characterize the methylene groups. 85

Figure 4.3. The ^{1}H NMR spectrum (500 MHz, $CDCl_3$) of mPEGOTs$_{500}$. 87

Figure 4.4. Representative ^{1}H NMR spectrum (500 MHz, $CDCl_3$) of the surfactant, mPEGpHBA-a$_{900}$. 88

Figure 4.5. MALDI spectra of both (a) mPEGpHBA-a$_{500}$ and (b) mPEGpHBA-a$_{900}$. In (a) the peaks belonging to the surfactant are outlined with the dashed line. *Artifacts from the α-cyano-4-hydroxycinnamic acid and 2,5-dihydroxybenzoic acid matrices at 650, 552, 462, 450, and 434 m/z. 89

Figure 4.6. Pictures of (a) unloaded micelles of mPEGpHBA-a$_{900}$ in nanopore water and (b) the loaded micelles of all three PEG-based surfactants with their monomer to surfactant mass loading ratios. 90

Figure 4.7. The difference in interfacial volume of surfactants with differing tail lengths. 91

Figure 4.8. Performance of the synthesized surfactants in this work (green) compared to commercially available surfactants (orange) and benzoxazine-based surfactants from literature (blue). 92

Figure 4.9. (a) Changing micelle diameter over time for the loaded mPEGpHBA-a$_{900}$ micelle and the (b) micelles solutions at 100 hours, all solutions were loaded at a monomer to surfactant mass ratio of 1.5. . 93

Figure 4.10. First heat scans from DSC of the (a) neat surfactants and *p*HBA-a, (b) surfactants blended with *p*HBA-a, and (c) lyophilized micelles of surfactants loaded with *p*HBA-a. 94

Figure 4.11. ^{1}H NMR (500 MHZ, $CDCl_3$) of PAGE surfactant with the addition of (a) 1 g of AGE or (b) 4 g of AGE during the synthesis. **Chloroform*; ***tetrahydrofuran*..... 96

Figure A1. (a) Plots for the peak exotherm temperature of cure of BA-a in blends with $mPEGOH_{2000}$ (■), $mPEGOTs_{2000}$ (●), and $mPEGOTs_{900}$ (▲) as a function of PEG wt %. (b) Plots for the onset temperature for cure of BA-a in blends with $mPEGOH_{2000}$ (■), $mPEGOTs_{2000}$ (●), and $mPEGOTs_{900}$ (▲) as a function of PEG wt %. Empty triangles (▽) are used to identify the onset and max cure temperatures of pure BA-a monomer. 118

Figure A2. DSC curves of BA-a/$mPEGOTs_{900}$ from the first heat after liquid nitrogen quench. The wt % of PEG in each sample is listed above the data curve. The y-axis is correlated to the curve of the pure mPEGOTs, all other curves have been offset for clarity. 119

Figure A3. ^{1}H NMR spectra (500 MHz in D6-DMSO) of extractable polymer from cured (a) $mPEGOH_{2000}$ blends and (b) $mPEGOTs_{2000}$ blends. The original content of PEG in (a) and (b) are 20, 40, and 50 wt % (i-iii). 121

Figure A4. FTIR tracer plots for sp^3 ν_{CH} stretching at 2973 cm^{-1} from the effluent of PBA-a blends with (a) $mPEGOH_{900}$ and (b) $mPEGOTs_{900}$ from TGA..... 122

Figure A5. FTIR tracer plots for ν_{CO} ether stretch at 1136 cm^{-1} from the effluent of PBA-a blends with (a) $mPEGOH_{900}$ and (b) $mPEGOTs_{900}$ from TGA. 122

Figure A6. FTIR tracer plots for sp^2 ν_{CH} stretch at 3048 cm^{-1} from the effluent of PBA-a blends with (a) $mPEGOH_{900}$ and (b) $mPEGOTs_{900}$ from TGA. 123

Figure A7. The TGA thermograms for PBA-a blends with (a) $mPEGOH_{900}$ and (b) $mPEGOTs_{900}$. The $T_{D5\%}$ and the char yield at 475 °C of (c, e) $mPEGOH_{900}$ and (d, f) $mPEGOTs_{900}$ blends were determined from the thermograms. Triangles (▲) are used to identify the $T_{D5\%}$ and char yield at 475 °C of pure BA-a monomer in (c-f). 124

Figure A8. The generation of the *p*-TSA fragment with increasing temperature as determined with (i) TGA thermogram, (ii) FTIR tracer plot of the signal at 885 cm^{-1} from the TGA effluent, (iii) TGA-MS spectrum scan for m/z 91 of the blend sample (●) and pure BA-a (▼), and (iv) a DSC thermogram of the 1:1 BA-a:$mPEGOTs_{900}$ blend. 125

Figure A9. TGA-FTIR absorbance maps of blends composed of BA-a with (a) $mPEGOH_{900}$ and (b) $mPEGOTs_{900}$ with PEG wt % content of 20, 40, 50, 60, 70, and 100 % (i-vi). TGA-FTIR absorbance maps of pure PBA-a (c) and pure *p*-toluene sulfonic acid (d). For datasets i-vi in (a), i-iv in (b), and those in (c-d), the FTIR absorbance data for the final isotherm is included in the maps. The absorbance scale is shown as a colored intensity bar beside each map. 126

Figure B1. (a) Silicon molds filled with silica blends for DMA sample preparation prior to cure, and (b) the cured samples. 128

Figure B2. ^1H NMR of 50:50 poly(lactic-*co*-glycolic acid) in $CDCl_3$. 128

Figure B3. ^1H NMR spectrum of tosylated polysulfone in $CDCl_3$. 129

Figure B4. ^1H NMR of tosylated poly(D,L-lactic acid) in $CDCl_3$. 129

Figure B5. X-ray diffraction patterns of blends of BA-a with $mPEGOH_{2000}$ at (a,b) 40, (c,d) 50, (e,f) 60, (g,h) 70, and (i,j) 80 wt %. The plots in the right column are the baseline corrected versions of those in the left column. 130

Figure B6. X-ray diffraction patterns of blends of BA-a with $mPEGOTs_{2000}$ at (a,b) 40, (c,d) 50, (e,f) 60, (g,h) 70, and (i,j) 80 wt %. The plots in the right column are the baseline corrected versions of those in the left column. 131

Figure B7. Storage modulus (a-c) and loss modulus (d-f) of PBA-a blends with $mPEGOH_{500}$, $mPEGOTs_{900}$, $mPEGOTs_{2000}$ at varying weight loading. 132

Figure B8. TGA scans of neat SiOH, SiOTs, and SiPh particles from 30-400 °C. 133

Figure B9. The exothermic peak from the DSC heat scan of the 60 wt % SiOTs blend and the fitted components of each peak as determined with CasaXPS. 133

Figure B10. The pH change of as PLGA degrades in PBS at 37 °C over several days with an exponential fit of the data. 134

Figure C1. ^{1}H NMR spectrum (500 MHz, $CDCl_3$) of *p*-toluenesulfonyl chloride. 135

Figure C2. ^{1}H NMR spectrum (500 MHz, $CDCl_3$) of *p*-toluenesulfonic acid. 135

Figure C3. ^{1}H NMR spectrum (500 MHz, $CDCl_3$) of mPEGpHBA-a_{500}. 136

Figure C4. ^{1}H NMR spectrum (500 MHz, $CDCl_3$) of mPEGpHBA-a_{2000}. *Chloroform, **excess pHBA-a 136

List of Tables

Table 1.1. The resulting micellar geometry as determined by the shape of the surfactant and its corresponding packing parameter.. 17

Table 4.1. The diameter, polydispersity index (PD), and mass loading of monomer of the three PEG-based surfactants. 90

Table A1. Equilibrium melting points for BA-a/mPEGOH and BA-a/mPEGOTs blends..... 118

Table A2. Enthalpy of benzoxazine cure exotherms for BA-a/mPEGOH and BA-a/mPEGOTs blends. 119

Table A3. Enthalpy of melting for PEG in BA-a/mPEGOH, BA-a/mPEGOTs, PBA-a/mPEGOH and PBA-a/mPEGOTs blends..... 120

List of Schemes

Scheme 2.1. Proposed pathways (A-C) for the generation of cationic species to initiate the ROP of BA-a. Pathways A and B show the nucleophilic attack by the oxygen atom or the nitrogen atom from the oxazine ring of a BA-a at the tosylate end group of mPEGOTs, respectively. Pathway C shows the thermal dissociation of mPEGOTs. All three pathways show the formation of a free-tosylate that is associated with the generation of possible cationic ROP initiators. 42

Scheme 2.2. Proposed mechanism for the generation of HOTs catalyst, subsequent initiation and propagation of BA-a monomers, and the grafting of mPEG to cured blends of BA-a with mPEGOTs..... 44

Scheme 3.1. α,ω-Bistosylate polymer attaching to PBA-a 53

Scheme 3.2. PBA-a growing around tosylated particle 54

Scheme 3.3. Degradation of poly(lactic acid) via hydrolysis and the morphology after degradation in a polymerized blend..... 76

Scheme 4.1. Synthesis of *p*HBA-a from formaldehyde, aniline, and *p*-hydroxybenzyl alcohol 84

Scheme 4.2. The synthesis of $mPEGOTs_{500}$ from $mPEGOH_{500}$ 86

Scheme 4.3. Reaction for mPEGpHBA-a from mPEGOTs and *p*HBAa 87

Scheme 4.4. Polymerization of allyl glycidyl ether with *p*HBA-a 95

Scheme 4.5. Polymerization of glycidyl methyl ether with *p*HBA-a 97

Chapter 1: Introduction

1.1 Thermoplastics and thermosets

Engineering polymers are typically divided into two categories, thermoplastics and thermosets. Usually, thermoplastics are linear polymeric chains with low to very high molecular weight (~1 to >1000 kDa). Thermoplastics are termed as such due to possessing more elastic properties upon heating to or above the glass transition temperature. Thermoplastics typically have low modulus, low glass transition temperatures, good toughness, and good overall solubility. Thermoplastics are typically thermally stable with low melting temperatures which allows for re-processing and recycling. Common thermoplastics exist in most everyday commodities such as the polyethylene in plastic bags, nylon and polyester in clothing, polytetrafluoroethylene in the Teflon of cookware, polystyrene in Styrofoam, or even the polyvinyl chloride in vinyl records hence their common name. Thermosets, as their name suggests, are polymers that "set" upon heating, typically by polymerizing a monomer by the addition of heat, UV-radiation, or an activating compound. Thermosets tend to have high modulus, high glass transition temperatures, good thermal resistance, and low flammability. Common thermosets include polyurethane in mattresses, epoxy resin in adhesives and protective coatings, and bismaleimide in circuit boards. One of the most common uses of thermosets is the production of fiber reinforced polymers, also known as composites, which are used in car, aircraft, and naval frames, as well as gas and oil pipelines. The mechanical properties and low density of these composites make them desirable over traditional materials such as steel or wood. Many thermosets have high moduli and low fracture resistance despite their strength, meaning that upon failing they are more likely to break rather than stretch. The toughening of thermosets can be achieved by the alloying of a thermoset resin with a thermoplastic.

1.2 Benzoxazine and polybenzoxazine

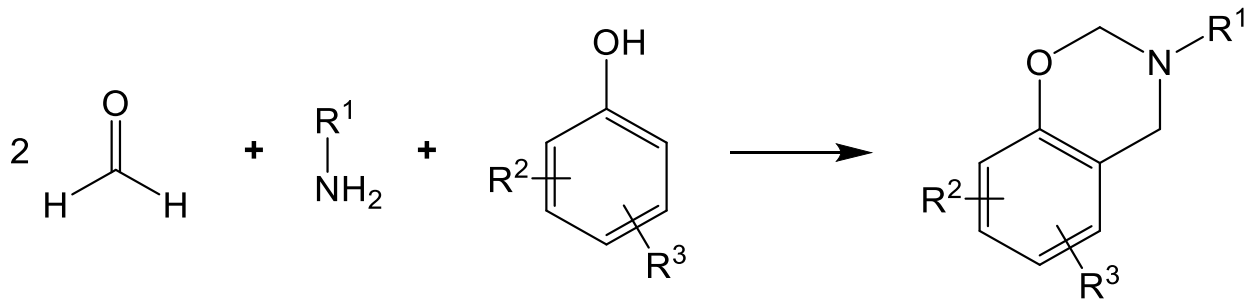

Figure 1.1. Synthesis of benzoxazine monomer from a phenol, a primary amine, and formaldehyde. R^1-R^3 can be a variety of substituents to target different functionalities.

One thermoset that has recently gained much popularity is the class based on benzoxazines (BA). Benzoxazine materials are a relatively new and expanding field with a large and diverse scope of applications. The synthesis of these small molecules, by the condensation of a phenol and an amine with formaldehyde (Figure 1.1), was first published in 1944 by Holly and Cope. The polymerization of large molecular weight polybenzoxazines (PBA) from multi-functional monomers wasn't explored until 1985.[1,2] Ning and Ishida were the first to study the properties these thermosets in 1994.[3] These relatively new materials have good mechanical, thermal, and dielectric properties. Polybenzoxazine materials, resins, and pre-impregnated fiber are currently marketed by Henkel and Huntsman. Current applications in industry of PBAs include aerospace and naval composites, automotive frames and components, composite pipes for gas or oil, prepreg tooling, circuit boards, protective coatings, and paints.[4,5] Current literature has demonstrated their function in aerogels, self-healing materials, shape memory materials, batteries, and other textile applications.[6-12]. The mentioned properties of this relatively new material make PBAs desirable in various fields.

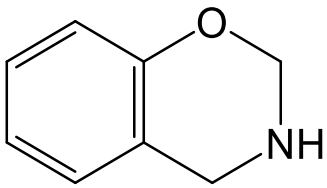

3,4-dihydro-2H-1,3-benzoxazine

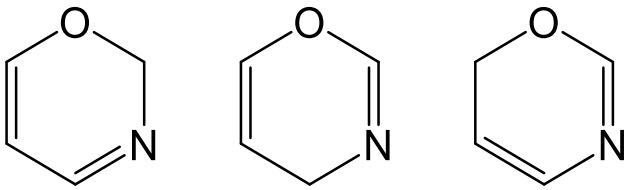

2*H* 4*H* 6*H*

Figure 1.2. Nomenclature of benzoxazine and the oxazine substructure.

Benzoxazines have a heterocyclic fused ring structure containing a benzene and oxazine ring. The IUPAC name of the benzoxazine which has the thermal ring opening polymerization (ROP) functionality is 3,4-dihydro-2H-1,3-benzoxazine. The 1,3-benzoxazine refers to the position of the oxygen and nitrogen, where 1,2- and 1,4- benzoxazine do not show the same polymerizable capabilities. The oxazine structure is a diene containing ring with three isomers denoted as 2*H*, 4*H*, and 6*H*, which signifies the presence of a hydrogen and specifies the position lacking a double bond. Finally, the 3,4-dihydro prefix specifies the saturated bond, in this case the N-C bond. In this work, the use of the name benzoxazine refers only to 3,4-dihydro-2H-1,3-benzoxazine and molecules containing this substructure. Benzoxazine monomers are often termed by their starting materials in a "phenol"-"amine" format. For instance, benzoxazine synthesized from phenol and aniline is typically called P-a, or monomer synthesized from biphenol A and aniline is termed BA-a. Another example would be *p*-hydroxybenzyl alcohol and aniline: *p*HBA-a.

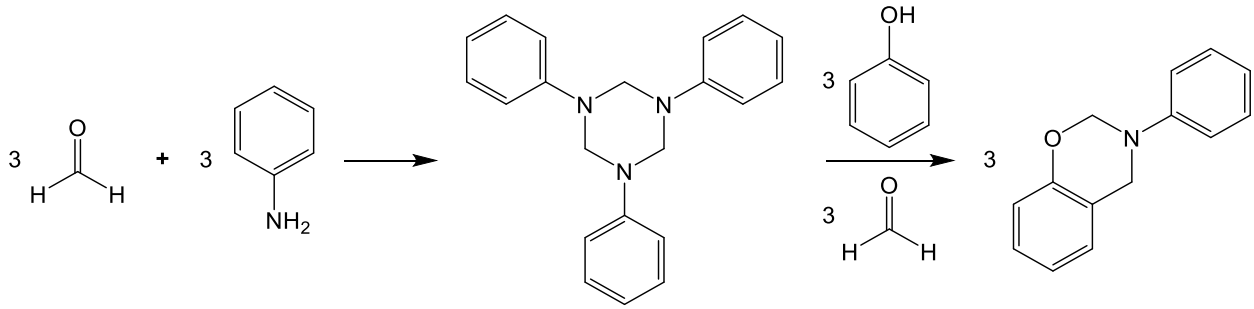

Figure 1.3. Synthesis of mono-functional benzoxazine, 3,4-dihydro-2H-3-phenyl-1,3-benzoxazine.

Ishida has reported the presence of an intermediate species in the formation of benzoxazine monomer. In the case of aromatic amines the formaldehyde and aryl amine will form hexahydro-1,3,5-triphenyl-1,3,5-triazine which further undergoes the formation of the hetero cyclic oxazine ring with the phenol species (Figure 1.3).[13]

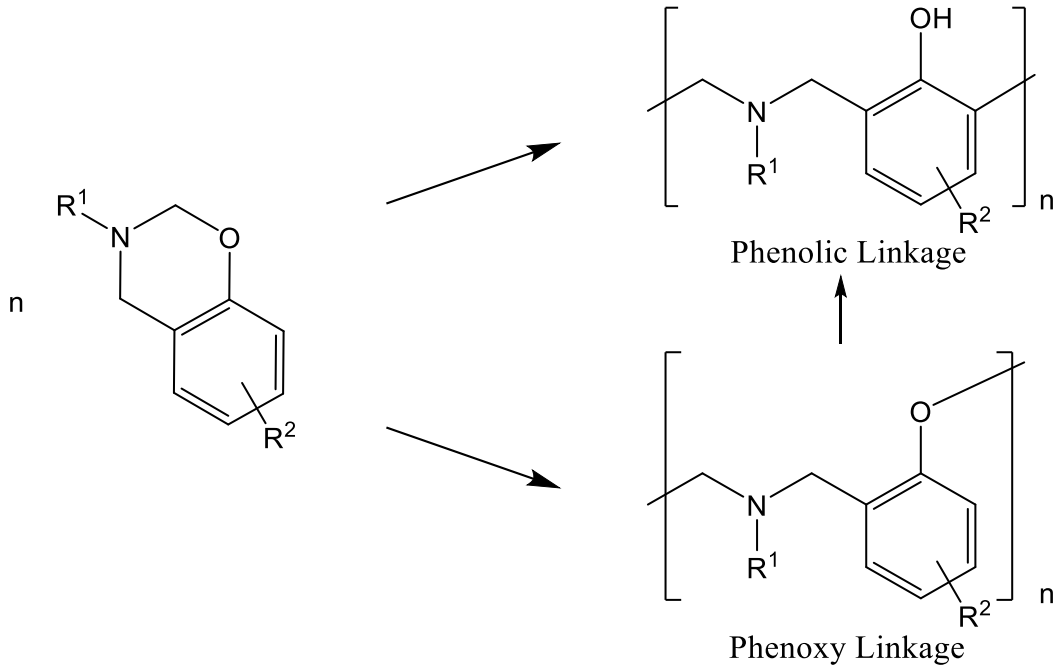

Figure 1.4. The thermal polymerization of benzoxazine monomer into the phenoxy and phenolic form of polybenzoxazine.

Upon heating benzoxazine monomers, the heterocyclic ring undergoes a cationic ROP seen in Figure 1.4.[14-16] The polymerization of thermosets is colloquially termed a “cure”. The mechanism of this curing

process has been determined to result in the formation of an iminium cation which further activates adjacent monomer.[17-19] It is proposed that the ROP may form two different ring open structures noted as the phenoxy and the phenolic linkages (Figure 1.4).[20-22] The former is considered the less thermodynamic intermediate that will convert to the latter upon further heating.

1.3 Known benzoxazine cure accelerants and the polymerization mechanism

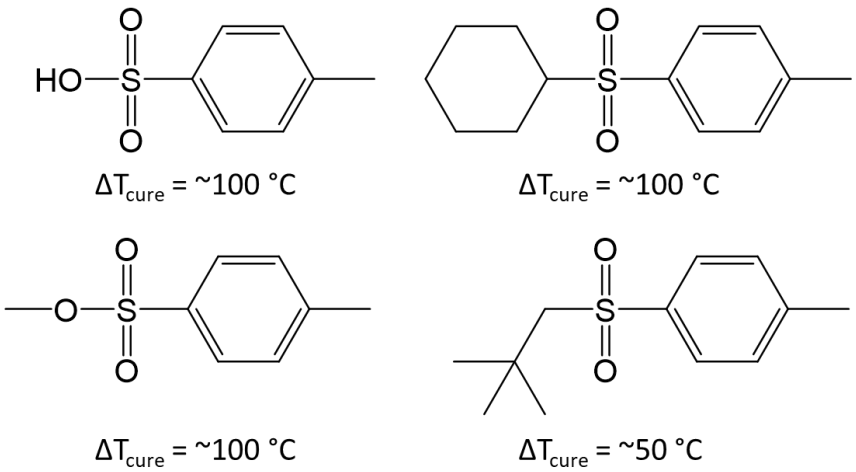

Figure 1.5. Tosylate initiators for the ROP polymerization of benzoxazine studied by Endo et al. listed with their reduction in cure temperature when loaded at 1 mol %.

Several groups have studied many small molecules that act as accelerants to the cure of benzoxazine. These typically include Lewis acids, organic acids and bases, imidazoles, transition metal compounds, and metal-organic frameworks.[16,23-28] Ishida and Rodriguez have characterized several organic acids, reducing the curing temperature by 50 °C.[23] Ishida and Wang were able to identify many chlorinated accelerants such as PCl_5, PCl_3, and $POCl_3$ as well as organic triflates that cure benzoxazines at room temperature over a 20 hour period.[16] First row transition metal complexes of acetylacetonate have reduced the curing temperature up to 60 °C.[24] Tosylates are among these well-known organic accelerants.[25,29] Endo et al. studied several tosylates (Figure 1.5), reducing the curing temperature significantly.

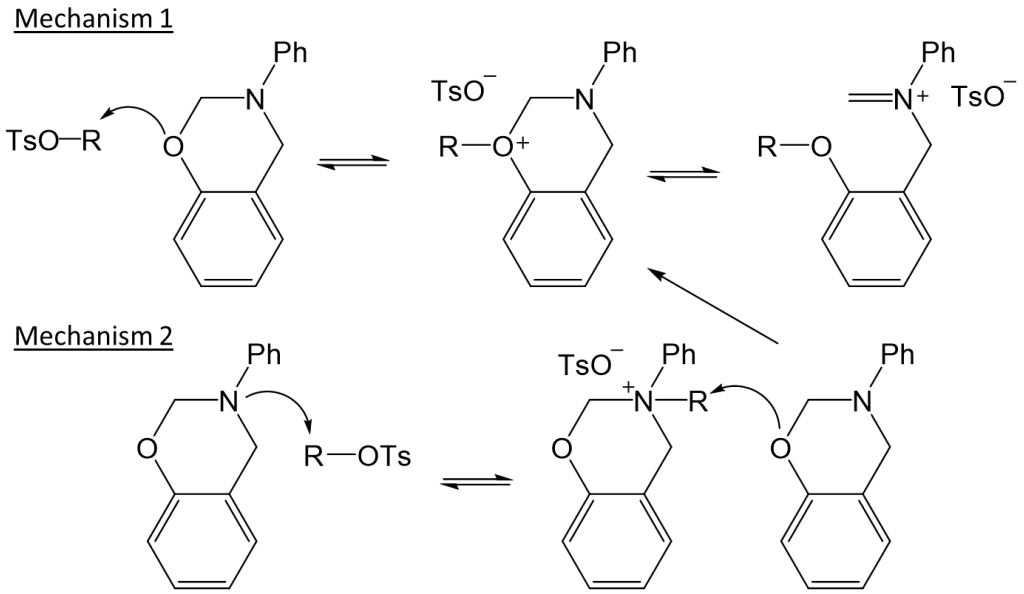

Figure 1.6. Mechanisms proposed by Endo et al. responsible for the accelerated ROP of benzoxazine.

The mechanism largely thought to be responsible for the acceleration of the cationic ROP is the nucleophilic attack from the oxazine ring from the lone pair of either the nitrogen or oxygen onto the proton or alkyl substituent of the tosylate, effectively giving the oxazine ring a positive charge (Figure 1.6). In the case of the latter, the ring converts into the iminium cation (Figure 1.6) previously discussed which then initiates further ROP polymerization. In the case of the former the alkyl or proton attached to the now positively charged nitrogen is then attacked by an oxygen from an adjacent oxazine ring, which then leads to the previously discussed pathway.[25]

(a) (b)

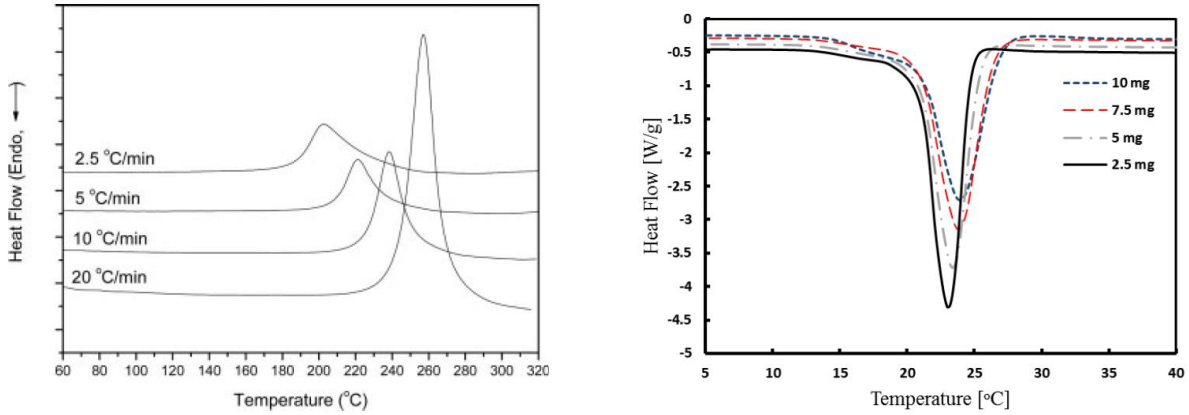

Figure 1.7. Effect of (a) heat rates[30] and (b) sample size[31] on thermal events in the DSC heat curve. All data was reproduced with permission.

The polymerization of benzoxazine is typically studied with differential scanning calorimetry (DSC). There are many modifiable parameters to this instrument and sample preparation that all have an effect on the obtained data. For instance, it is typical to have some "thermal lag" in the system where the average temperature of the sample, or the temperature at the center of the sample, is less than that read by the thermocouple in the furnace. This results in a cure temperature being read at a higher temperature than actual. This thermal lag may also be exaggerated by the ramp rate of the instrument. For instance, it is known that temperature rates of 10-20 °C will show thermal events happening at higher temperatures than what is found with temperature rates of 3-5 °C (Figure 1.7a). Another factor that may result in this thermal lag is the sample size. Larger samples are more likely to have a different temperature at the core of the sample than at the surface or than that which is being read by the instrument due to a slower transfer of heat through a larger sample. Finally, the thermal history of a sample may strongly effect the results found in DSC. Samples which may have differing crystallinity or even partial curing will have a different temperatures of cure or different thermal events during the DSC heat scans. The blend technique used to disperse the accelerant may also effect the results obtained from the DSC heat scans. Additives may be co-dissolved or melt mixed, the homogeneity of these methods is important for the dispersion of

the accelerant. All of these mentioned factors are necessary to take into consideration when evaluating thermal measurements from literature.

1.4 Benzoxazine functionalization

Since Ning and Ishida's work in 1994, publications in this field have expanded significantly, the synthesis of new benzoxazine monomers to develop new functionalities have been a very active area of research. The polybenzoxazine material can be easily functionalized for desired properties through the synthesis of new small monomers or co-polymerization. The wide molecular design flexibility of these molecules makes them good candidates to replace traditional phenolic resins such as resole and novolac, such resins present the risk of small, toxic compounds such as formaldehyde. The utility of these monomers can be manipulated to out preform existing thermosets such as bismaleimide and epoxies, or even thermoplastics using cresol and methylamine based monofunctional benzoxazine or molecular analogues of the former.[32] Bis- or tri- functionalized benzoxazine can typically be synthesized by the use of a similarly functionalized amine or phenol starting material. These multi-functional monomers will yield densely cross-linked materials, which exhibit good mechanical properties and considerable thermal resistance.[3,33-38] In the case of the mono-functional benzoxazine (Figure 1.8a), the monomer must be ortho and para substituted on the benzene ring to impede any crosslinking to achieve the thermoplastic product, this leads to only phenoxy linkages unlike in the bis- and tri- functional benzoxazine monomer.

(a)

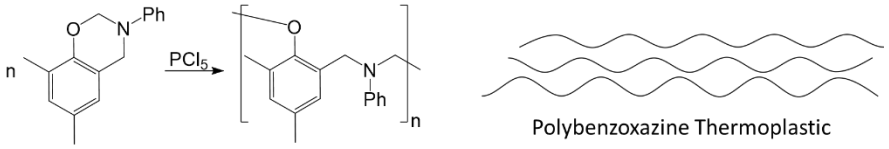

(b)

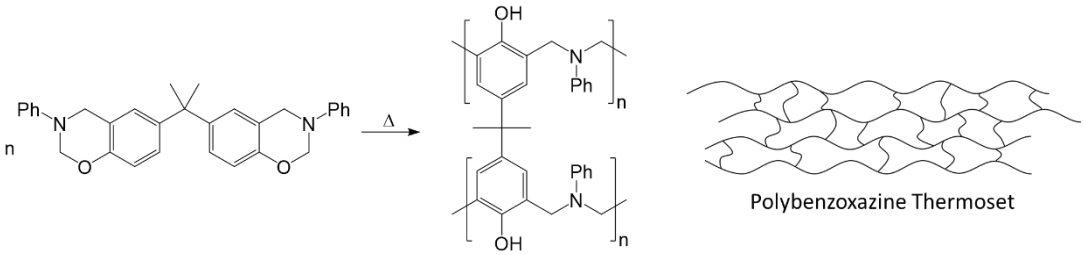

(c)

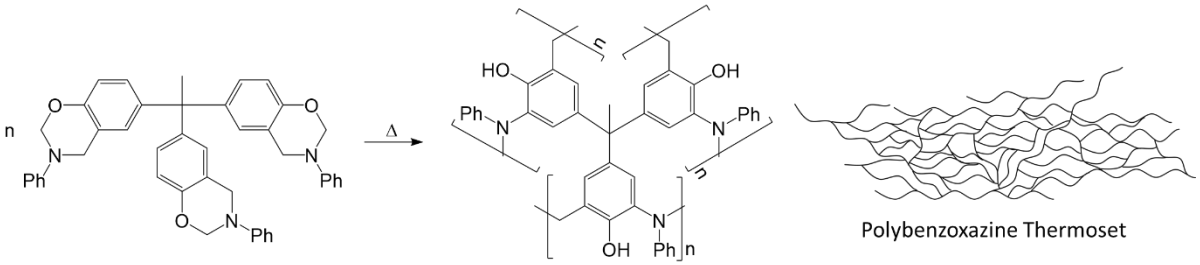

Figure 1.8. The polymerization of (a) mono-, (b) bis-, and (c) tri- functional benzoxazine into linear or densely cross-linked polybenzoxazine networks.

Already, many unique benzoxazines exist, synthesized for specified applications beyond those of traditional PBAs. Properties targeted in recent literature of monomer design encompass liquid benzoxazines,[39-43] elastic properties,[32] high modulus,[44-48] modified surface chemistry,[49-51] telechelic materials for highly dense crosslinking,[52,53] thermal stability,[54] reduced curing temperature,[55-58] low flammability,[53] and altered solubility.[55,59-61]

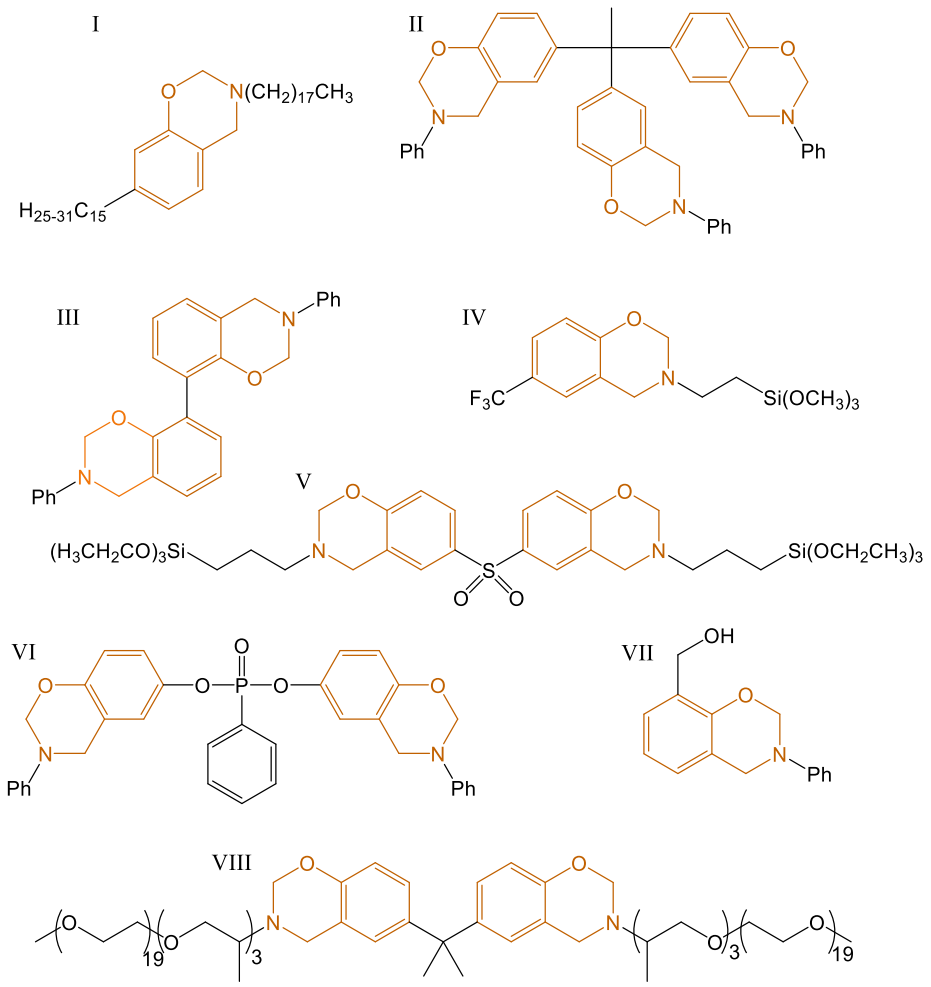

Figure 1.9. Novel benzoxazine molecules functionalized by alternative starting materials, the benzoxazine functional group is colored in orange.

The intended application is as listed: I liquid,[42] II and III high modulus,[44,52] IV modified surface chemistry,[50] V and VI improved thermal stability,[54,62] VII reduced curing temperature,[56,63] VIII modified solubility.[61]

Benzoxazine can be further synthesized into the main-chain or side-chain of polymers yielding a polymer with the potential for further crosslinking. Such polymers possess high molecular weight,[64,65] reduced cure temperature and increased thermal stability,[66] by installing thermally curable groups within the polymer's main-chain or side-chain (Figure 1.10).

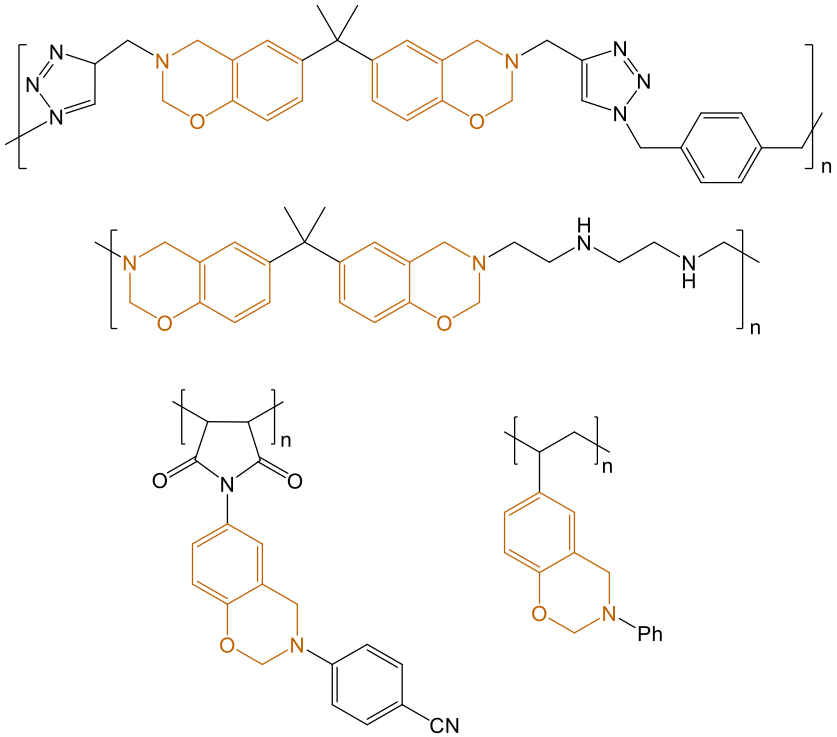

Figure 1.10. Synthesized polymers from literature containing benzoxazine in the main or side chain which possess the ability to further polymerize upon thermal activation to yield a densely crosslinked material. The benzoxazine functional group is colored in orange.

Synthesis of the monomer can also be done cost-effectively with no by-product, thereby reducing or eliminating subsequent purification steps. Solventless syntheses are also known and typically apply the amine or phenol component as the reaction media.[13,33,67] The Lomonaco group has also had success in synthesizing monomer in a matter of minutes using microwave technology, even in large quantities.[68] Furthermore, there has been extensive work done on the development of "green chemistry" benzoxazine monomer from natural sources. These monomers can be synthesized from cardanol, catechol, furfurylamine, stearylamine and other renewable materials.[46,68-71]

1.5 Benzoxazine in industry

Processing of benzoxazine monomer remains one of the largest obstacles in this field. Current thermosetting resins such as phenolic resins, like resole or novolac, remain the leading competitors to

benzoxazines of similar expenses due to their shorter cure times, lack of post cures, and lower curing temperatures, as well as ease of casting and lower melting temperatures despite the superior mechanical properties of benzoxazines. This is largely due to the high melting point, high curing temperatures, and longer curing times of benzoxazine, which have been addressed in synthesizing benzoxazine monomers with properties that are intrinsic to the molecule without the need of additives.[56,63,72-74] Many of these enhanced benzoxazine monomers also possess melting temperatures that begin to encroach on the curing temperature which only allows for a very narrow temperature window for processing.[66,75,76] These problems are addressed in this work by the introduction of blended tosylated polymers with benzoxazine to yield melting temperatures between 35-50 °C, curing temperatures of 140-210°C, and possible increased conversion of monomer thereby alleviating the need of a post cure, depending on the selected polymer/particle blend and composition.

One of the most common commercially available benzoxazines is BA-a, a bisphenol A (BPA) based benzoxazine. Recently there has been growing concern regarding the health and environmental impact of BPA and its prevalence in a variety of common plastics and coatings. While there is not much known about the effects of BPA based benzoxazines, there are several groups working to design similar benzoxazines with comparable properties and equivalent synthetic methods.[77,78]

1.6 End group influence on polymer

End group functionalization of polymers often play a role in polymer chemistry and behavior. Karaman et al. studied the surface energy and acid-base parameters of poly(ethylene glycol) (PEG) and its tosylated analogue. They found that the addition of a tosyl end group to PEG of 400 g/mol molecular weight significantly increased both its surface energy and basic characteristics.[79] End group influence on polymer miscibility at the lower critical solution temperature (LSCT) of poly(2-isopropyl-2-oxazoline) was studied by Huber et al. They found that the termination of the polymer with hydrophilic groups increased the LCST while the opposite was observed in the case of hydrophobic end groups.[80] Beuermann et al.

determined the dependence of crystallization and morphology of poly(vinylidene fluoride) (PVDF) on end groups. They found that the choice of end group can affect the degree of crystallinity of PVDF from 26-64 %. It was also observed with AFM that the end group influenced the structure of their PVDF thin films.[81] In this work the homogeneity of the blends prior to cure was determined with the percent crystallinity using differential scanning calorimetry (DSC) or post-cure with X-ray diffraction (XRD). A significant difference of BA miscibility in polymer was observed between the functionalized polymers and their unmodified precursor. This difference was largely attributed to the behavior of the end group of these polymers.

1.7 Targeting benzoxazine processability

Poly(ethylene glycol) blends or co-polymers with PBA have been studied previously by several groups, most notably are F.-C. Chang, S. Zheng, and P. Verge, the latter directly interested in incorporating PEG into the molecular PBA network by α,ω-termination of PEG with mono-functional benzoxazine.[82-84] Since the disclosure of the second chapter of this work, K. Koschek's group has reported findings that are in agreement with our own. Koschek's group reported the grafting of poly(ε-caprolactone) (PCL) onto the PBA network concurrently with the polymerization of the benzoxazine monomer.[7] Unlike in most of our blends where one terminus of the polymer is tosylated, Koschek's group studied blends of α,ω-tosylated PCL polymers with PBA-a. The hydroxyl group that is produced upon ROP of PBA-a performs an S_N2 substitution with the tosylated PCL thereby crosslinking two polymer chains resulting in a highly interconnected polymer network. Koschek was able to determine the shape-memory of these blends by the cured material's shape fixity and recovery properties.

1.8 Gordon-Taylor relationship of polymer blends

$$T_{g,ab} = \frac{w_a T_{g,a} + k w_b T_{g,b}}{w_a + k w_b} \quad (1)$$

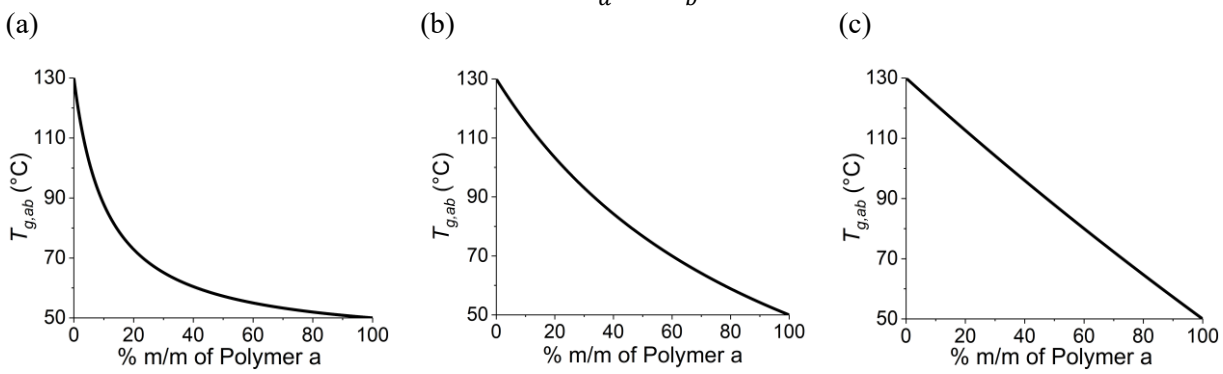

Figure 1.11. Example of Gordon-Taylor relationship between two arbitrary glass transition temperatures of 130 and 50 °C with the fitting constant, *k*, of (a) 0.10, (b) 0.50, and (c) 0.90.

The miscibility of a two polymer mixture can be estimated based on the fit of the Gordon-Taylor relationship (Equation 1). The glass transition temperature of polymer blends ($T_{g,ab}$) is expected to be found anywhere in the interval of the glass transition temperatures of each pure polymer, $T_{g,a}$ and $T_{g,b}$, weighted by the weight percent of each polymer, w_a and w_b. The homogeneity of these polymers can be assessed by the value of the fitting constant, *k*. Figure 1.11 demonstrates expected Gordon-Taylor relationships for varying *k* values where $T_{g,b} > T_{g,a}$. When there is little homogeneity in the sample, *k* is closer to 0 as seen in Figure 1.11a where *k* is 0.10. In systems with good homogeneity *k* is closer to 1 as seen in Figure 1.11c where the *k* is 0.90. At low homogeneity the glass transition temperature of the blended material is largely dominated by one of its components. However, once the fitting parameter approaches 0.50, the differences between the glass transition temperatures vary little from a system with a fitting parameter of 1. This example shows the insignificance in the improvement of a *k* value from 0.50 to 1. Few groups have been able to determine any Gordon-Taylor relationships between such polymer blends with BA.[83,85,86] The grafting of our polymers onto the PBA network improves the homogeneity of such blends resulting in a Gordon-Taylor relationship found in the glass transition temperature as

determined with differential scanning calorimetry and dynamic mechanical analysis, resulting in highly tunable blend properties by composition.

Further blends of PBA have been studied including polymers such as poly(caprolactone),[86,87] polysulfone,[88] polycarbonate,[85] poly(ether imide),[89] poly(imide-siloxane),[90] polyarylene ether nitriles,[91] and others.[92-94] Gu et al. studied polysulfone blends with benzoxazines. After installing sulfonate groups along the backbone of these polymers they discovered a reduction in the cure temperature of the benzoxazine monomer, noticing a trend of decreasing curing temperature with increasing sulfonate content, as explored in this work.[88] Drawbacks of the inclusion of PEG are further explored and addressed in this work. The increase of PEG content in these PBA materials results in weakening of the overall polymer with decreased storage modulus. PEG also imparts some flammability and smoke density which are undesirable in the aforementioned fields that have expressed interest in the PBA materials. The capabilities and chemistry investigated in the PEG/PBA blends can also be assigned to a wide variety of other blends, which in this work include polylactic acid, polysulfone, and silica additives. Each polymer incorporates and imparts its own unique chemical and mechanical properties onto the novel PBA material. In this work it was found that the PSU and silica blends provide increased modulus and possible reduced flammability or chemical sensitivity, while still providing homogenous blends and reducing the cure temperature by 17 and 79 °C, respectively, similarly seen in the PEG blends. The chemistry resulting in the tosylation of such polymers is well established and easily implemented.

1.9 Water-soluble, benzoxazine-based surfactants

Processing of benzoxazine typically includes solvent casting, solvent baths, and hot melting. Easier alternatives to these processing methods have come under much interest, several solutions including liquid benzoxazine monomers (typically increasing the flammability of BA).[39,73,95] The Taden, Ishida, Krajnc, and Notley groups have recently published several studies on the synthesis and utility of benzoxazine-based surfactants for aqueous media. [59-61,96,97] Such methods are attractive because of the decrease in

toxicity and risks associated with the fabrication of such materials using baths of water at or near room temperature. Benzoxazine based surfactants are more desirable over their commercially available counterparts such as cetyltrimethylammonium bromide (CTAB), sodium dodecyl sulfate (SDS), etc. due to the incorporation of the surfactant into the final cured PBA material. Many routes for the synthesis of such surfactants have been explored. Non-polymerizable surfactants often form moieties in the finished product as it comes out of phase with the macromolecular structure of the PBA which makes the incorporation of these co-polymerizable surfactants attractive. Such deformities or faults in materials like protective coatings, interfaces and thin films or even aerospace applications with narrow acceptable parameters for mechanical failure may lead to fractures and faults in the product. Co-polymerizable surfactants, like Benzoxazine-based surfactants, avoid these complexities.

1.10 Surfactant Geometry

Table 1.1. The resulting micellar geometry as determined by the shape of the surfactant and its corresponding packing parameter.

Critical Packing Parameter	Surfactant Shape	Micelle Geometry
$cpp < \frac{1}{3}$	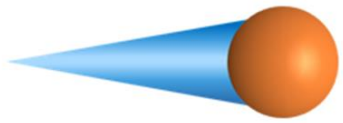 Cone	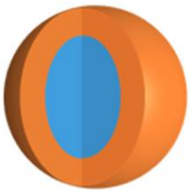 Sphere
$\frac{1}{3} < cpp < \frac{1}{2}$	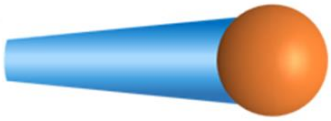 Truncated Cone	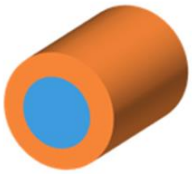 Cylinder
$\frac{1}{2} < cpp < 1$	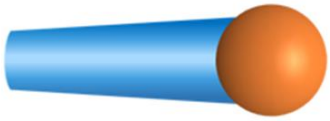 Truncated Cone	Vesicle
$cpp \approx 1$	Cylinder	Lamellar
$cpp > 1$	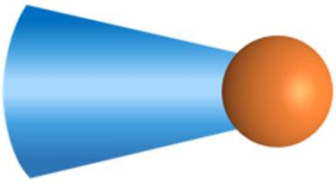 Inverted Truncated Cone	Inverted Sphere

A surfactant is shorthand for surface active agent, its shape and functionality tends to translate to the overall structure of the micelle. The micelle shape can effect monomer loading and the critical micelle concentration (CMC), the lowest concentration required to form micelles within a solution. It is typical for nonionic surfactants to have lower CMC values than those of ionic surfactants, however oxyethylene based nonionic surfactants may increase the CMC as well.[98] The surfactant shape can be determined by its critical packing parameter (CPP) which can be estimated by Equation 2,[98] where V is the volume of the tail, A is the area of the head group and, and l is the length of the tail. Therefore the CPP represents a unitless ratio that can be manipulated by changing one of these three factors.

$$\mathrm{CPP} = \frac{V}{A \cdot l} \tag{2}$$

1.11 Biodegradability of thermoset composites

The disposal of composites and materials made from PBAs has also been under much investigation. Currently, most fiber reinforced polymers are largely disposed by solvolysis, which requires heating the composites in large baths of water or organic solvents at high temperatures for long periods of time until the monomer degrades into a more suitable condition for disposal.[99-102] Most other parts are left to sit in landfills for centuries in the cases of most plastics and thermosets. Several groups are working to reduce the burden of disposing these materials by synthesizing reversible benzoxazine monomers or forming new co-curing components that will "de-polymerize".[103-105] This not only leads to green disposable alternatives but may actually aid in reusing monomer/starting materials to synthesize new monomer which will also reduce the expenses of these highly engineered materials. Alternatively, the incorporation of a biodegradable component can also fulfill this need. Poly(lactic acid) (PLA) may also provide the opportunity for installing biodegradable thermoplastic into the network for easier disposal of PBA blend materials.[106,107]

1.12 Scope of project

The aims of the work in this thesis is to provide solutions to current processing obstacles of polybenzoxazines as well as explore new applications to this unique polymer. The following represents the main objectives in this work:

1. To formulate liquid benzoxazine blends with thermoplastics at room temperature.
2. To increase homogeneity between benzoxazine monomer and these thermoplastics by end group functionalization.
3. To reduce the curing temperature of polybenzoxazine by installing a thermally latent catalyst on the end group of these thermoplastics.
4. To induce grafting of the thermoplastic on the polybenzoxazine network in order to maintain homogeneity of the now cured polybenzoxazine and thermoplastic.
5. To increase the modulus of blended polybenzoxazine materials.
6. To increase thermal stability of polybenzoxazine.
7. To increase the strength of the polybenzoxazine materials by blending with high modulus, end group functionalized thermoplastics, or functionalized particles.
8. To synthesize a water-soluble benzoxazine-based surfactant with competitive monomer loading to commercially available surfactants.
9. To synthesize a surfactant with the ability to co-polymerize with loaded monomer in order to reduce faults from non-polymerizable aggregates in the material.
10. To study the effect of chain length and functionalization on the surfactant geometry.

Chapter 2: Pegylated polybenzoxazine from miscible blends of poly(ethylene glycol) and benzoxazine monomer

Reproduced with permission from Brown, E. A.; Rider, D. A. Pegylated polybenzoxazine Networks with increased thermal stability from miscible blends of poly(ethylene glycol) and a benzoxazine monomer. *Macromolecules* **2017**, *50*, 6468-6481. Copyright 2017 American Chemical Society.[*Link*]

2.1 Introduction

Polybenzoxazines, PBA or P(BA)s, are an emerging class of thermosetting resins that display excellent properties such as high glass transition temperatures, low water absorption and flammability, near-zero volumetric cure shrinkage, and very good dielectric, thermal and mechanical properties even at modest polymer molecular weights.[108] Crosslinked P(BA-a)s are typically produced from monomers containing two or more benzoxazine rings per molecule and the ring-opening polymerization (ROP) of these rings leads to a macromolecular networked structure mostly consisting of Mannich-bridged phenolic moieties. The synthetic scope for benzoxazine monomers, which usually consists of the condensation of formaldehyde with a primary amine and a phenolic molecule, is very large and has led to a wide class of P(BA)s. Recent examples include P(BA)s with hydroxyl, phenyl, maleimide, propargyl, allyl, and carboxy crosslinking groups, or aliphatic residues for tailored thermal stability, low-brittleness and other properties.[3,43,64,109-116] The ROP is commonly triggered by a high temperature condition (from 160-270 °C)[20,74,109,117,118] but other cure conditions such as electrochemical oxidation[14] or photoinitiation have been reported.[119] The high temperatures required for the thermal ROP of benzoxazines have in part contributed to the lack of widespread deployment of these resins into various industries. Accelerators such as organic acids[23] and bases,[26] Lewis acids,[16] imidazoles,[28] transition metal compounds,[24] and metal-organic frameworks[27] can reduce this polymerization temperature.

Functionalizing PBA with other polymers offers interesting opportunities for creating hybrid materials with stable, tunable physical, chemical and mechanical properties.[120] Accordingly, PBA functionalized with polystyrene,[109,121,122] poly(methyl methacrylate),[123] polyesters,[109] polyethers,[124,125] poly(ε-caprolactone),[126]

polysiloxanes,[127,128] and polyacetylenes[129] have been synthesized. PBA with blended additives including silicates,[130-132] carbon black,[133] lignin,[134] and nanoparticles and nanotubes[135] are also well-described. For some applications, improved flexural and impact properties in P(BA)s would be desirable and could be achieved by the incorporation of complementary low glass transition temperature (T_g) polymer.[136-138] Curing benzoxazine monomers in a polymer matrix often leads to phase separated polymer-polymer blends due to reduced entropic contributions as the molecular weight of the PBA increases.[20] Previously for example, solutions of a bisphenol A benzoxazine [PBA-a or P(BA-a)] monomer in *α,ω*–dihydroxy poly(ethylene glycol) (*α,ω*–HO-PEG-OH) were studied for miscibility and subsequent thermal ROP.[139] In this case, cured solutions afforded a phase separated blend of PBA-a and *α,ω*–HO-PEG-OH, where the phenolic hydroxyl groups of the PBA-a were in a non-associated form, i.e. lacking any significant hydrogen-bonding within the PBA-a network or to the PEG phase. Less-well described are blends where the complement polymer is capable of several roles such as solubilizing the benzoxazine monomer, accelerating its cure and controllably grafting to the resulting PBA-a network so as to permit adjustment of the chemical and thermal properties of the hybridized material. We therefore present herein a study on the solubility, polymerization and the molecular characterization of blends of BA-a in end group mono-tosylated poly(ethylene glycol) (mPEGOTs). More specifically, we prepare and characterize blends of BPA-based benzoxazine (BA-a) with either *α*–hydroxyl-terminated (mPEGOH) or tosylate-terminated mPEGOTs. Contrary to the mPEGOH blends, a decrease in the cure temperature is found for the BA-a/mPEGOTs combination. Infrared spectroscopy and mass spectroscopy were used to monitor heated blends and have identified free tosylate as a possible catalyst in curing blends of BA-a/mPEGOTs. In contrast to cured mPEGOH blends, ^{1}H NMR and FTIR revealed that the PBA-a network synthesized in mPEGOTs consists of a phenolic rich molecular structure with strongly H-bonded hydroxyl residues and grafted PEG-chains. Scanning electron microscopy confirmed that P(BA-a)-*graft*-mPEGOTs [P(BA-a)-*g*-mPEGOTs] is homogeneous in its microstructure. The tuning of the T_g and the thermal stability of the P(BA-a)-*g*-mPEGOTs was also demonstrated in mPEGOTs blend series. Since most PBA-a alloys are synthesized from monomer/monomer blends,[140] this work has novelty arising from the demonstrated access

to well-defined PBA-a alloys from BA-a/polymer blends. We expect that the details of the novel reaction and covalent bonding between curing BA-a and mPEGOTs may apply universally to other miscible benzoxazine/polymer blends and would allow for greater tuning of the resulting properties of the graft co-polymers based on tuned molecular weight and structure in the initial tosylated polymer. The potential applications of such chemistry and alloys is large in scope and may lead to novel materials for the biomedical plastics, electronics, membranes and aerospace industries.

2.2 Experimental

2.2.1 Materials. The bisphenol-A benzoxazine (BA-a) monomer was used as received from Hunstman. The methoxypoly(ethylene glycol) ($mPEGOH_{2000}$; M_n 2000), methoxypoly(ethylene glycol) tosylate ($mPEGOTs_{2000}$; M_n 2000), and methoxypoly(ethylene glycol) tosylate ($mPEGOTs_{900}$; M_n 900) were acquired from Sigma Aldrich. The methoxypoly(ethylene glycol) ($mPEGOH_{900}$; M_n 900) was used as received from Polymer Source. Acetone (99.7 % purity) was used as received from Fisher Scientific. Chloroform (99.8 % purity) was used as received from J.T. Baker. Deuterated dimethyl sulfoxide (99.9 % purity) was used as received from Cambridge Isotope Laboratories, Inc. Neutral aluminum oxide was used as received from Acros Organics.

2.2.2 Methods. A Vega TS 5136MM scanning electron microscope (SEM), operated with an accelerating voltage of 15 kV, was used to capture micrographs of samples that were coated with a thin layer of gold and platinum to dissipate charge (nominal Au thickness ~1 nm). Cured blend samples were prepared for SEM by fracturing the sample followed by a soak in chloroform for 30 minutes before drying in ambient conditions. A Nicolet iS10 FTIR spectrometer equipped with an attenuated total reflectance (ATR) accessory was used for FTIR studies (64 scans at 4 cm^{-1} resolution per spectra). A Bruker AVANCE-III, HD 500 MHz NMR spectrometer was used to collect ^1H NMR spectra. Samples for NMR were prepared from cured materials that were soaked in DMSO-d6 for 30 minutes.

2.2.3 Preparation of Blends of Poly(ethylene glycol) and N-Phenyl Bisphenol A Benzoxazine. The preparation of blends of either mPEGOH or mPEGOTs with N-phenyl bisphenol A benzoxazine (BA-a)

follows a modified procedure outlined by Lü et al.[83] The general procedure for the preparation of BA-a blends is as follows: separate solutions of 1.45 g BA-a in 2.90 mL acetone and 2.05 g of either mPEGOH, $mPEGOTs_{900}$, or $mPEGOTs_{2000}$ in 4.10 mL of acetone were prepared. Appropriate volumes from each solution were then combined to total 1 mL in a 10 mL round bottom flask. Each sample was dried in vacuo and then dried in a vacuum oven at 50 ˚C for 9 hours.

2.2.4 Thermal Analysis. A TA Instruments Q500 thermogravimetric analysis (TGA) instrument equipped with an inline Thermo Scientific iS10 Fourier Transform Infrared (FTIR) Gas Cell Spectrometer was used for TGA/TGA-FTIR experiments.[141] TGA experiments were performed with a 1 min isotherm at 75 °C followed by a 25 °C/min ramp from 75 to 30 °C and then a 10 °C/min ramp from 30 °C to a minimum of 400 °C to analyze the weight changes during the melting and curing of BA-a, mPEGOH, mPEGOTs and their blends, and to determine any char yields. An isothermal transfer line (225 °C) was used to direct effluent from the TGA sample furnace to the FTIR spectrometer using dry nitrogen as a carrier gas (flow rate = 90 mL/min). The background signal of FTIR spectra was collected from a 5 minute isotherm before and after this temperature program. FTIR spectra (consisting of 4 scans at 8 cm^{-1} resolution and acquired at a 2.7 sec interval) were corrected for background created from a time averaged signal (5 min) for the blank nitrogen carrier gas. A Perkin Elmer 4000 thermogravimetric analysis (TGA) instrument equipped with an inline Hiden QGA gas analysis mass spectrometer (MS) was used for TGA-MS experiments. Effluent from the sample was carried to the MS spectrometer via an isothermal transfer line (80 °C) and dry nitrogen gas flowing at 20 mL/min.

A TA Instruments Q100 differential scanning calorimetry (DSC) instrument was used for DSC-based cure studies on all samples. Blends were heated (in hermetically sealed DSC pans) for 3 min at the elevated temperature of 100 °C for mPEGOH blends and 50 °C for mPEGOTs blends. The pans were rapidly transferred to liquid nitrogen for a –200 °C quench then loaded into the DSC instrument. For cure studies, the samples were then scanned at 5 °C/min from –70 °C to 75 °C to –70 °C to 75 °C (heat, cool, heat). The samples were heated and quenched as before and then scanned at 5 °C/min from -70 °C to 260 °C to -70

°C to 260 °C. Exothermic cure was estimated by integration of the exothermic peak using a tangential sigmoidal baseline (see Figure A1 and Table A2 in the supporting information).

2.3 Results and discussion

2.3.1 Miscibility of BA-a in mPEGOH and mPEGOTs and Crystallization. The miscibility of N-phenyl bisphenol A benzoxazine (BA-a) monomer in hydroxyl or tosylate end group functionalized poly(ethylene glycol) (PEG) was investigated in order to better describe the polymerization, cross-linking and grafting reactions that may occur in their heated blends. Mixtures of BA-a with either methoxypoly(ethylene glycol) ($mPEGOH_{2000}$; M_n = 2000 Da) or methoxypoly(ethylene glycol) tosylate ($mPEGOTs_{2000}$ or $mPEGOTs_{900}$; M_n = 2000 and 900, respectively) were prepared by first co-dissolving in acetone, a common solvent for both BA-a and the PEG-based polymers. The solvent was evaporated at low pressure and temperature to create blended samples which were then sealed in hermetic vessels. The vessels were heated to melt any PEG-based crystallites and then thermally quenched in liquid nitrogen prior to thermal analysis by DSC. Shown in Figure 2.1 are the heating curves for the BA-a, $mPEGOH_{2000}$, and $mPEGOTs_{2000}$ and the BA-a/mPEG blends. Similar heat curves for the $mPEGOTs_{900}$ series are found in the supporting information (Figure A2). The PEG polymer used for samples in Figure 2.1a was $mPEGOH_{2000}$ and that for samples in Figure 2.1b was $mPEGOTs_{2000}$. The bottom-most curves in Figure 2.1a and 2.1b depict the thermograms for the isolated $mPEGOH_{2000}$ and $mPEGOTs_{2000}$. Each curve shows no evidence for an exothermic transition which confirms crystallization of the polymer occurred during the quench step. There was also little evidence for a glass transition temperature in the heating curves which suggests that there is relatively little amount of amorphous content in these PEG samples. Each curve however depicts a notable endotherm with peak temperature values of 51 °C and 50 °C for the $mPEGOH_{2000}$ and $mPEGOTs_{2000}$, respectively. This endotherm corresponds to the melt transition (T_m) of PEG for which the T_m values agree with previous reports for other PEG samples of similar molecular weight and structure.[142,143] The enthalpy of melt (ΔH_m) values for the $mPEGOH_{2000}$ and $mPEGOTs_{2000}$ were found to be 149 and 165 J/g, respectively, and are also in agreement with similar molecular weight PEGs.[144-147] The

top-most heating curve in Figures 2.1a and 2.1b depict the thermograms for the isolated BA-a monomer and show no evidence for crystallization, melting or curing. A notable difference between the blends with $mPEGOH_{2000}$ and $mPEGOTs_{2000}$ was observed in the change of their respective ΔH_m before and after cure of the benzoxazine content (Table A3). Generally the former series maintained similar ΔH_m in two successive heat curves with the second heat cycle mostly characterizing the sample after a cure event has occurred. The latter series however had a significant decrease in the ΔH_m of the PEG in the second heat curve with no endotherm observed at all for blends ≤ 50 wt % mPEGOTs. We hypothesize that a random grafting of the PEG onto the PBA-a network occurs in this series and is responsible for suppressing crystallization of the grafted PEG (vide infra) in the second heating scan in the DSC curves.

From the first heat cycle in the DSC curves for the BA-a/$mPEGOH_{2000}$ blends, it is apparent that crystallization and melting of PEG is not impeded by the presence of BA-a monomer for blends with compositions that range from 40 to 100 wt % mPEGOH. BA-a/$mPEGOH_{2000}$ blends with an overall PEG content less than 40 wt % exhibit complete suppression of the melt endotherm and are therefore comprised of a majority amorphous state that hosts the dissolved BA-a. Similarly, from the DSC curves for the BA-a/$mPEGOTs_{2000}$ blends, crystallization and melting of PEG is not impeded by BA-a monomer when blends are formulated with the composition range of 50 to 100 wt % mPEGOTs. BA-a/$mPEGOTs_{2000}$ blends with an overall PEG content less or equal to 50 wt % exhibit complete melt suppression. Similarly, BA-a/$mPEGOTs_{900}$ blends with an overall PEG content less or equal to 60 wt % exhibit complete melt suppression. The similar blend range for miscibility between BA-a and mPEGOTs and mPEGOH suggests that the end group of mPEGOTs is not important for compatibilizing the solute.[79] Huang et al. have previously observed a similar affect for PEG blended with a similar benzoxazine monomer.[84] Also evident in Figure 2.1a is a significant decrease in the T_m of $mPEGOH_{2000}$ with increasing BA-a content in its blends. The melting point depression in Figure 2.1a is due to the thermodynamic effect of incorporating the miscible phase into a crystalline mPEGOH phase.[84,139] There is less melt point depression in the BA-a/mPEGOH

system. The lowest melt points of the $mPEGOH_{2000}$ and $mPEGOTs_{2000}$ in the BA-a-richest blends are found at relatively similar values of 43 and 38 °C, respectively.

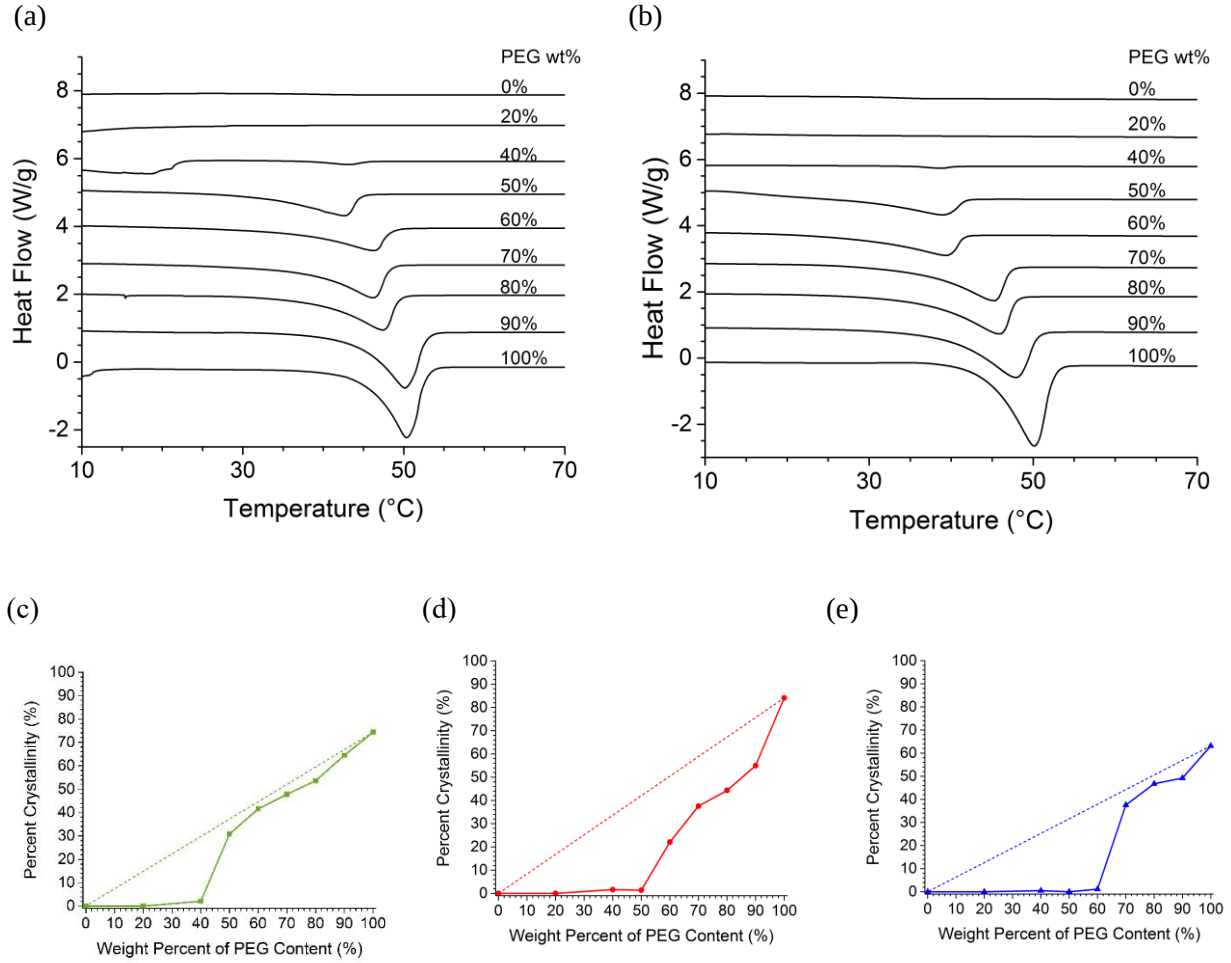

Figure 2.1. DSC curves from the first heat cycle after quenching (exothermic direction is up) of BA-a blends with either (a) $mPEGOH_{2000}$ or (b) $mPEGOTs_{2000}$. Curves have been offset for clarity. Plots for the percent crystallinity of (c) $mPEGOH_{2000}$, (d) $mPEGOTs_{2000}$, and (e) $mPEGOTs_{900}$. The dash line in (c-d) represents the theoretical crystallinity of PEG assuming no interaction with non-crystallizable BA-a.

The inhibition of crystallization can be better represented by plotting the theoretical percent of crystallization of the PEG component versus the blend composition. Figures 2.1c-e report the percent of crystallization of the mPEG component versus the BA-a blend composition for the $mPEGOH_{2000}$, $mPEGOTs_{2000}$, and $mPEGOTs_{900}$ series. The enthalpy of melt for a completely crystallized PEG has been

reported as ~205 J/g,[148,149] and is used to determine the percentage of crystallization in each blend sample discussed above. The enthalpy of crystallization for the pure $mPEGOH_{2000}$ was used to determine the degree of crystallization which corresponded to a value of 74 %, a value that agrees with previous reports for similar PEG materials quenched from its melt state.[144,150] The degree of crystallization for the pure $mPEGOTs_{2000}$ and $mPEGOTs_{900}$ had values of 84 % and 63 %, respectively. The difference in molecular weight of the two polymers is responsible for the difference in the degree of crystallinity of the two mPEGOTs polymers.[151] If the crystallization of PEG was not influenced by the inclusion of the BA-a solute, then the percent of crystallization should correspond to the product of the fractional content of mPEG in the blend and the enthalpy of melt for the pure mPEG. Each plot in Figures 2.1c-e reports this theoretical percent of crystallization as a dotted line. In the $mPEGOH_{2000}$ series (Figure 2.1c), the percentage of crystallinity in the polymer does not deviate significantly from the predicted value for blends with ≥ 50 % polymer content. In this same series, there is a dramatic decrease in crystallinity from the expected trend when the content of BA-a is more than 60 wt % which indicates a miscibility range for the polymer and the BA-a monomer. In the $mPEGOTs_{2000}$ and $mPEGOTs_{900}$ series (Figures 2.1d and 2.1e, respectively), similar characteristics are found in the corresponding plots but with an important difference. The miscibility range, indicated by the break from trend of the high PEG content blends (excluding pure PEG), is wider. Generally, the crystallization of the polymer is uninhibited for blends that are greater than 70 wt % $mPEGOTs_{2000}$ or $mPEGOTs_{900}$.

2.3.2 Cure of BA-a in mPEGOH and mPEGOTs blends. The thermal ROP of BA-a proceeds at elevated temperatures (> 160 °C) and involves a cationic polymerization mechanism.[14,152] A DSC cure study was conducted to understand the cure of the BA-a/mPEG blends. The temperature scan range of all the DSC runs were limited to 260 °C to minimize the influence of PEG degradation in this study. Shown atop in Figure 2.2a is the DSC trace for pure N-phenyl bisphenol A benzoxazine (BA-a) which depicts an exotherm with a peak value and an onset value of 220 and 205 °C, respectively. This exothermic signal corresponds to the energy of the thermal ROP reaction which was calculated to be 242 J/g, a value that agrees with

previous literature.[153] As PEG is introduced in the $mPEGOH_{2000}$ blend series, the exotherm of the thermal ROP reaction for BA-a was found to shift to higher temperatures. Most curves are symmetric and monomodal with peak values in the range of 232-240 °C. The onset of these peaks were also found to shift to higher temperatures as well (215-226 °C). There appears to be neither a trend in the exotherm temperature values with composition of the blend nor any significant distinction of highly miscible blends from phase separated samples (i.e. samples described in Figure 2.1a with < 40 wt % PEG). The increase in the temperature required to cure the BA-a into PBA-a suggests that the mechanistic steps for initiation and propagation do not benefit from any interaction with PEG repeat units, or with the hydroxyl end group of the polymer. The additional temperature for cure is likely a consequence of kinetic factors such as reduced heat transfer across the excluded and melted PEG phase to the monomer for polymerization. Inspection of the DSC curves for blends of BA-a with mPEGOTs reveals important distinctions. The DSC trace of the pure BA-a sample that was heated at 50 °C, similar to the mPEGOTs blends, is shown atop in Figures 2.2b-c. The enthalpy of the thermal ROP reaction was calculated to be 287 J/g for this sample with a peak and onset exotherm at 227 and 217 °C. As $mPEGOTs_{2000}$ is enriched in its BA-a blend series, the exotherm of the thermal ROP reaction for BA-a was found to decrease to lower temperatures with most peaks values in the range of 186-207 °C. The onset of these peaks were also found to shift to lower temperatures (161-193 °C). The exotherm curves remain monomodal until the $mPEGOTs_{2000}$ content exceeds a value of 50 wt %. Based on the miscibility range inferred from Figure 2.1b, it follows that the higher temperature exotherm shoulders would correspond to the cure of BA-a that is more closely associated with the once crystalline domains of the mPEGOTs. Overall, it appears that a beneficial interaction for polymerization exists between BA-a with $mPEGOTs_{2000}$ and, since the *p*-toluenesulfonate group distinguishes this polymer from the aforementioned one, we propose that this end group is responsible for the reduction in energy required for initiation and propagation step in the polymerization of BA-a. In the three selected blends with $mPEGOTs_{900}$, the presence of the *p*-toluenesulfonate end group decreases the temperature of the thermal ROP reaction for the BA-a as well with peak temperatures between 170-185 °C and onset temperatures

between 150-172 °C, significantly lower than the mPEGOTs$_{2000}$ blends. The blends with high mPEGOTs$_{900}$ content at 60 and 80 wt % exhibit bimodal exotherms similar to the mPEGOTs$_{2000}$ blends.

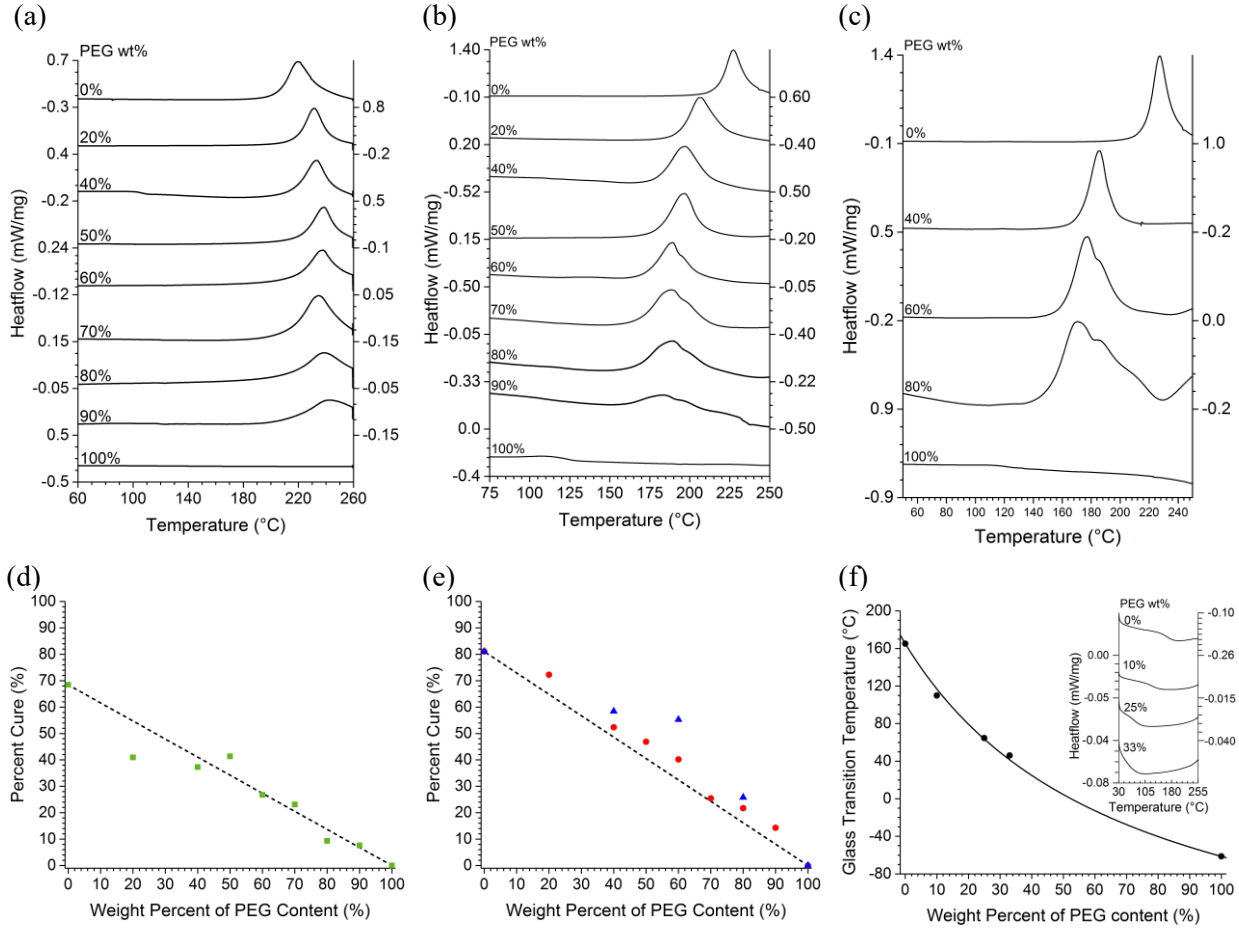

Figure 2.2. DSC cure study of quenched blends of benzoxazine with (a) mPEGOH$_{2000}$, (b) mPEGOTs$_{2000}$, and (c) mPEGOTs$_{900}$. Plots for the percent cure of blends with (d) mPEGOH$_{2000}$, (e) mPEGOTs$_{2000}$ (●) and mPEGOTs$_{900}$ (▲). The dash line represents the theoretical cure of benzoxazine assuming no interaction with PEG. (f) Plot for the T_g of the PBA-a for cured samples from the mPEGOTs$_{900}$ series. The theoretical curve superimposed over the data points is the result of fitting a Gordon–Taylor relation.

The standard enthalpy of cure for the thermal ROP reaction for the BA-a used in this work is 354 J/g.[154,155] The exothermic signal for the exotherm atop in Figure 2.2a corresponds to a percent cure value of 68 % under the conditions used for the in-situ cure in the DSC. If the polymerization or cure reaction of BA-a

into pure PBA-a was not influenced by the inclusion of the PEG, then the percent of cure should correspond to the product of the fractional content of BA-a in the blend and the enthalpy of cure for the pure BA-a. The dotted lines in Figures 2.2d-e reports these theoretical percent of cure predictions. The exotherm data in Figure 2.2a was quantified by integration in order to estimate and report the enthalpy of cure for BA-a in these blends (see data in Figure 2.2d). As PEG is introduced in the $mPEGOH_{2000}$ blend series, the percent of cure of the BA-a closely follows the theoretical curve, suggesting that the thermal ROP of BA-a largely proceeds in the $mPEGOH_{2000}$ without complication or side reaction. This also suggests that the hydroxyl-terminus of the PEG-OH does not undergo any reaction with the BA-a or PBA-a under these conditions and would result in a phase-separated or interpenetrating network mixture of the PBA-a and $mPEGOH_{2000}$. The corresponding data for the $mPEGOTs_{2000}$ and $mPEGOTs_{900}$ blend series shows significant differences. The exothermic signal for the thermal ROP of BA-a atop in Figures 2.2b-c represents a percent cure value of 81 %. Likewise the exotherm data in Figure 2.2b-c was calculated by integration and the percent of cure was reported in Figure 2.2e. As the PEG is introduced in this series, the percentage of cure into pure PBA-a deviates positively from the predicted trend suggesting that there is a more complete cure reaction and/or a secondary exothermic reaction. Chemical information gleaned from FTIR and ^{1}H NMR supports the latter of these hypotheses. The amount of positive deviation from the theoretical BA-a cure trend line appears to be maximized when the BA-a:mPEGOTs is highest and exhibits no crystallization of the PEG component (i.e. 50 and 60 wt % $mPEGOTs_{2000}$ and $mPEGOTs_{900}$ samples, respectively). The lower melt viscosity for the lower molecular weight $mPEGOTs_{900}$ appears to favor higher exotherm values in this regime.

The Gordon-Taylor relation can be used to generate a metric that quantifies the miscibility arising from favorable intermolecular interactions between components in polymer alloys.[156] This relation, shown in eq. 1, calculates the glass transition temperature of miscible polymer-polymer systems ($T_{g,ab}$), using glass transition values of the independent blend components ($T_{g,a}$) and ($T_{g,b}$), and the weight fraction of each polymer in the blend (W_a and W_b).

$$T_{g,ab} = \frac{w_a T_{g,a} + k w_b T_{g,b}}{w_a + k w_b} \quad (1)$$

The constant, k, in the Gordon-Taylor equation is a fitting parameter that provides curvature to the $T_{g,ab}$ versus blend composition curve and usually takes on values from 0-1. The k values often increase as the number and strength of favorable intermolecular interactions increases in blend systems.[157,158] Shown as an inset in Figure 2.2f are the DSC curves for the PBA-a created from the thermal ROP of BA-a and selected cured PEG blends from the $mPEGOTs_{2000}$ series. All samples were cured using a heating program consisting of 10 °C/min scans from 25 °C to 260 °C to 25 °C to 260 °C. A glass transition value for pure PBA-a of 165 °C was found which also agrees with previous work.[153,155,159-161] A glass transition value for pure PEG (M_n = 2000 Da) is also included on the plot.[162,163] PEG-rich blends (those with $mPEGOTs_{2000}$ >33 wt %) were not included in the plot. The fit of the Gordon–Taylor equation to the T_g values of the cured blends in Figure 2.2f was quite good (R^2 value of 0.998) and gave rise to a fit constant k equal to 0.41. This fitting value suggests there are very favorable molecular bonding interactions between the PEG and the cured BA-a material.

A FTIR study of cured blends of BA-a with $mPEGOH_{2000}$ and $mPEGOTs_{2000}$ was conducted in order to interrogate functional groups capable of intermolecular interactions as indicated in the Gordon-Taylor analysis above. The PBA-a that results from the thermal ROP of BA-a is expected to have phenol-based hydroxy residues that are capable of acting as a hydrogen bond donors. The oxygen atoms in the backbone of PEG are well-known H-bond acceptors[164] and, together, these groups could lead to favorable intermolecular bonding interactions for improved miscibility to favor a more hybridized structure. Shown in Figure 2.3 are the C-H and O-H stretch regions of the FTIR spectra of the cured samples from the BA-a/$mPEGOH_{2000}$ series. The spectra atop in both Figures 2.3a and 2.3b display the FTIR data for pure PBA-a with signals for both sp^3 CH_3 and CH_2 residues (ν_{CH3}: 2870-2970 cm^{-1}; $\nu_{CH2,}$: 2850-2925 cm^{-1}, respectively) and aromatic sp^2 CH residues ($\nu_{aromatic\ CH}$: 3010-3050 cm^{-1}) as well as a broad signal for phenol hydroxyl groups ($\nu_{O\text{-}H\ phenol}$: 3360 cm^{-1}).[165,166] The broadness of the OH-stretch peak reflects a wide distribution of weakly hydrogen-bonded hydroxyl groups that are characteristic of phenolic polymers.[84,85,160,167] As PEG

is increased in content in the blend series for $mPEGOH_{2000}$ (down the stack plot in Figure 2.3a), the intensity of the peak associated the ν_{CH2} stretching mode of sp^3 bonded CH_2 strengthened and evolved in accordance with the increase in the methylene content in the PEG loaded sample. The signal for the aromatic sp^2 CH residues ($\nu_{aromatic\ CH,}$: 3010-3050 cm^{-1}) also became less prominent with increasing PEG content. The broad signal associated with phenol hydroxyl groups became reduced with increasing PEG content and, displayed its maximum signal at a near constant wavenumber of 3360 cm^{-1}, which indicates a similar chemical distribution of polymeric hydroxyl groups regardless of blend composition. Only the sample with 90 wt % PEG showed a shift in this hydroxyl stretch, showing the peak at 3424 cm^{-1}, which indicates reduced hydrogen bonding. Therefore, as a whole, PBA-a phenol groups are largely weakly associated with the PEG constituent across the entire compositional range of samples. Inspection of Figure 2.3b shows some similarities and differences in cured samples from the $mPEGOTs_{2000}$ series. In similarity to the aforementioned series, as the $mPEGOTs_{2000}$ increases in these samples (down the stack plot in Figure 2.3b), the transmission peak associated ν_{CH3} sp^3 bonded CH_3 decreased in favor of increased ν_{CH2} signal for sp^3 bonded CH_2. Similarly, the $\nu_{aromatic\ CH}$ signal for the aromatic sp^2 CH residues became less prominent with increasing PEG content. In contrast however, the hydroxyl stretching band shifted to a lower frequency of about 3250 cm^{-1} when the $mPEGOTs_{2000}$ content was between 40-70 wt %. The samples with 80 and 90 wt % $mPEGOTs_{2000}$ also showed this low frequency peak but only as a prominent shoulder on the overall hydroxyl peak. The dotted and dashed lines in Figures 2.3a and 2.3b track the maximum signal of the hydroxyl stretching mode for the mPEGOH and mPEGOTs series. The low frequency hydroxyl stretch mode is associated with hydrogen bonding interactions between ring-opened BA-a and the PEG chain and indicates a hydroxyl hydrogen bond interaction that is much stronger in mPEGOTs blends than that found in the pure PBA-a polymer (atop in Figure 2.3) or in mPEGOH blends. Clearly, a molecular scale integration of the PBA-a and mPEGOTs has occurred in this series of blends.

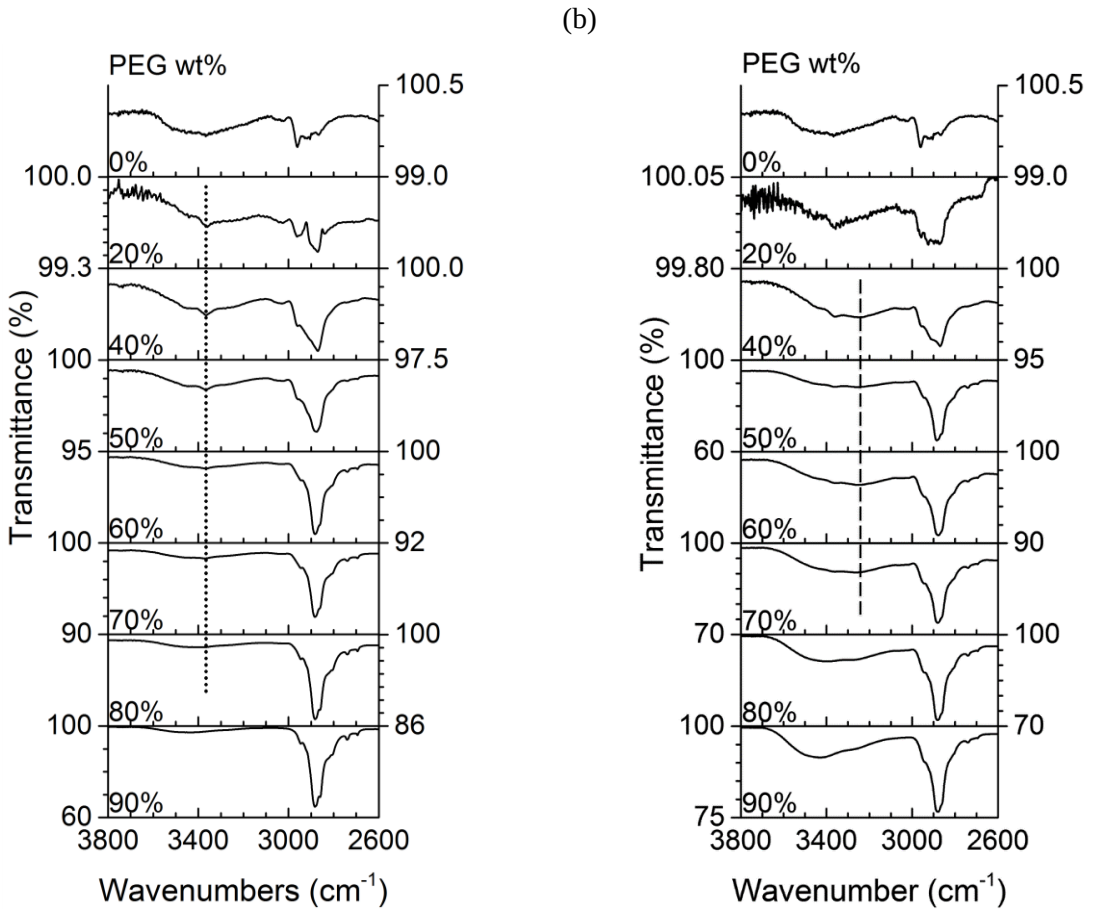

Figure 2.3. FTIR spectra (C-H and O-H stretch region) for cured blends of BA-a with (a) $mPEGOH_{2000}$ and (b) $mPEGOTs_{2000}$. The minima for the OH stretch signal for selected samples are connected by dotted and dashed lines in each figure. The dotted line at 3372 cm^{-1} in (a) tracks the wavenumber corresponding the highest signal for the hydroxyl-region and indicates that the phenolic residues in the mPEGOH series are largely free of H-bonding. The dashed line at 3245 cm^{-1} in (b) tracks the wavenumber corresponding the highest signal for the hydroxyl-region and indicates that the phenolic residues in the mPEGOTs series have significant H-bonding.

^{1}H NMR spectra of extractable polymer segments from cured blends (Figure A3) confirms that the molecular structure of the PBA-a network generated in mPEGOTs blends is enriched in phenolic groups. Previous work has shown that when BA-a is cured with a short cure time or without a catalyst, the resulting PBA-a polymer consists of a more phenoxy–rich structure with more methylene signals in the 4.3–5.0 ppm range in the ^{1}H NMR spectrum. A prolonged cure time or the introduction of a Lewis acid catalyst[20,27,168]

accesses the more phenolic-rich structure typically evidenced by a greater intensity of methylene peaks in the 3.5–4.0 ppm range.[20] The aromatic region of the spectrum also becomes more well-defined with greater intensity to fewer peaks in the 6.5-7.0 ppm range for phenolic-rich PBA-a. Based on the three broad methylene peaks at 4.5, 5.0, 5.4 ppm in Figure A3a, the PBA-a network that results from the thermal ROP of dissolved BA-a in mPEGOH appears to be enriched in the less thermodynamically stable phenoxy molecular structure. Conversely, the lack of significant peaks in the 4.3–5.0 ppm range and the greater intensity associated with a shoulder peak (δ = 3.8 ppm) on the foot of PEG methylene peak (δ = 3.5 ppm) in the ^{1}H NMR for BA-a/mPEGOTs blends (Figure A3b) indicates a significant enrichment in the more thermodynamically stable phenolic structure in these crosslinked PBA-a networks. The appearance of more well-defined aromatic peaks at 6.5, 6.7 and 6.9 ppm in the spectra of these cured blends also supports this structural assignment.

The excess exothermic energy in the cure DSC study and the high level of molecular mixing for the cured BA-a/mPEGOTs series suggests that a reaction occurs between the two components during the thermal cure process. In order to probe at the nature of the chemical reaction between BA-a/mPEGOTs and at the thermal stability of the resulting materials, Thermogravimetric-Fourier Transform Infrared (TGA-FTIR) and Thermogravimetric-Mass spectroscopy (TGA-MS) studies were performed. Lower molecular weight mPEGOH and mPEGOTs (both with M_n = 900 Da) were selected in order to better emphasize signal associated with the end groups of the polymers. FTIR intensity maps for temperature vs. wavenumber of the TGA-FTIR data sets are included in the Supporting Information file (Figures A4-6). The corresponding TGA curves are also shown in the Supporting Information file (Figure A7). Generally, TGA curves for the BA-a/mPEGOH$_{900}$ samples show two main weight loss events with onset temperature values of ~220 °C and ~370 °C. Those with more PEG content show more pronounced weight loss at 370 °C. TGA curves for the BA-a/mPEGOTs$_{900}$ show one major weight loss event at 380 °C. Interestingly, the thermal stability of the cured blends increases as mPEGOH and mPEGOTs are introduced. This thermal stability is reflected in the plots for the temperature for 5 % weight loss ($T_{D5\%}$) versus the PEG content (Figures A7c-d). The

increase in the thermal stability in the mPEGOH series is modest however, with a maximum value in Figure A7c of 225 °C for the 70 wt % mPEGOH sample which is only 12 °C above that of pure PBA-a. Remarkably, the influence of the mPEGOTs on the thermal stability is much more pronounced. Cured blends are generally much more thermally stable than those from the mPEGOH series and, notably more stable than pure PBA-a. As the mPEGOTs content is set from 0 to 20 wt %, the $T_{D5\%}$ increases by ~50 °C (see Figure A7b). This metric for thermal stability also appears to follow a relatively good correlation to the composition of the blend, where mPEGOTs content in excess of 20 wt % adjusts the thermal stability to a lower value but still in excess of that of pure PBA-a. The char yield at 475 °C for pure PBA-a is 41 %. The char yield of BA-a/mPEGOH blends appears to follow a decreasing linear trend for the samples with greater than 20 wt % mPEGOH. Only the sample with 20 wt % mPEGOH blend exhibits a char yield in excess of that of the pure PBA-a. The 475 °C char yield of BA-a/mPEGOTs blends appears to decrease with increasing mPEGOTs but does so with a non-linear dependence on the mPEGOTs content. Most of the tested blends exhibit 475 °C char yield values (28-39 %) close to that of the pure PBA-a. It appears once again that blends from the mPEGOTs favor good thermal stability even in the high temperature range past the main mass loss event. We hypothesize that the increased thermal stability of the BA-a/mPEGOTs blends arises from the increased phenolic structure deduced by the ^{1}H NMR data. The less thermodynamically stable phenoxy linkages that were enriched in the BA-a/mPEGOH blends may lead to a greater content of labile bonds and increased reactivity at lower temperatures and consequently reduced mass during the thermal stress of the TGA analysis.

FTIR intensity tracer plots that relate the intensity of absorbance for vibrational modes associated with volatiles from the samples were created and reported in the supporting information file (Figures A4-6) and Figures 4a, 4b and 4c(*ii*). In the $mPEGOH_{900}$ series, the tracer plots for the ν_{CH3} (2973 cm^{-1}) all showed that a methyl-containing volatile is liberated at approximately 380 °C with its peak intensity at 430 °C (with the exception of the pure PBA-a and mPEGOH constituents, see Figure A4a). Similarly, an ether-containing volatile (detected with a ν_{CO} at 1136 cm^{-1}) is liberated with similar onset and peak temperature values for

blends. This peak shifts to lower temperature for the mPEGOH and is not present in the pure PBA-a (see Figure A5a). Volatiles associated with a $\nu_{\text{aromatic CH}}$ at 3048 cm^{-1} are liberated from mPEGOH blends with an onset and peak temperature of 250 °C and 280 °C, respectively, (see Figure A6a). Pure PBA-a shows a similar volatilization of aromatic compounds bearing sp^2 CH units suggesting an excellent retention of carbon at high temperatures, a high char yield characteristic that is well-documented for P(BA-a)s.[87,154] No significant signal for sulfonate containing groups (that would be identified by a $\nu_{\text{S-OH}}$ stretch at 885 cm^{-1}, see Figure 4a) was found for pure PBA-a, $mPEGOH_{900}$ or their blends. Given the phase separated state that was indicated in the DSC study of the BA-a blends with $mPEGOH_{2000}$ and the fact that PEG is known to degrade at ~360°C,[169,170] we hypothesize that additional reduced thermal stability may arise from a higher surface area PBA-a material that is generated when phase-separated PEG is volatilized from the blends. Significant loss of mPEGOH is confirmed with the ether signal in the TGA-FTIR in Figure A5a which aligns with this hypothesis.

As expected, the TGA-FTIR study for the $mPEGOTs_{900}$ series shows differences in its tracer plots. In general, signals for volatiles with methyl, ether and sulfonate residues were detected. Furthermore, samples that demonstrated high miscibility of BA-a for mPEGOTs (40-60 wt % mPEGOTs) showed signals for these volatiles at higher temperatures than those that were phase separated (see Figure 2.1c). Particularly interesting was the lack of signal for volatiles containing aromatic groups. This result indicates a better retention of sp^2 carbon and explains the increased fractional char yield for mPEGOTs samples (see Figure A7 for a comparison of the TGA plots for blends for 40-60 wt % mPEGOH with 40-60 wt % mPEGOTs). The tracer plots for the S-OH stretch at 885 cm^{-1} vs. temperature for BA-a blends with $mPEGOH_{900}$ and $mPEGOTs_{900}$ are reported in Figures 2.4a and 2.4b, respectively, and also include the analogous data acquired from the TGA-FTIR for *p*-toluene sulfonic acid (*p*-TSA). In the latter, the onset for the major signal is 220 °C and shows a maximum intensity at 250 °C. A weak signal for the $\nu_{\text{S-OH}}$, beginning at ~110 °C, largely coincides with the onset for the first mass loss event found by TGA. The coinciding signals for the major *p*-TSA flux and that of the pure $mPEGOTs_{900}$ strongly suggests that heating the tosylate capped

mPEG leads to a scission of the *p*-TSA group from the polymer allowing for liberated *p*-TSA to act as a catalyst for the thermal ROP of BA-a. The detection of the S-OH signal for miscible blends at higher temperatures suggest that the *p*-TSA also has additional intermolecular interactions in the BA-a blends which would demand additional energy for volatilization. The hypothesis for generating *p*-TSA from heated mPEGOTs was also confirmed in a TGA-MS study of the BA-a/mPEGOTs$_{900}$ blend where the mPEGOTs content was 50 wt %. Shown as plot *iii* in Figure 2.4c is the partial pressure signal associated with the tolyl molecular ion fragment (m/z = 91 Da) of volatilized *p*-TSA[171] as the temperature is ramped. A control experiment confirmed that this signal did not originate from curing BA-a into PBA-a (see Supporting Information Figure A8). Co-plotted with this data are the corresponding TGA, DSC and $\nu_{S\text{-}OH}$ tracer data. Plot *iii* in Figure 2.4c shows that two fluxes of *p*-TSA evolve from the sample, where the initial rise in signal for the tolyl fragment begins at ~100 °C and plateaus by a temperature of 180 °C, a temperature range which largely coincides with the onset for the first mass loss event found by TGA. A weak qualitative signal for the $\nu_{S\text{-}OH}$ in the tracer plot is also found near this temperature. The secondary MS signal for the tolyl fragment initiates at ~200 °C which closely aligns with the maximum in the cure exotherm as found in the DSC (see plot *iv* in Figure 2.4c). These two fluxes of evolved *p*-TSA suggest that two mechanisms are involved in the generation of the molecule with the lower temperature event associated with generation of initiators and the higher temperature event being strongly associated with the ROP of BA-a.

(a) (b)

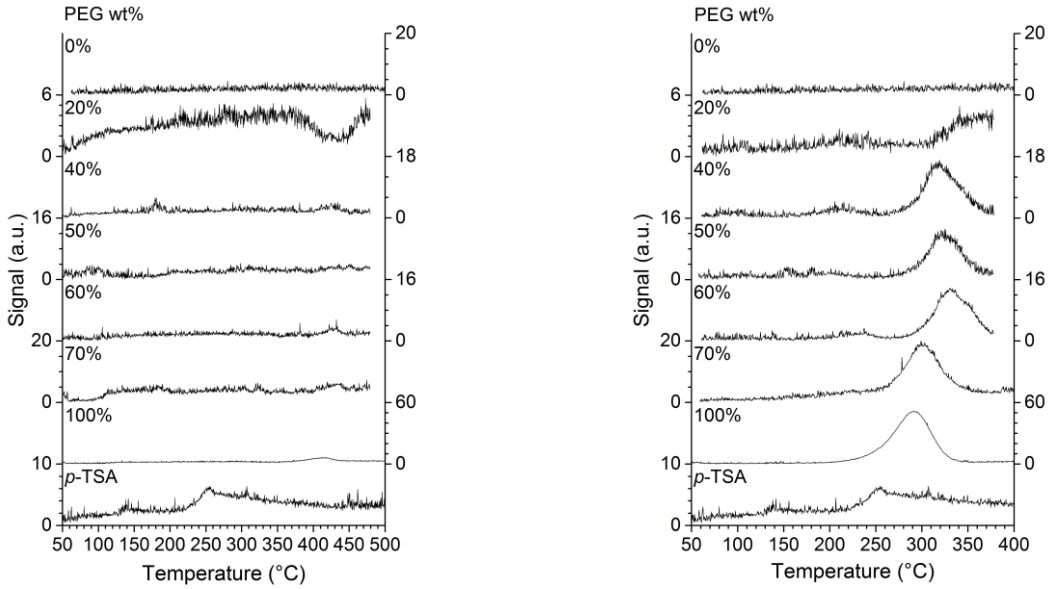

(c)

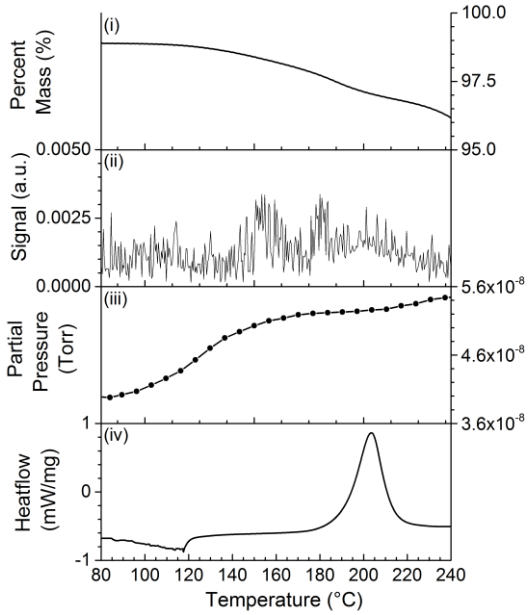

Figure 2.4. FTIR tracer plots for S-OH stretch at 885 cm^{-1} of the effluent from PBA-a blends with (a) $mPEGOH_{900}$ and (b) $mPEGOTs_{900}$ from thermogravimetric analysis. The generation of the *p*-TSA fragment with increasing temperature (c) as determined with (i) TGA thermogram (ii) Tracer plot of the signal at 885 cm^{-1} (iii) TGA-MS spectrum scan for m/z 91 and (iv) a DSC thermogram of the 1:1 BA-a:$mPEGOTs_{900}$ blend.

Scanning electron microscopy (SEM) was used to investigate the microstructure of the cured BA-a blends (see Figure 2.5). Following a cure condition (identical to that used in the DSC study), the $mPEGOH_{2000}$ and $mPEGOTs_{2000}$ samples were extracted with chloroform and then cooled for cleavage prior to the SEM study. All samples from the $mPEGOH_{2000}$ series showed a highly porous morphology. The sample that was weighted the most with $mPEGOH_{2000}$ (90 wt %) exhibits the most heterogeneous structure with large void spaces that are greater than 10 µm in size. The void space in these samples has arisen from regions that were previously occupied by the $mPEGOH_{2000}$, material that was extracted by the chloroform solvent. As the $mPEGOH_{2000}$ content is decreased (Figures 2.5a-g) the void space is observed to decrease and the uniformity in the PBA-a phase increases. The ability to tune the void content in the cured PBA-a from blends with $mPEGOH_{2000}$ may prove useful for tuning transparency, macroscopic density and strength characteristics in cured macroscopic parts made from these blends. Indeed, all cured mPEGOTs/PBA-a materials are a transparent yellow-orange materials while those of cured mPEGOH/PBA-a are orange and opaque. The PBA-a-richest samples tend to adopt a fused particle like morphology with complex and wide interconnections that makes measurements of the void and particle size difficult. There is little evidence for any structural implications that would be from the miscible condition that was observed for uncured samples with <40 wt % $mPEGOH_{2000}$ (Figure 2.1a). The SEM data therefore agree with the conclusion from the FTIR study that the polymerization of BA-a monomer leads to a PBA-a that is phase-separated from the $mPEGOH_{2000}$ polymer. Lü and coworkers found a very similar result for PBA-a that was cured in HO-PEG-OH (where the molecular weight was 20000 Da).[83] A similar morphology for PBA-a and PEG blends has been described in some detail by Huang et al.[84] The SEM study of the cured $mPEGOTs_{2000}$ blends led to a different conclusion regarding the morphology and structure of the PBA-a. For cured samples with a completely suppressed crystallization of $mPEGOTs_{2000}$ (Figure 2.1b) and a high content of hydrogen-bonded hydroxyl groups (<50 wt % $mPEGOTs_{2000}$), a highly continuous and smooth morphology was indicated in the SEM images (see Figures 2.5l-n). The microstructure of cured samples where there was crystallization of $mPEGOTs_{2000}$ resulted in a porous microstructure, reminiscent of that in the $mPEGOH_{2000}$ series. This structure is highly uniform, where sphere-like nanoparticles of PBA-a become larger and more

well-defined as the $mPEGOTs_{2000}$ content increases (varying from ~50 to ~500 nm in diameter for the 60 to 90 wt % mPEGOTs samples, respectively). A rather abrupt transition in particle size was found between samples that were 80 and 70 wt % $mPEGOTs_{2000}$ which coincides with the threshold ratio needed to suppress some of the crystallization of the $mPEGOTs_{2000}$ (Figure 2.1b). This in combination with the data from the SEM, DSC, and FTIR studies highly support a more hybridized and bonded chemical structure for cured BA-a/mPEGOTs samples. We therefore assign a graft structure to P(BA-a)-*g*-PEG samples.

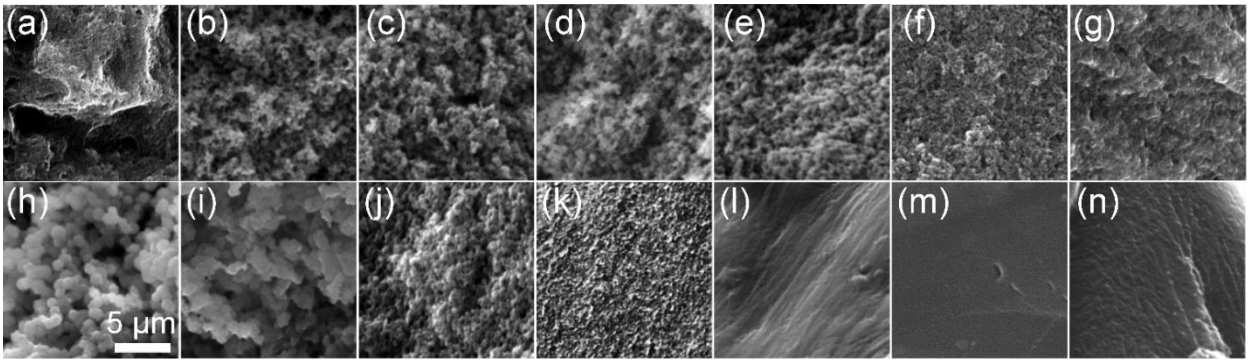

Figure 2.5. SEM images for chloroform extracted PBA-a blends with decreasing $mPEGOH_{2000}$ (a-g) and $mPEGOTs_{2000}$ (h-n) content. In (a-g) the original $mPEGOH_{2000}$ content was 90, 80, 70, 60, 50, 40 and 20 wt %, respectively. In (h-n) the original $mPEGOTs_{2000}$ content was 90, 80, 70, 60, 50, 40 and 20 wt %, respectively. The scale bar in (h) applies to all SEM images.

2.3.3 Mechanistic aspects for the cure of BA-a/mPEGOTs blends. There are several proposed mechanisms for the thermal cure benzoxazine rings.[21,172,173] Ishida et al. have reported a mechanism for the cationic ring-opening polymerization of benzoxazines via alkylation or protonation of the oxygen or amine centers of the oxazine ring by low steric demand sulfonic acid or alkylsulfonates.[15,18,32,119] By extension, when polymerization of the BA-a/mPEGOTs blends are considered, a pegylated cationic oxonium species would result from the nucleophilic attack by the oxygen site of a BA-a monomer at the tosylate end group of the mPEGOTs (see Pathway A in Scheme 2.1). This oxonium would establish an equilibrium with the ring-opened iminium species, both of which may initiate ROP of other BA-a monomers. In the alternative Pathway B, the nitrogen center of the BA-a monomer acts as the initial nucleophile and a pegylated ammonium species is afforded by reaction with the mPEGOTs. This species may undergo a secondary

nucleophilic attack by another BA-a molecule to produce the same pegylated cationic oxonium species discussed in Pathway A. Corey and Sudo et al. have also found that thermal dissociation of bulky alkyl *p*-toluenesulfonates can produce free *p*-toluenesulfonate ($^{-}$OTs) and cationic species such as the cyclohexyl secondary carbocation for initiation of BA-a.[25,174] The thermal dissociation of the mPEGOTs is shown as Pathway C in Scheme 2.1 and would produce a primary carbocation by this mechanism. We propose that the high reactivity of primary carbocation makes pathway C unlikely, and favors the generation of the cationic initiators by either Pathway A or B. Both of these routes lead to free $^{-}$OTs as a byproduct in the early stages of the thermal cure of the BA-a/mPEGOTs blends. The TGA-MS experiment described above detected this early flux of $^{-}$OTs (i.e. a tolyl molecular fragment) which further supports a thermal initiation of BA-a by its nucleophilic attack on the mPEGOTs.

Scheme 2.1. Proposed pathways (A-C) for the generation of cationic species to initiate the ROP of BA-a. Pathways A and B show the nucleophilic attack by the oxygen or nitrogen atom from the oxazine ring of a BA-a at the tosylate end group of mPEGOTs, respectively. Pathway C shows the thermal dissociation of mPEGOTs. All three pathways show the formation of a free-tosylate that is associated with the generation of possible cationic ROP initiators.

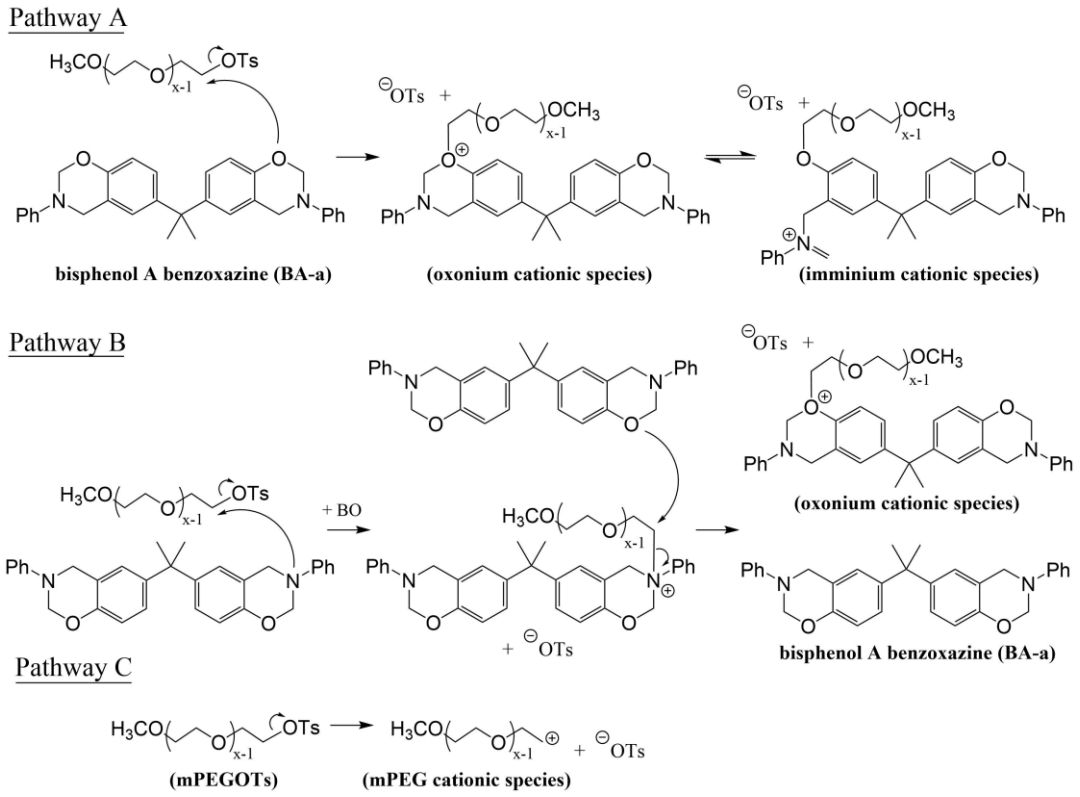

Previous groups have successfully used *p*-toluenesulfonic acid (HOTs) to accelerate the cure of BA-a. In these studies it was concluded that the strong nucleophilic and good leaving group characteristics of HOTs led to monomer conversion and reduced curing temperatures.[20,21,24,25] Any HOTs generated in the blends from the mPEGOTs series could therefore act as an accelerant by analogous mechanisms. We also draw attention to alternative pathways that lead to cationic benzoxazinyl molecules to initiate the cationic polymerization of other neutral BA-a monomers. Shown in Scheme 2.2 are these initiation and propagation steps. For clarity, the scheme first considers the conversion of one benzoxazinyl functional group from BA-a followed by a separated step for the cross-linking reaction for the other benzoxazinyl functional group.

This proposed mechanism also applies the pegylated cationic oxonium species that was in common in both Pathway A and B in Scheme 2.1, and does not focus on other cationic species such as the iminium species or show the formation of N,O-acetal-type linkages that are also known for P(BA-a)s.[17,20,21] After initiation and the generation of an initial flux of $^{-}$OTs, a free BA-a monomer attacks the cationic center of the oxonium initiator and the cationic charge is transferred to this attacking BA-a. Proton transfer restores the aromaticity in the attacking BA-a unit and leads to the Mannich bridged structure that is shown atop at the middle of Scheme 2.2. The process repeats itself with new BA-a monomer that adds to the cationic molecule so as to extend the polymer in a chain growth process. The ROP reaction of each benzoxazinyl functional group therefore leads to the more thermodynamically favored phenolic residue that should be further considered for reaction with mPEGOTs. These newly created phenol residues nucleophilic attack the tosylate end group of other mPEGOTs molecules and lead to random mPEG grafts along the PBA-a backbone with concomitant formation of HOTs, a byproduct associated with this propagation step. This secondary flux of HOTs was detected by both TGA-MS and TGA-FTIR. In the control series, the PBA-a was found to phase-separate from mPEGOH during the thermal ROP,[83] and cured at higher temperatures. The pegylated oxonium initiator originating in the mPEGOTs blends would be expected to have high solubility in the BA-a/mPEGOTs miscible phase, which would allow the onset temperature for cure to be reduced relative to that of phase-separated analogues. The Gordon-Taylor-predicted T_g values for the cured BA-a/mPEGOTs blends and the FTIR evidence for strongly hydrogen bonded OH groups suggests that the grafting reaction of mPEG to the PBA-a proceeds to a large extent leading to a hybridized graft co-polymer with a high compatibility with free mPEGOTs and/or BA-a.

Scheme 2.2. Proposed mechanism for the generation of HOTs catalyst, subsequent initiation and propagation of BA-a monomers, and the grafting of mPEG to cured blends of BA-a with mPEGOTs.

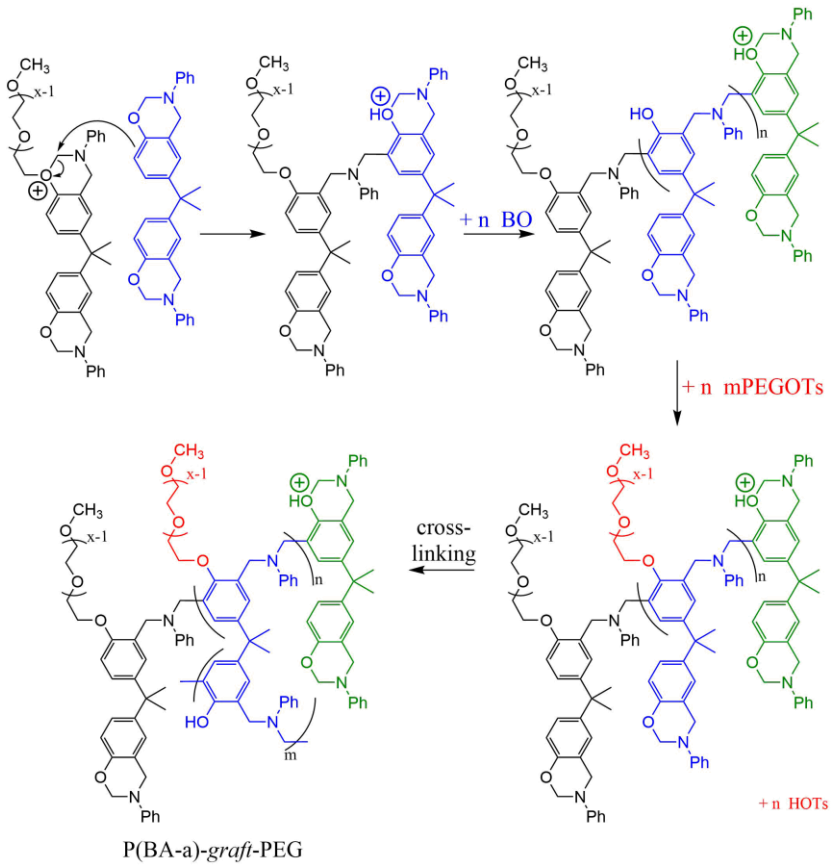

2.4 Conclusions

The roles of end group functionalized methoxypoly(ethylene glycol) (mPEG) for solubilizing, accelerating, and grafting to a polybenzoxazine network derived from bisphenol A-based benzoxazine (BA-a) was studied. The nature of the end group had little effect on the miscibility range for BA-a in a mPEG-based matrix, where a wide loading range of ~100-40 wt % BA-a was possible. When the end group of the mPEG was a hydroxyl (OH) residue, the temperature required for ring-opening polymerization (ROP) of dissolved BA-a increased subtly by ~5-10 °C. Conversely, when the end group of the mPEG was a *p*-toluenesulfonate (OTs) residue, a significant decrease in temperature of the ROP was found with the onset for cure occurring at ~20-60°C less than that of the pure BA-a monomer. This onset for the cure temperature was linearly correlated to the weight loading of mPEGOTs in the blends and supports the assignment of the role of the

mPEGOTs as an accelerant for BA-a cure. In-situ monitoring of the headspace above curing blends using FTIR and MS identified free tosylate and suggests that the mPEGOTs is activated by nucleophilic attack by BA-a at ~110 °C in order to create HOTs catalysts and cationic initiators for the ROP of BA-a. The molecular structure of soluble extracts and the glass transition of cured mPEGOTs blends indicate that a significant amount of grafting has occurred in these materials, where, a phenolic rich structure consisting of hydrogen-bonded phenols is present. The cured mPEGOH blends are more phenoxy-rich and have insignificant hydrogen bonding in any phenols. All cured mPEGOTs/PBA-a materials are a transparent yellow-orange materials while those of cured mPEGOH/PBA-a are orange and opaque. A homogeneous P(BA-a)-*graft*-PEG molecular structure is assigned for the former whereas a phase-separated PBA-a/PEG structure is assigned for the latter. Scanning electron microscopy supports this assignment where a highly voided PBA-a results from solvent extraction of PEG from the phase-separated cured mPEGOH/PBA-a materials.

The resulting P(BA-a)-*graft*-PEG exhibit improved and tunable thermal and physical properties. The glass transition of the P(BA-a)-*graft*-PEG can be adjusted predictably over a wide temperature range (40-160 °C experimentally demonstrated) where values follow a Gordon-Taylor relation based on the composition of the initial mPEGOTs/BA-a blend. Most P(BA-a)-*graft*-PEG exhibit higher thermal stability with a temperature of 276 °C (based on a 5 wt % mass loss $T_{D5\%}$ metric) where most samples were more stable than pure PBA-a ($T_{D5\%}$ = 214°C) or materials created from phase-separated mPEGOH/PBA-a ($T_{D5\%}$ = 202-225 °C). We expect that the highly tunable properties demonstrated thus far will also be found in other mechanical and chemical characteristics and some of this remains as our future work in this area.

Chapter 3: Alternative blends of bisphenol A benzoxazine with polymers and particles

3.1 Introduction

There is much left to be explored in the topic of blends of benzoxazines with tosylated complements. Further investigation into the mechanical properties of the existing cured BA-a blends with PEG for both the OH and OTs series is of interest. There is also a need to further explore the role of alternative tosylated polymers for the cure acceleration and bonding to BA-a. Several blends of thermoplastics with benzoxazines has been researched as mentioned in chapter 1 and 2 (polycarbonate, polysulfone, polymethyl methacrylate, etc.).[85-90,160,175] However, outside of our own PEG system the Koschek group is the only other group studying these tosylated polymers.[7] Koschek et al. have so far defined a bis-tosylated polycaprolactone (PCL) system and found unique characteristics beyond its reduced cure and toughening. The crosslinking of PBA-a with flexible PCL increased the shape memory capabilities of these thermoset materials. This example further widens the scope of this topic and justifies further work in this area.

This chapter not only further defines the existing PEG systems but explores the possibility of BA-a blends with other additives with a range of chemical and mechanical properties. The most robust additive of these blends are that of silica particles which is already a well-defined system. The survey of polymers chosen for these blends are polysulfone (PSU) and poly(lactic acid) (PLA). Both of these polymers impart their own unique properties onto these blends and address issues presented in the PEG blends. While the decreased mechanical properties and reduced hardness in mPEGOTs blends may be attractive for some applications, the complement of increased mechanical properties is also desirable.

Talc, silica, and other silicates have long been used to increase the mechanical properties of thermosets.[176-181] Such additives in benzoxazine are typically added at 1-10 wt % with a typical increased modulus of 5-8 GPa.[182] Weight loading outside of this range remains fairly uncharacterized. Monomer blends with functionalized silica have yet to be fully developed. As with polymers, tosylated silica can be used to both decrease the curing temperature of benzoxazine and produce a stronger and more durable

material. The organic surface alone will also affect the interaction between the particles and the monomer. For this reason, phenyl-functionalized silica was chosen to determine the effect of improved wetting and compatibility of a silica surface rich in aromatic rings while lacking the sulfonate group.

Polysulfone has a higher storage modulus than PEG (about 1.9 GPa at room temperature), a high T_g of 186 °C, and thermal stability with a $T_{d5\%}$ of 460 °C.[183-187] PSU also has very low flammability, low smoke density, and a high limiting oxygen index which make blends of BA-a and PSU very desirable for composite applications in the naval and aerospace fields.[188,189] As plastics became an increasingly integral material in today's technology so did the need to classify the smoke density of these products. Smoke density is quantified by the method standardized by the American Society for Testing and Materials where a sample of known area is ignited and burned under controlled conditions and the transmission of a beam of light passed through its smoke is monitored.[190] Such standards are incredibly useful to the naval and aerospace fields. Polysulfone has a vast amount of applications including membranes for hemodialysis and food processing, proton-exchange membranes in fuel cells, and various medical applications.[191-195]

Currently PLA and its analogue, poly(lactic-*co*-glycolic acid) (PLGA), have been typically thought of as biodegradable plastic alternatives.[196-200] PLGA has been researched as an alternative to PLA which possesses a dramatically shorter biodegrable lifespan.[201-204] The Saiani group has found that the majority of the degradation of bulk PLGA (50:50 molar ratio of lactic to glycolic acid) happens within one month in phosphate buffer at 37 °C. As PLGA degrades and glycolic and lactic acid is produced into the solution, the degradation can be tracked by the pH.[205] These polymers can be produced from renewable resources such as corn and are typically used in food packaging, drug delivery, and biomedical devices.[206-208] Tosylated PLA and PLGA do not only offer the labile accelerant but also the acid generated during the degradation of these polymers during the cure.

3.2 Experimental

3.2.1 Materials. The bisphenol A benzoxazine (BA-a) monomer was used as received from Hunstman. The methoxypoly(ethylene glycol) ($mPEGOH_{2000}$; M_n = 2000), methoxypoly(ethylene glycol) tosylate ($mPEGOTs_{2000}$; M_n = 2000), methoxypoly(ethylene glycol) tosylate ($mPEGOTs_{900}$; M_n = 900), *α,ω*-dihydroxy polysulfone (PSUOH; M_n = 22000) and triethylamine (≥99% purity) were acquired from Sigma Aldrich. Methylene chloride (99.9 % purity), methanol (99.9%), and potassium phosphate monobasic (>99% purity) was purchased from Fisher Scientific. Chloroform (99.8% purity), sodium phosphate dibasic (99.8% purity), and sodium azide were received from J.T. Baker. Methoxypoly(ethylene glycol) ($mPEGOH_{500}$; M_w 500), D,L-lactide (99% purity), and *p*-toluenesulfonyl chloride (99% purity) was received from Acros Organics. The 1,4-butanediol (99% purity) and tin (II) 2-ethylhexanoate (96% purity) were purchased from Alfa Aesar. Hydroxy terminated poly(D,L-lactic acid) (PDLLAOH; M_w = 25000) was purchased from Polysciences. The 1,4-dioxane-2,5-dione (97 % purity) was purchased from Maybridge. Deuterium oxide (>99% purity), chloroform-d3 (>99% purity), and acetonitrile-d3 (>99% purity) were purchased from Cambridge Isotope Laboratories. Silica flash (SiOH), and sulfonic acid and phenyl functionalized silicas (SiOTs and SiPh) were received from Silicycle and conditioned in a vacuum oven at 120 °C for 12 h to remove water from the particles. Sodium chloride was purchased from Macron Fine Chemicals. 4-Dimethylaminopyrdine (DMAP; 98% purity) was purchased from Oakwood Chemicals.

3.2.2 Methods. A PANalytical X'Pert Pro diffractometer using monochromatic Cu Kα radiation (λ = 0.15418 nm) was used for X-Ray Diffraction (XRD) studies. XRD data fitting was done using an X'Pert HighScore Plus software package. A Vega TS 5136MM scanning electron microscope (SEM) was used to capture micrographs with an accelerating voltage of 15 kV. Cured polymer blend samples were prepared for SEM by fracturing the sample and soaking it in chloroform for 1 hour then allowing it to dry in ambient conditions. All SEM samples were coated with a thin layer of gold and platinum to dissipate charge (nominal Au thickness ~1 nm). A Nicolet iS10 FTIR spectrometer with an attenuated total

reflectance (ATR) accessory was used for FTIR studies (64 scans at 4 cm^{-1} resolution per spectra). A Bruker AVANCE-III, HD 500 MHz NMR spectrometer was used to collect all ^{1}H NMR spectra.

3.2.3 Preparation of blends. The general procedure for the preparation of either PLA, PLGA, or PSU with N-phenyl bisphenol A benzoxazine (BA-a) is as follows: to a 25 mL flask the desired mass of polymer and BA-a were added to a combined mass of 3 g and dissolved in dichloromethane (10 mL). Each sample was concentrated in vacuo and then dried in a vacuum oven for 12 hours. The silica blends were prepared in a similar fashion to the polymer blends in 5 mL of dichloromethane and then concentrated in vacuo while rotated at >200 rpm to ensure dispersion of the particles in the monomer followed by further drying in a vacuum oven for 12 hours.

3.2.4 Dynamic mechanical analysis sample preparation. Dried PEG blends were deposited into silicon molds with dimensions of 60 x 6 x 1 mm and then heated at 125 °C for 4 h in a vacuum oven to remove any residual solvents. The samples were then ramped to 225 °C and allowed to cure for 2.3 h while still under vacuum. The silica blends were dissolved in minimal amounts of dichloromethane and stirred to maintain good dispersion of the particles before being solvent casted into the same molds as the PEG samples. The silica blends were then heated at 150 °C for 20 min to remove the majority of the solvent, and then they were allowed to heat at 150 °C for an additional 3.6 h under vacuum to remove residual solvent. The silica blends were then cured at 225 °C for 2.3 h under vacuum. (See Figure B1 in Appendix B).

3.2.5 Preparation of PSU/PBA-a films. To a vial the desired amounts of BA-a and polysulfone are added and dissolved in chloroform to maintain a concentration of 100 mg/mL of polysulfone. A 38 x 38 mm glass substrate is spin coated with 0.4-0.8 mL of the blend solution at an acceleration of 2650 rpm/s to 2000 rpm for 60 s. The slides are then cured in a vacuum oven at 225 °C for at least 1.5 h. The film is then lifted from the glass substrate in a water bath.

3.2.6 Thermal analysis. Thermogravimetric analysis (TGA) experiments were performed with a TA Instruments Q500. Each scan began with a 5 min isotherm at 30 °C followed by a 10 °C/min ramp to 600 °C. A TA Instruments Q100 differential scanning calorimetry (DSC) instrument was used for DSC-based cure studies on all samples. In hermetically sealed, aluminum DSC pans an average of 3 mg per sample of polymer or silica blends were scanned. All DSC scans started with a 5 min isotherm at 30 °C then ramped to 260 °C, then to 30 °C and back to 260 °C at 5 °C/min with a modulated temperature of ±0.53 °C every 40 s. Exothermic cure was estimated by integration of the exothermic peak using a tangential sigmoidal baseline unless indicated otherwise.

3.2.7 Mechanical analysis. Dynamic Mechanical Analysis (DMA) was performed with a TA Instruments Q800 equipped with a film tension clamp. PEG blends were equilibrated and held at an isotherm at -50 °C then scanned at a frequency of 1 Hz and a ramp of 5 °C/min to 275 °C to survey the blends entire range of mechanical characteristics. Silica blends were scanned from room temperature to 280 °C at a frequency of 1 Hz and a ramp of 2 °C/min. A minimum of three stress-strain curves of each PSU/PBA-a film was obtained with an ADMET load cell with a cross-head speed of 0.55 mm/min.

3.2.8 Degradation of PDLLA and its blends with benzoxazine. Pure hydroxy terminated poly(lactic acid) (PDLLAOH), tosylate terminated poly(lactic acid) (PDLLAOTS), and both of their blends with BA-a were studied in this experiment. Blended samples were cured similar to the DMA sample preparation method from the 50:50 blends. The procedure for the degradation of PDLLA was adapted from C. Shih.[209] The general procedure is as follows: PDLLA (10 mg) (20 mg of the 50:50 blend), was dissolved in a 9:1 acetonitrile-d3/D_2O solvent (0.5 mL). To the solution DMAP (23 mg, 0.19 mmol) was added. The solution was heated at 65 °C for several days and ^{1}H NMR spectra were acquired periodically as indicated.

3.2.9 Degradation of PLGA. The degradation of PLGA was adapted from Saiani et al.[205] A phosphate buffer solution (PBS) was prepared by dissolving NaCl (4.00 g), KH_2PO_4 (0.10 g), Na_2HPO_4 (0.61 g), and

NaN_3 (0.10 g) in 500 mL of nanopure water, the pH was adjusted to 7.4 using HCl (0.1 M). To the PBS (20 mL) PLGA (0.300 g) was added and heated at 37 °C. The pH was measured with a pH sensor from Vernier that was calibrated against a phthalate buffer solution (4.01 pH) and a phosphate buffer solution (7.00 pH).

3.2.10 50:50 PLGA polymerization

Poly(lactic-co-glycolic acid) To a 50 mL round bottom flask with a gas inlet, D,L-lactide (1.00 g, 6.95 mmol) and 1,4-dioxane-2,5-dione (0.537 g, 4.62 mmol) was added for an initial 60:40 lactide to glycolide monomer ratio. The flask was stirred while heated at 130 °C under nitrogen until all solids melted. A solution of tin(II) 2-ethylhexanoate [$Sn(Oct)_2$; 0.033 g, 81 μmol] in 1,4-butanediol (1.01 g, 11.2 mmol) was prepared and used immediately. To the flask 0.055 g of the $Sn(Oct)_2$/diol solution was added via needle injection. The reaction stirred under inert gas for 24 h before quenching in an ice bath. The polymer was dissolved in methylene chloride (50 mL) and precipitated in methanol before being dried in a vacuum oven for 24 h. The polymer was collected as a white solid. ^{1}H NMR (500 MHz, $CDCl_3$, ppm): δ 5.20 (m, O-C*H*-C), 4.78 (m, O-CH_2-C), 1.58 (m, CH_3). M_n= 2,700 g/mol; PDI = 1.46 by GPC.

3.2.11 Tosylation of polymers

α,ω-Bistosylate polysulfone (PSUOTS) The following procedure represents the tosylation of both polysulfone and PDLLA. To a 100 mL round bottom flask with a gas inlet Mn 22000 polysulfone (5.00 g, 0.227 mmol) was added and stirred in chloroform (23 mL) until completely dissolved. In chloroform (4.5 mL) *p*-toluenesulfonyl chloride (0.869 g, 4.56 mmol, 20 equiv) was dissolved. To the stirred polymer solution triethylamine (1.82 mL, 13.0 mmol) was added under inert gas. To the reaction flask the end group solution was added drop wise. The reaction was stirred for 16 h under inert gas at room temperature. The reaction mixture was precipitated in methanol and dried in a vacuum over for 12 h. To remove the *p*-toluenesulfonic acid contaminant the polymer was dissolved in chloroform (25 mL) and passed through a silica column with subsequent chloroform. The eluent was concentrated in vacuo

yielding a white transparent solid (3.23 g). ^{1}H NMR (500 MHz, $CDCl_3$, ppm): δ 7.84 (d, main chain Ar*H*), 7.80 (d, 2H, end group Ar*H*), 7.35 (d, 2H, end group Ar*H*), 7.23 (d, main chain Ar*H*), 7.00 (d, main chain Ar*H*), 6.93 (d, main chain Ar*H*), 2.45 (s, end group CH_3), 1.69 (s, CH_3). M_n= 26,000 g/mol by ^{1}H NMR.

Tosylate ether poly(D,L-lactic acid) (PDLLAOTs) Polymer was collected as clear, colorless solid. ^{1}H NMR (500 MHz, $CDCl_3$, ppm): δ 7.80 (d, end group Ar*H*), 7.36 (d, end group Ar*H*), 5.19 (m, main chain O-C*H*-C), 2.45 (s, end group CH_3), 1.56 (m, repeat unit CH_3). M_n= 7700 g/mol by ^{1}H NMR.

3.3 Results and Discussion

3.3.1 Characterization of PLGA and tosylated materials by ^{1}H NMR. The ^{1}H NMR spectrum of the 50:50 PLGA (Figure B2) matches that found in literature.[210] The integration of the peak at 5.20 ppm, corresponding to the methine of the lactic acid repeat unit, and the peak at 4.80 ppm, corresponding to the methylene of the glycolic acid repeat unit, have a ratio of 1:2, confirming the synthesis of 50:50 PLGA. The 1,4-butanediol initiator is not observable in the ^{1}H NMR spectrum.

As seen in Figures B3 and B4, both the polysulfone and the poly(D,L lactic acid) have successfully been tosylated from the presence of their doublets at 7.80 and 7.35 ppm corresponding to the aromatic protons of the end group. Any residual *p*-toluenesulfonic acid (HOTs) has been successfully removed as determined from the lack of a doublet near 7.30 ppm. The absence of doublets at 7.90 and 7.40 ppm signifies that the excess starting material of *p*-toluenesulfonyl chloride (TsCl) has also been successfully quenched and removed.

Scheme 3.1. α,ω-Bistosylate polymer grafting to PBA-a

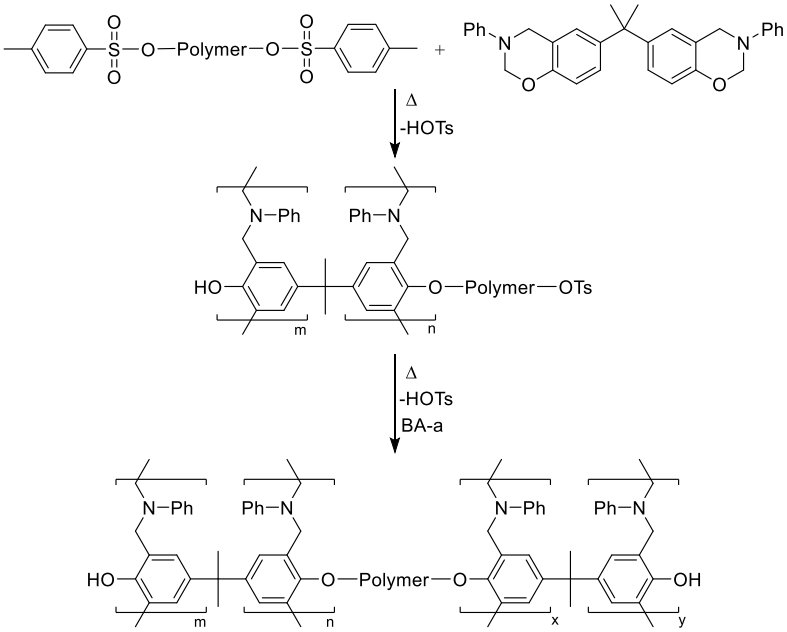

The grafting of poly(ethylene glycol) (PEG) onto PBA-a was determined in the previous chapter by SEM, DSC enthalpy, the trending glass transition temperature, and FTIR. It is then plausible that alternative tosylated polymers or materials may also yield unique grafted materials via a similar mechanism as the PEG blends after curing their blends. In the case of *α,ω*-bistosylate polymers such as the synthesized PSUOTs (Figure B3), the possibility of crosslinking exists as shown previously with bis-tosylated PCL.[7] These newly crosslinked materials may also show some interesting shape-memory behavior. In chapter 2 it was proposed that pathway A and B of the grafting of PEG onto the PBA-a network were more energetically favorable. This is likely the case for PDLLAOTs (Figure B4) as well considering the sp^3 carbon *α* to the tosylate group. However, in the case of the PSUOTs, the *α* carbon is within a rigid phenyl group and is unlikely to undergo an S_N2 displacement of the tosylate by the bulky polybenzoxazine. In the case of PSUOTs, pathway C which results in the dissociation or elimination of the tosylate and a secondary and resonance stabilized carbocation may be the more energetically favorable route.[211]

Scheme 3.2. PBA-a growing around tosylated particle

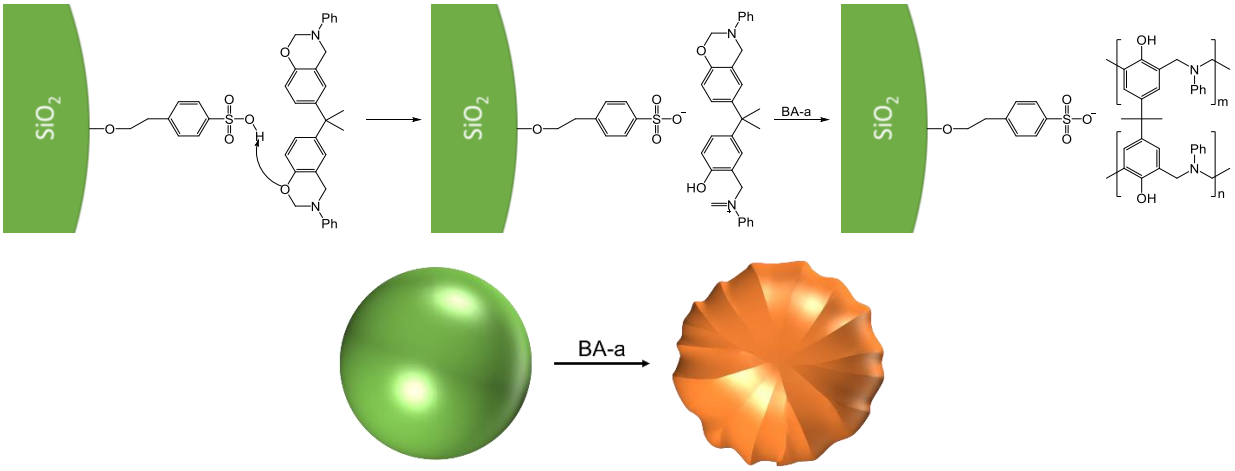

The purchased tosylated silica particles are fundamentally different from the tosylated polymers in that the attachment to the additive is from the benzene group and not across the sulfate (Scheme 3.2). Such an orientation will not result in the release of the HOTs accelerant and therefore will also not result in the grafting of the benzoxazine onto the particle surface. Instead the tosylated particle surface may react more similarly to neat HOTs, the effects of which have been well established by other groups.[20,21,24,25] Instead of grafting, it is proposed that the monomer nearest to the particles will densely polymerize first due to the high concentration of accelerant which will form a hard PBA-a shell over the particle that is not directly grafted, sitting in a matrix of less dense PBA-a. It is expected that the functionalized silica particles will have a higher affinity and homogeneity with the PBA-a than that of non-functionalized silica.

3.3.2 Crystallinity of PEG blends by XRD.

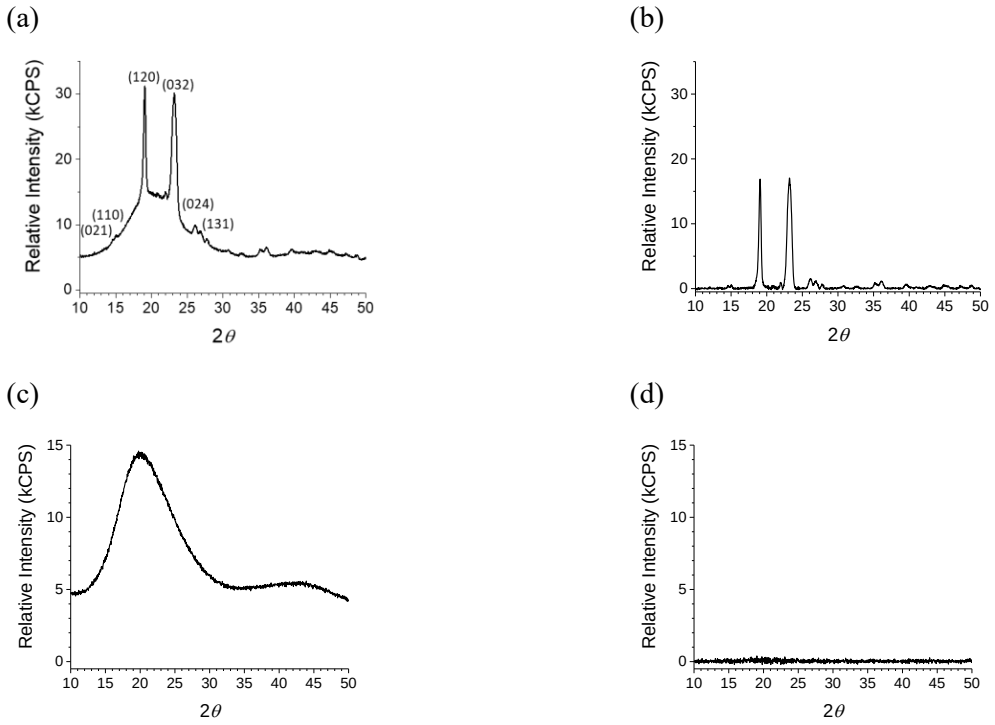

Figure 3.1. X-ray diffraction patterns of blends of BA-a at 40 wt % PEG with (a,b) $mPEGOH_{2000}$ and (c,d) $mPEGOTs_{2000}$. The plots in the right column are the baseline corrected versions of those in the left column.

An XRD study on the $mPEGOH_{2000}$ and $mPEGOTs_{2000}$ series with 40-80 wt % PEG revealed intensity maxima at 2θ angles of 14.5°, 15.1°, 19.1°, 23.2°, 26.1°, 26.8° and 32.5°, which, are due to diffraction from the (021), (110), (120), (032), (024), (131) and (114) planes in crystallized PEG, respectively (Figure 3.1, see Figures B5 and B6 for the complete series).[212] The large halos are the result of amorphous PBA-a and grafted PEG in the case of the mPEGOTs series. The degree of crystallinity was determined from the ratio of the area of the diffractogram that excluded amorphous halos with that of the total area for the diffractogram that included areas for diffraction from crystallites and halos from amorphous material.[213] The degree of crystallinity of the cured mPEGOH blends was significantly higher than that of their mPEGOTs blend counterparts (Figure 3.2).

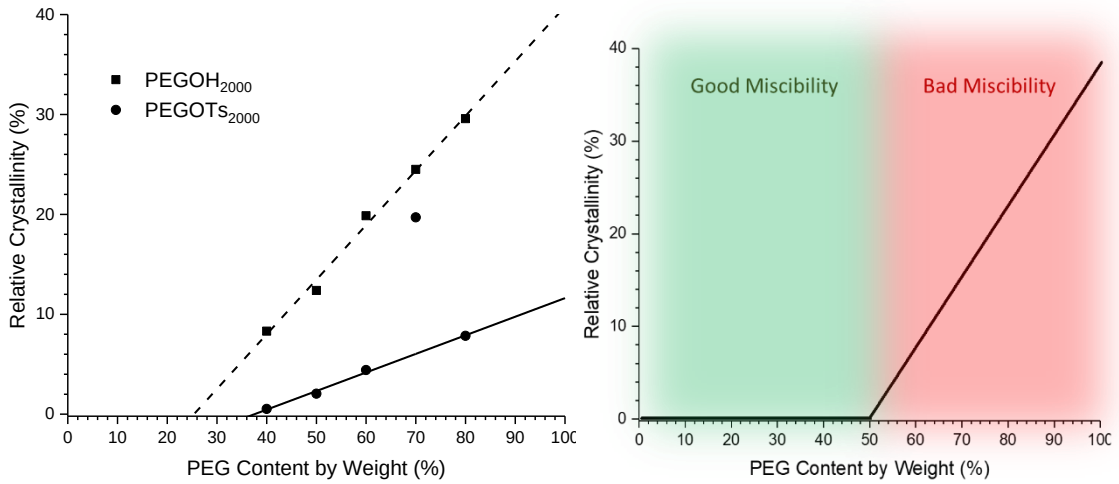

Figure 3.2. (a) The percent crystallinity of BA-a blends with $mPEGOH_{2000}$ from the spectra in Figures B5 and B6. The dotted and solid lines are the linear fits of the $mPEGOH_{2000}$ and $mPEGOTs_{2000}$ blends respectively. The fit for the $mPEGOTs_{2000}$ blends ignores the data point at 70 wt %. (b) A sketch of predicted crystallinity behavior dependent on PEG/PBA-a miscibility.

Both the mPEGOTs and mPEGOH blends show a linear trend of increasing sample crystallinity with increasing PEG content. The trend starts after reaching a similar threshold determined by the percent crystallinity from the enthalpy values of their DSC data. By XRD this threshold starts at 40 wt % PEG in the $mPEGOTs_{2000}$ blends and, theoretically from the linear fit, near 23 wt % PEG in the $mPEGOH_{2000}$ blends. The crystallinity values determined by XRD for both series are significantly smaller than that found by DSC analysis. This difference may be attributed to the phases of PEG in the cured samples that were analyzed by XRD being constricted by the surrounding PBA-a and impeding it from assuming its preferred crystalline packing. While in the case of the crystallinity before the cure, determined by DSC, the polymers have more mobility in the surrounding benzoxazine monomer. Overall, the XRD analysis is in agreement with the DSC crystallinity study, that these PEG blends have good miscibility with BA-a up to 40-60 wt % PEG content.

3.3.3 Mechanical studies of PEG blends.

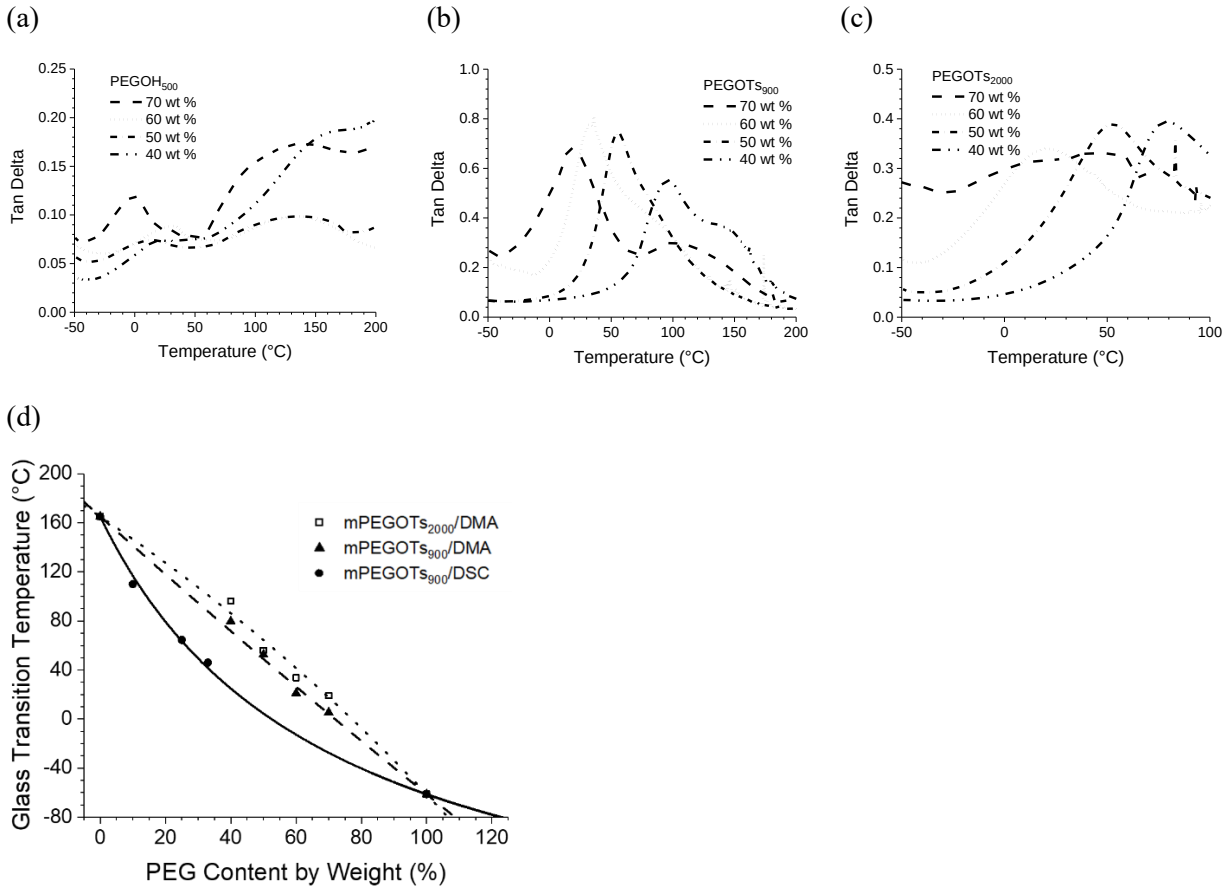

Figure 3.3. Tan delta from the DMA of benzoxazine blends with either (a) $mPEGOH_{500}$, (b) $mPEGOTs_{900}$, or (c) $mPEGOTs_{2000}$ at various weight loading. (d) The glass transition temperatures and the respective Gordon-Taylor fits determined from the peak tan delta signals in b-c for blends with $mPEGOTs_{900}$ (triangles, dashed fit, k = 0.95) and $mPEGOTs_{2000}$ (empty squares, dotted fit, k=1.25) overlaid with the glass transition temperatures and the fit for $mPEGOTs_{900}$ (circles, solid line, k = 0.41) as determined from the DSC data in chapter 2.

The glass transition temperatures were determined from peaks in the tan delta signals from the DMA scans of the PEG blends (Figure 3.3a-c, see Figure B7 for storage and loss modulus). Regardless of the amount of PEG content in the $mPEGOH_{500}$ series there is an obvious bimodal system in its tan delta signal, one peak near 0-30 °C and the other near 140-160 °C. The first and lower temperature T_g is likely

from the phases of higher PEG content while the higher temperature T_g is from the higher PBA-a content phase. The bi-modal system is present in all samples due to low homogeneity between mPEGOH and PBA-a across the entire series of the mPEGOH blends. The heterogeneity of these samples has also widened the temperature range where the T_g values are found. The tan delta scans in both of the tosylated series show a shifting maxima over the different weight loadings. With increasing polybenzoxazine content, the glass transition temperature was found to increase. These glass transition temperatures are plotted in Figure 3.3d and overlaid with the glass transition temperatures determined from the DSC scans of $mPEGOTs_{900}$ blends. Like with the DSC results, the T_g has a strong Gordon-Taylor relationship with a *k* of 0.95 for the $mPEGOTs_{900}$ blends and a *k* of 1.25 for the $mPEGOTs_{2000}$. The difference between these k values may be due to a difference in thermal history of the samples. The k values from the DMA data that are closer to 1 indicate very good mixing and good homogeneity between the blend components. The similarity between the fits and data of the tosylated blends despite the difference in their molecular weight suggest that the grafting of these polymers into the benzoxazine network has a larger impact on its glass transition temperature, therefore the $mPEGOH_{500}$ blends are a comparable blend.

3.3.4 Thermal behavior of blends of PBA-a with PSU.

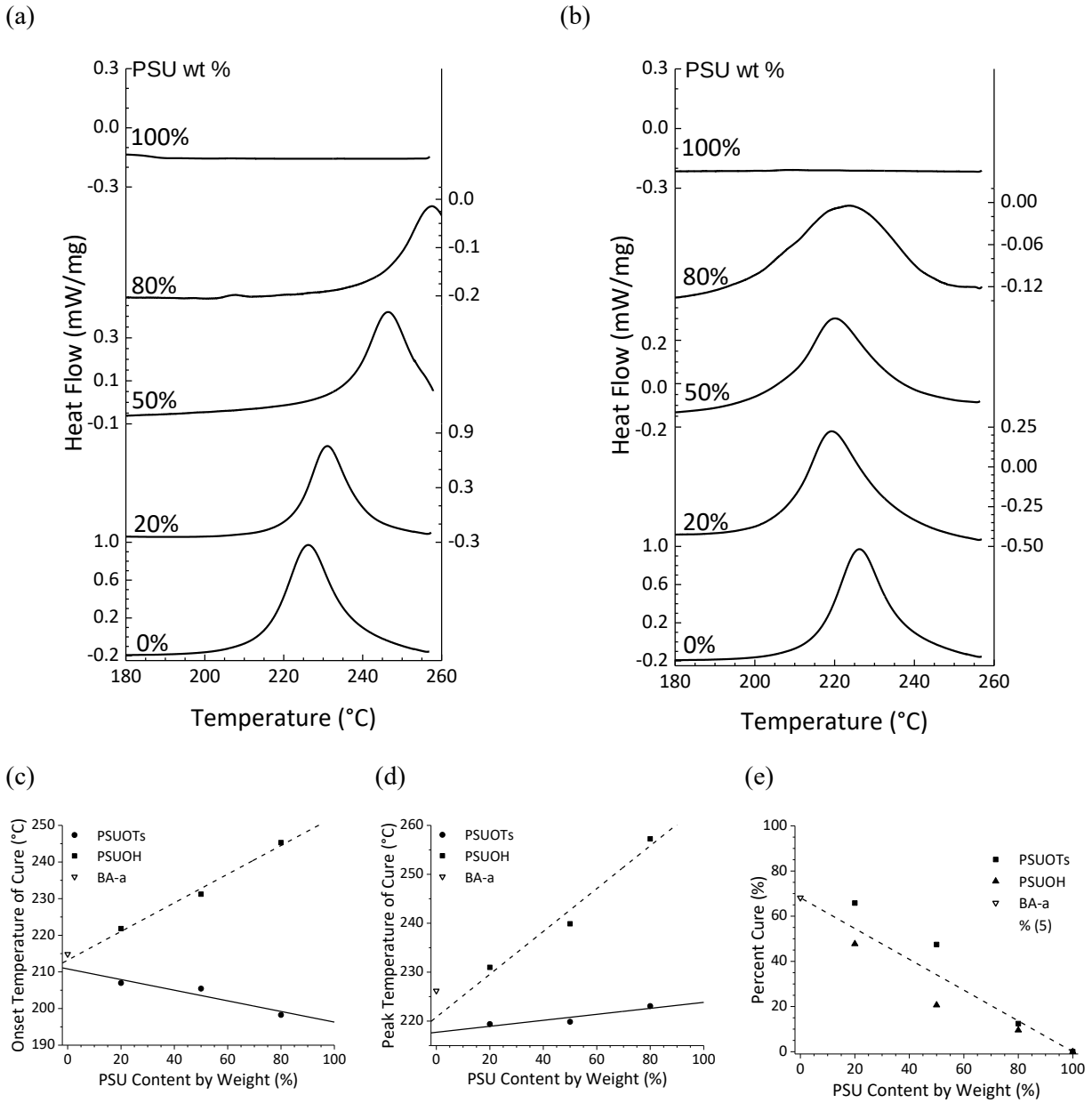

Figure 3.4. DSC heat curves from the first scan of blends of BA-a with (a) PSUOH and (b) PSUOTs. (c) The onset of cure and (d) the peak cure temperature of the blends with PSUOH and PSUOTs with linear fits in the dotted and solid lines respectively. (e) The percent cure was determined by the enthalpy of the exotherm from the scans in (a) and (b).

Similar to the PEG blends we see a decrease in the curing temperature and an increase in the enthalpy of cure of BA-a blends in the tosylated series. Again, we see an increase in temperature in both the onset and peak of the exotherm of cure in the PSUOH blends. While the onset of cure temperature decreased by ~15 °C with increasing PSUOTs (Figure 3.4c) the same was not seen for the peak cure temperature of such blends, instead there was a slight increase in the peak temperature while still remaining below that of pure BA-a by about 5-10 °C (Figure 3.4d). This is a result of the broadened exotherm of cure seen in the heat scans (Figure 3.4a), likely a result of the higher molecular weight of the blended polymer, slowing the cure. While the reduced cured temperature is not as significant as that of the mPEGOTs blends, it is significant with respect to end group concentration of the two polymers, 500 and 77 µmol/g in mPEGOTs and PSUOTs respectively. Interestingly, the increase in the curing temperatures are much more dramatic with an increase of about 40 °C in the 80 wt % sample when compared to the mPEGOH system where the increase of the peak was about 10 °C in the 90 wt % sample. This is likely due again to the higher molecular weight of the PSUOH. The noticeable broadening of the curing exotherm of the BA-a in the PSUOTs blends that is not present in the PSUOH blends speaks to the differences in the homogeneity of these two series. Likely, the BA-a in the PSUOH that polymerized did so in an isolated phase, separated from the polymer which results in an exotherm that looks very similar in shape to that of pure BA-a while shifted to a higher temperature.

As was seen in the mPEGOTs system, the PSUOTs system results in a higher enthalpy of cure of benzoxazine. It is again proposed that excessive enthalpy that is greater than what was projected is due to the grafting of the polymer onto the PBA-a network as it was the case in the mPEGOTs system. Furthermore, the large enthalpy may also be a result of higher monomer conversion due to being in phase with its polymer solvent.

3.3.5 Morphology of PSU blends.

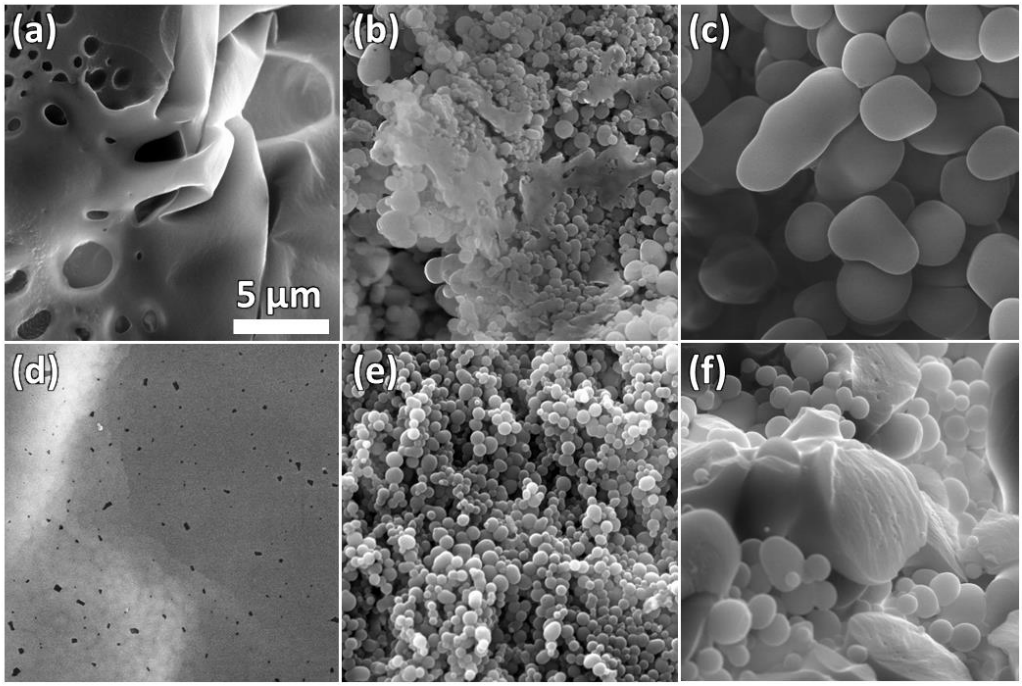

Figure 3.5. SEM images of PBA-a blends with either PSUOTs at 80, 50, and 20 PSUOH wt % (a-c) or PSUOH at 80, 50, and 20 PSUOTs wt % (d-f) after a rinse in chloroform. The scale in image (a) is relevant to all images.

The SEM images of the fractured surfaces of the PSUOH and PSUOTs blends show very different morphologies (Figure 3.5). Unlike in the PEG images the lower polymer content samples do not exhibit a uniformly smooth surface. Instead, nearly all samples present a morphology consisting of spheres. However, the 80 wt % PSUOH blend is an exception. The shapes of these spheres are much more uniform in the PSUOTs blends than they are in the PSUOH. The 20 wt % PSUOTs sample has two obvious features, smooth, uniform spheres and an underlying branched polymer network. The smooth surface of these branches are similar in texture to the homogenous P(BA-a)-g*raft*-PEG blends. This branched network is most likely the result of PSU grafted PBA-a from the BA-a and PSUOTs miscible phase. The spheres are similar to those seen in the heterogeneous mPEGOH blends from the immiscible BA-a. These spheres are uniform in both the 80 and 50 wt % as well. The uniformity in the PSUOTs blends that is not

seen in the PSUOH blends speaks to the difference in the homogeneity between these two different blends. In the PSUOH series as the PSU content increases the spheres seem to conglomerate. In the 80 wt % PSUOH, the spheres are not present and likely the result of the PBA-a forming its own isolated phase.

3.3.6 Mechanical characteristics of PSU blends. While polybenzoxazine is a highly desirable engineering material due to its remarkable mechanical, thermal, and dielectric properties, it suffers from its brittleness. Such brittleness inhibits the processing of polybenzoxazine films and thin films. The current remedy to this issue is to synthesize polymers with benzoxazine moieties in the main chain. Such polymers can be further polymerized to induce cross-linking by the ROP of the oxazine ring as discussed in chapter 1.[9,65,214,215] These benzoxazine units are usually connected by ether or aliphatic segments or other polymers and the films they produce are 0.1-1.0 mm in thickness.[215-217] As seen with polymer blends both in current research and in chapter 2, the inclusion of non-benzoxazine material impedes the benzoxazine ROP and pushes it to a higher temperature.[9,45,109] There are many groups producing films by co-polymerizing benzoxazine with other resins such as epoxy, these films are also typically 100 μm at the thinnest.[218,219] Some groups are mitigating the rigidity of the benzoxazine by blending it with polymers as we have done. Some of the existing films made from blends include benzoxazine blended with lignin,[220] poly diglycidyl ether of bisphenol A/butadiene acrylonitrile co-polymer[221], benzoxazine functionalized polycaprolactone,[222] and styrene-butadiene-styrene triblock co-polymers.[223] Of these, the Gu group achieved the thinnest benzoxazine-based thin film with a thickness of 40-50 μm.[221] As far as we are aware, there has yet to be a film produced incorporating benzoxazine that is ~1 μm; oligomer, main-chain benzoxazine polymer, co-polymer, blended, or otherwise.

(a)

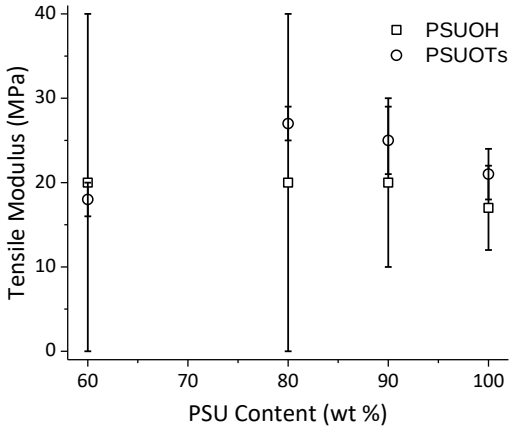

(b)

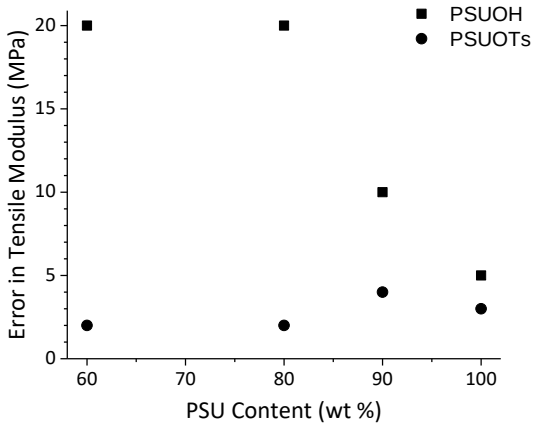

(c)

Figure 3.6. (a) Tensile modulus of PSU blends with PBA-a determined from stress-strain curves and (b) the error in the tensile modulus measurements plotted against PSU content. (c) An image of a representative film of 50:50 PSUOTs and PBA-a.

All PSU/PBA-a films that were prepared were transparent with an average thickness of ~1 μm. The higher content PBA-a films are more yellow in color. The higher content PBA-a films were also noticeably more stiff and easier to tear due to the lower content of flexible PSU material.

From the stress-strain curves of the PSUOH and PSUOTs blends the tensile modulus was determined by the linear slope of the data. The blends of PBA-a with PSUOH do not have any significant change in tensile modulus across the compositionally varied samples with values around 22 MPa. The measured tensile modulus of these films also exhibit a very large error (Figure 3.6a and 3.7b). The error in the

tensile modulus of the PSUOH/PBA-a films decreases as PSUOH content increases from 70 to 100 wt %. As more non-homogeneous PBA-a content becomes present in the blends the uniformity of the samples diminishes. The PSUOTs/PBA-a blends benefit from the homogeneity of the films with smaller error in the obtained tensile modulus values. There is also a statistically significant improvement in tensile modulus in the 80 wt % PSUOTs/PBA-a blend from that of pure PSUOTs, increasing from 20.6 to 26.5 MPa, almost 30 %. The possible formation of a P(BA-a)-*graft*-PSU material likely was responsible for the improvement in the tensile modulus and the reduced error due to a more homogeneous material compared to the PSUOH/PBA-a films.

3.3.7 Miscibility of blends of PBA-a with PSU.

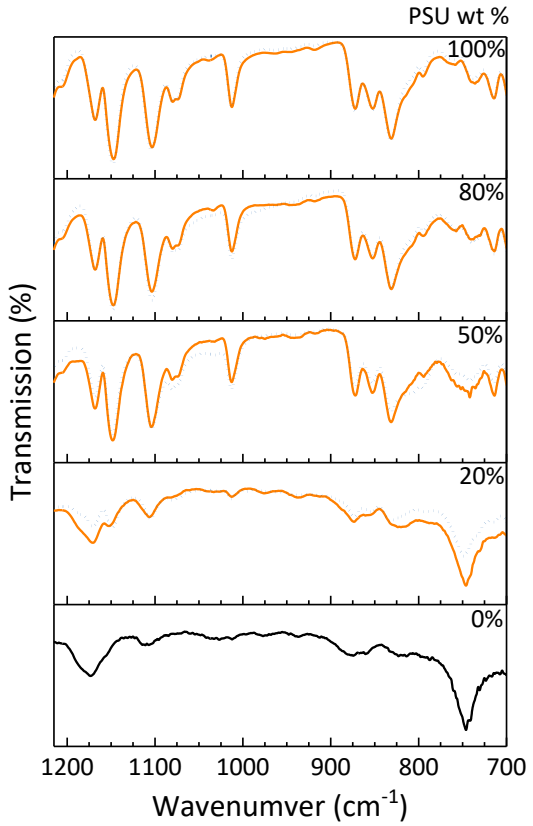

Figure 3.7. FTIR of the cured PBA-a and its blends with either PSUOH (blue, dotted line) or PSUOTs (solid, orange) from 1200 to 700 cm^{-1}.

The acquired FTIR spectra for the PSUOH and PSUOTs blends show fairly different profiles (Figure 3.7). Most noticeable are the difference in the intensities of the signals from the PSU component relative to the PBA-a signals between the two series across all compositions. The profile of the FTIR spectra for the blends with 80 and 50 wt % PSU in both series assume a similar shape to pure PSU. The only blends that have spectra similar to that of PBA-a is at 20 wt % PSU. From 1200-700 cm^{-1} the most noticeable peaks in the blends and pure materials are at 1174, 875, 831, and 747 cm^{-1}. The signal at 1174 cm^{-1} is from the PBA-a component in these blends from the asymmetric C-N-C stretch ($\nu_{as\ C\text{-}N\text{-}C}$).[224] This broader signal is only present in the 20 wt % PSU sample and is much stronger in the PSUOTs blend than in the PSUOH. The peaks at 831 and 875 cm^{-1} are the δ CH_{oop} deformation bands in of the aromatic rings in the PSU.[225] This 875 cm^{-1} signal is also weakly present in the PBA-a spectra from the tetra-substituted benzene ring of the phenolic linkage, confirming the ring opened structure.[226,227] The lack of a peak at 960-910 cm^{-1} corresponding to one of the modes of the benzene ring, only present when the oxazine ring is closed, also confirms the polymerization of the BA-a.[4] Finally there is a strong, isolated signal at 747 cm^{-1} that is considered to the ring breathing mode from benzoxazine.[4] The presence of stronger signals from PBA-a in the 20 wt % PSUOTs spectra suggests better miscibility than in other compositions or in the PSUOH blends as observed in the morphology in the SEM images.

3.3.8 Thermal behavior of particle blends. In the TGA scans of the silica particles (Figure B8), it was found that after the evaporation of water there was no significant mass loss up to 400 °C. Therefore, there is no degradation of the organic material of the phenyl- or tosylate-functionalized particles and they can be conditioned within this temperature range without deterioration.

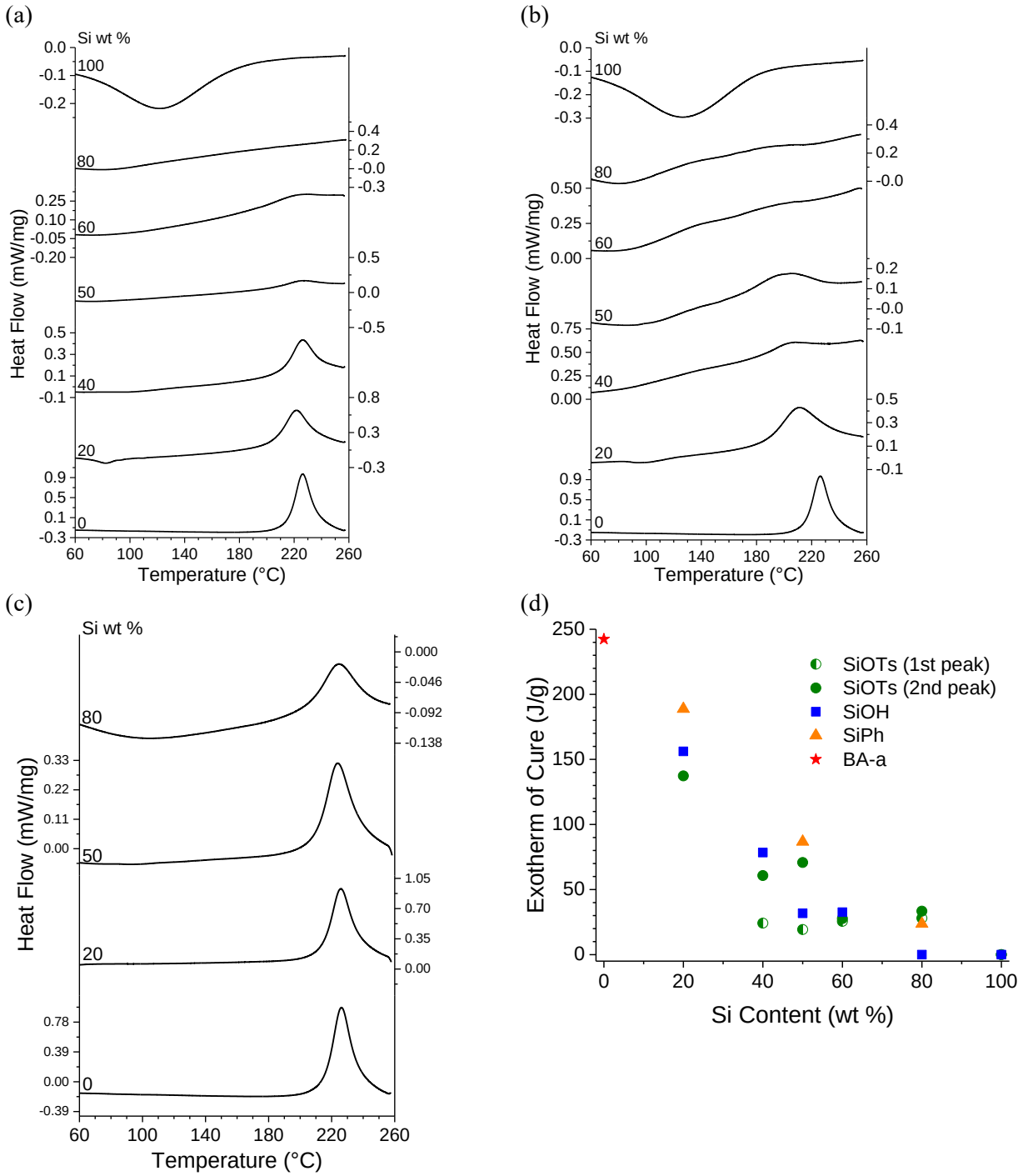

Figure 3.8. First heat scan from the DSC of blends of BA-a with (a) non-functionalized silica, (b) tosylated silica, and (c) phenyl functionalized silica. (d) The enthalpy values of the exothermic peaks from the polymerization of BA-a of all blends.

The shape of the exotherms from the first DSC heat scans are very different between the three blends of BA-a with SiOH, SiOTs, and SiPh. The blends with the phenyl functionalized silica have the least change across the range of compositions. The exotherm neither drifts nor broadens and remains gaussian in shape. The enthalpy of cure follows the expected trend of decreasing with decreasing BA-a (Figure 3.8d). The individual enthalpies of cure for the first and second peak of the SiOTs blends were fit with CasaXPS software with a residual STD <0.08, an example of the fitted exothermic peaks can be seen in Figure B9. The cure diminishes with increasing silica content but is not completely suppressed at the 80 wt % unlike the heat scan for the 80 wt % SiOH. In the SiOH blends the exotherm is slightly broadened but remains in the same position. There is no increase in cure temperature as has been seen in the hydroxy terminated polymers. The silica likely has less of an impact on the heat transfer across the blend like the polymer does, thus not increasing the curing temperature. As the silica content in the SiOTs blends increases, a bimodal exotherm appears, starting at the 40 wt % sample. The exotherms at both peaks are significantly broader compared to that of pure benzoxazine. The lower temperature exothermic peak has a similar onset and peak temperature across all compositionally varied blends. The higher temperature exothermic peak has lower onset and peak temperatures than that of pure BA-a.

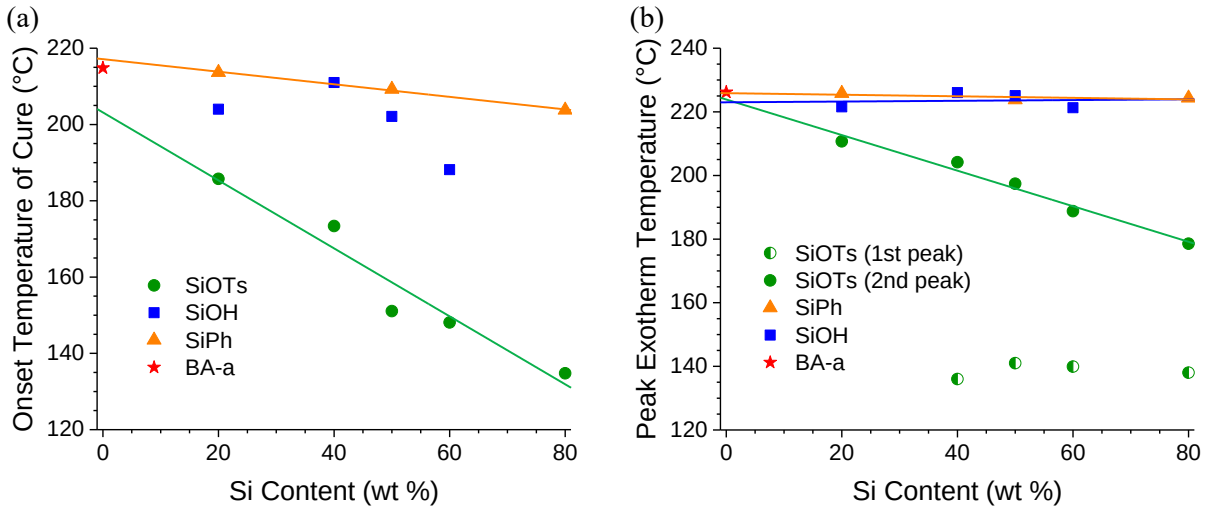

Figure 3.9. (a) The onset of cure and (b) the max curing temperature of PBA-a blends with silica as determined from DSC.

The onset temperature of the exotherm for samples in the SiOTs series decreased more significantly than other blends. The blend sample with 80 wt % SiOTs exhibited the greatest reduction in cure temperature with the onset of the exotherm appearing at about 80 °C lower than that of pure BA-a. The onsets for the cure of BA-a in SiPh and SiOH series only decreased by about 10-30 °C most likely from slight broadening of the exotherm rather than by cure acceleration. The onset temperature of cure for the SiOTs blends, plotted in Figure 3.9a, was of the higher temperature peak where the bulk of the exotherm was, the onset of the first peak remained near constant around 120 °C. The peak exotherm in both of the SiOH and SiPh remains the same as pure BA-a , the presence of organic content on the surface of the SiPh particles did not have an effect on the cure of the BA-a content. The blends containing SiOTs had a significant decrease in the peak exotherm, the mechanism of the accelerated cure from *p*-toluenesulfonic acid is likely also present in these blends where the sulfonic acid is exposed to BA-a. The peak exotherm from the first exotherm did not drift or show any trend and remained near 140 °C. This first exotherm is likely from the polymerization of the monomer that is closer to the surface of the SiOTs particles. As more SiOTs is added into the system, the enthalpy shifts from the second exotherm to the first.

3.3.9 Mechanical properties of PBA-a/particle blends.

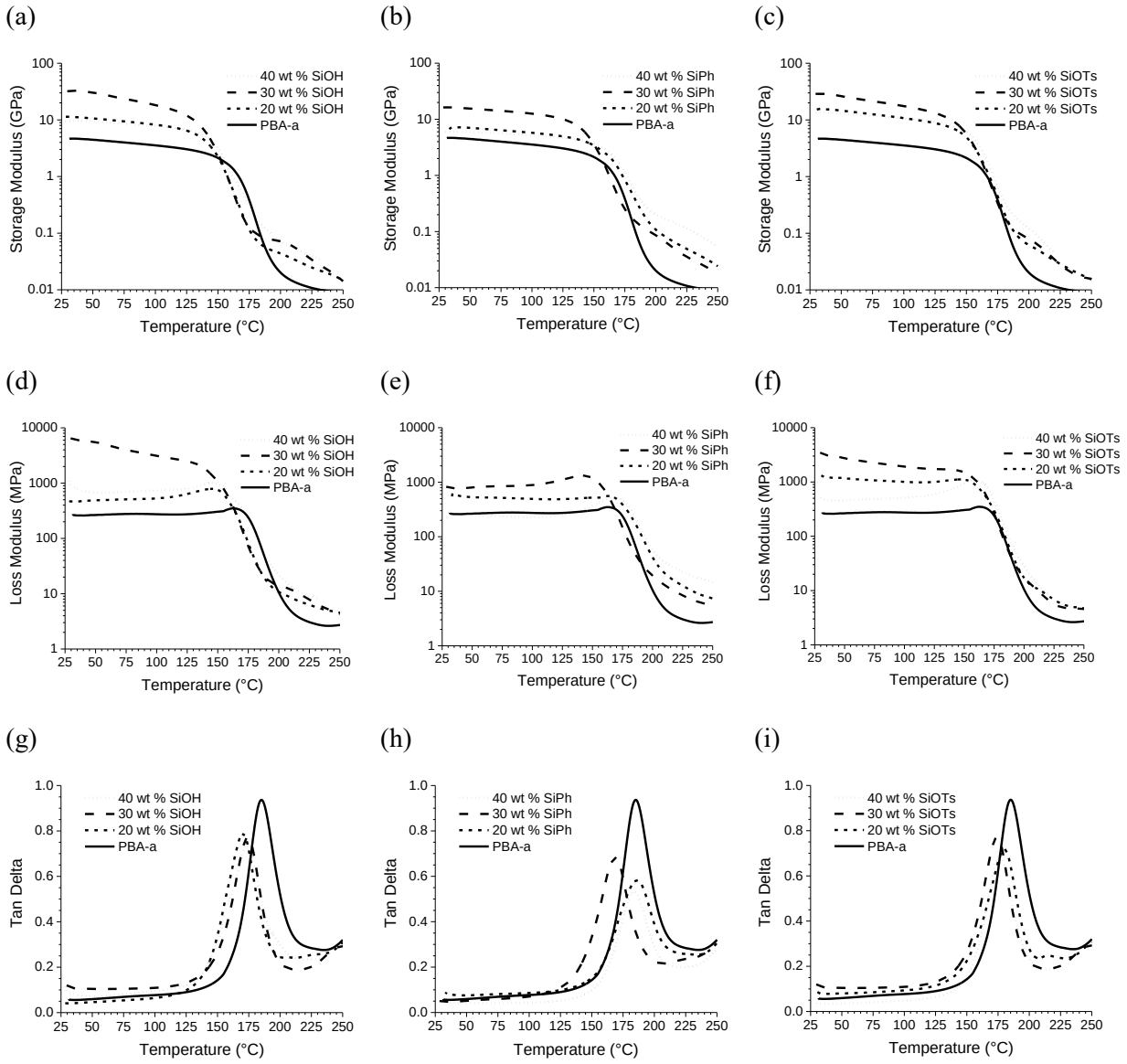

Figure 3.10. (a-c) The storage modulus, (d-f) loss modulus, and (g-i) the tan delta for blends of PBA-a with SiOH, SiPh, and SiOTs respectively at varying loading.

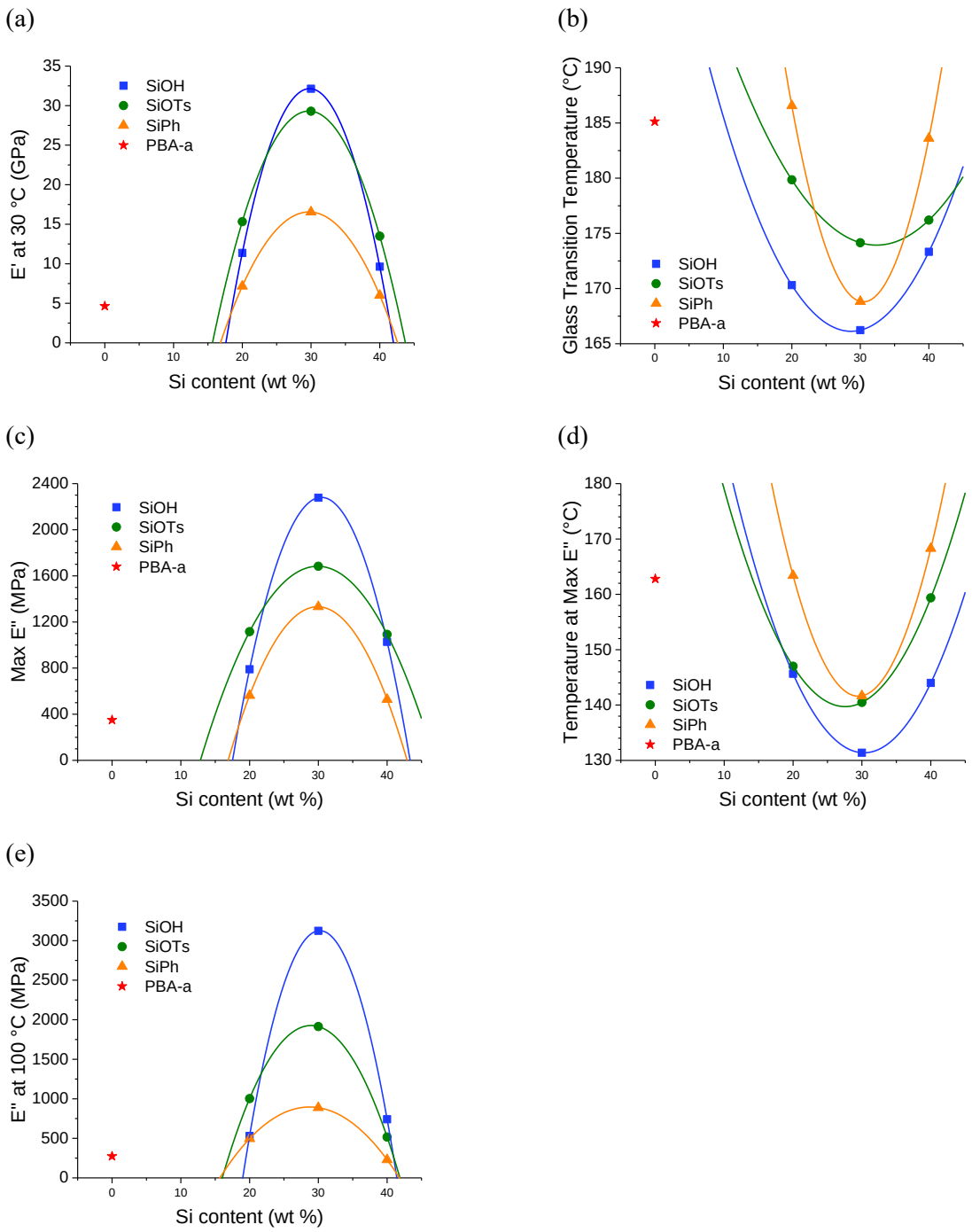

Figure 3.11. (a) The storage modulus at 30 °C, (b) glass transition temperature determined from the max signal of the tan delta, (c) the max loss modulus signal, (d) the temperature at max loss modulus, and (e) the loss modulus at 100 °C of pure benzoxazine and its blends with SiOH, SiOTs, and SiPh particles.

The storage modulus at 30 °C in all blends has an optimal mass loading at 30 wt %. There was a significant increase across the entire loading range in all blends from that of PBA-a at 5 GPa, with peaks at 32, 29, and 16 GPa for the SiOH, SiOTs, and SiPh blends respectively. While the SiOH particles preformed better at the 30 wt %, the SiOTs had higher storage modulus at 20 and 40 wt %, effectively widening the range of increased modulus. The storage moduli of the SiPh blends were lower than that of the other two. The mechanical properties of the SiPh blends did not benefit from the organic surface. The high modulus found in the SiOTs blends is from the presence of the accelerant causing a difference in the polymerization behavior of the PBA-a. Despite the increase in storage modulus there is a significant decrease in the glass transition temperatures in all blends across the loading compositions except for the 20 and 40 wt % SiPh. The glass transition temperature minima in all three blends are found in the 30 wt % at 166, 169, and 174 for the SiOH, SiPh, and SiOTs blends respectively. The glass transition temperature of the SiOTs blends were as impacted by the presence of the particles as the SiOH blends, possibly from the organic content. The SiPh particles had the least impact on the glass transition temperature of its blends.

3.3.10 Morphology of silica blends.

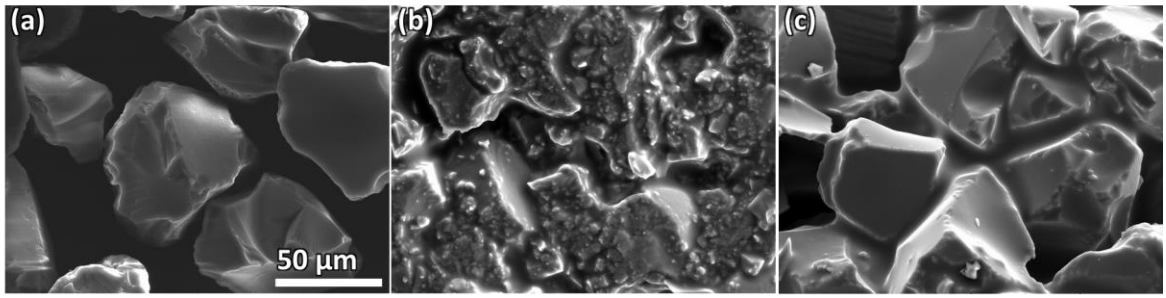

Figure 3.12. SEM images of (a) SiOTs and blends of PBA-a with (b) SiOTs and (c) SiOH at 50 wt % silica content.

There is a noticeable morphological difference between the cured SiOH and SiOTs blends in the SEM images in Figure 3.12. In the SEM image of the fractured SiOH blends the particles are well defined with

a smooth phase of PBA-a filling between the individual fragments. However, the images acquired of the fractured SiOTs blends reveal a rough and bumpy texture on the particles despite their originally smooth surface. The SiOTs particles are also indistinguishable from the PBA-a phase. This unique morphology is possibly from densely polymerized PBA-a, creating a shell over the particle and integrating them into the polymer network. The presence of the PBA-a shell on the particle is due to the initiation of the cure of the monomer at the surface of the tosylate functionalized silica.

3.3.11 Thermal behavior of blends of PBA with PDLLA.

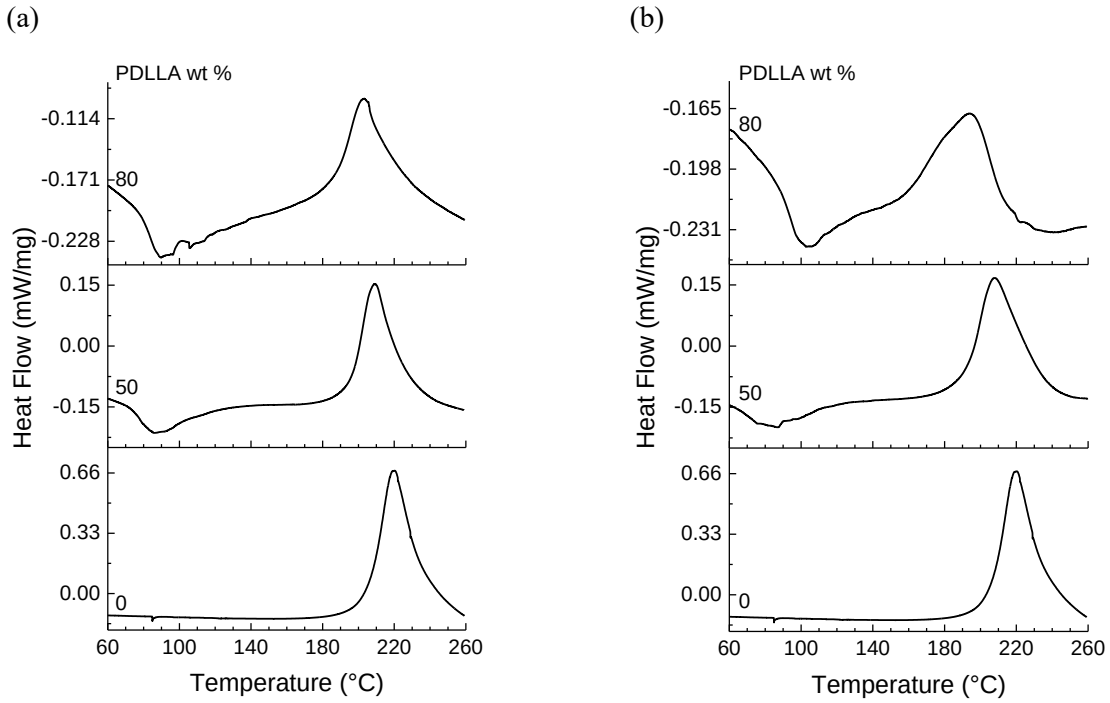

Figure 3.13. The first heat scans from DSC of blends of BA-a with (a) PDLLAOH and (b) PDLLAOTs.

There is a unique difference between the blends of the PDLLA and the other polymers, in that there is an acceleration in the benzoxazine polymerization in both the tosylated and non-tosylated blends. The tosylated blends show a slightly lower onset and peak curing temperatures at 191 and 208 °C for the 50 wt % blend and 155 and 194 °C for the 80 wt % blend. The PDLLAOH had an onset and peak curing temperature at about 190 and 205 °C for both the 50 and 80 wt %. The blends only benefit from the

presence of the tosylate at the higher loadings. As the blends reach the higher temperature the PDLLA likely begins to degrade.[228,229] As the polymer degrades to produce lactic acid and more of the carboxylic acid end group is exposed to the BA-a content which may then dominate the accelerated cure mechanism as seen in literature.[23] The degradation occurs in both the PDLLAOH and the PDLLAOTs resulting in the decrease in curing temperature for both blends.

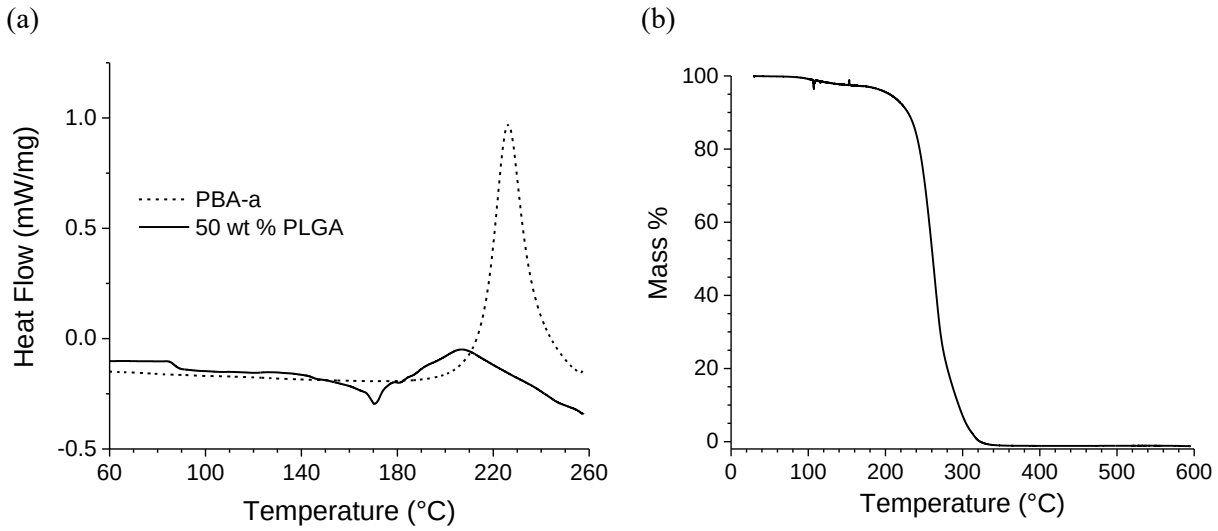

Figure 3.14. The (a) DSC curve of 50:50 PLGA blended at 50 wt % with BA-a and (b) the TGA curve of 50:50 PLGA.

As was seen in the PDLLAOH blend the PLGA blend also results in a reduction of the curing temperature with an onset of cure at 183 °C and the peak at 209 °C (Figure 3.14a). The PLGA is significantly more sensitive to hydrolysis and thermal degradation than the PDLLA and will result in the presence of the carboxylic acid that reduces the cure of the BA-a as well. The endotherm just before the cure at 170 °C is likely the result of the degradation of the polymer which has a $T_{D5\%}$ at 220 °C for the major mass loss event as determined by the TGA of PDLLA in Figure 3.14b. The degradation of pure PLGA was characterized by monitoring the change in pH of the sample in PBS. As lactic acid and glycolic acid is freed into the solution via hydrolysis by water, the pH expectedly decreased (Figure B10). These findings were in agreement with literature.[205]

3.3.12 Degradation of blends of PBA-a with PDLLA.

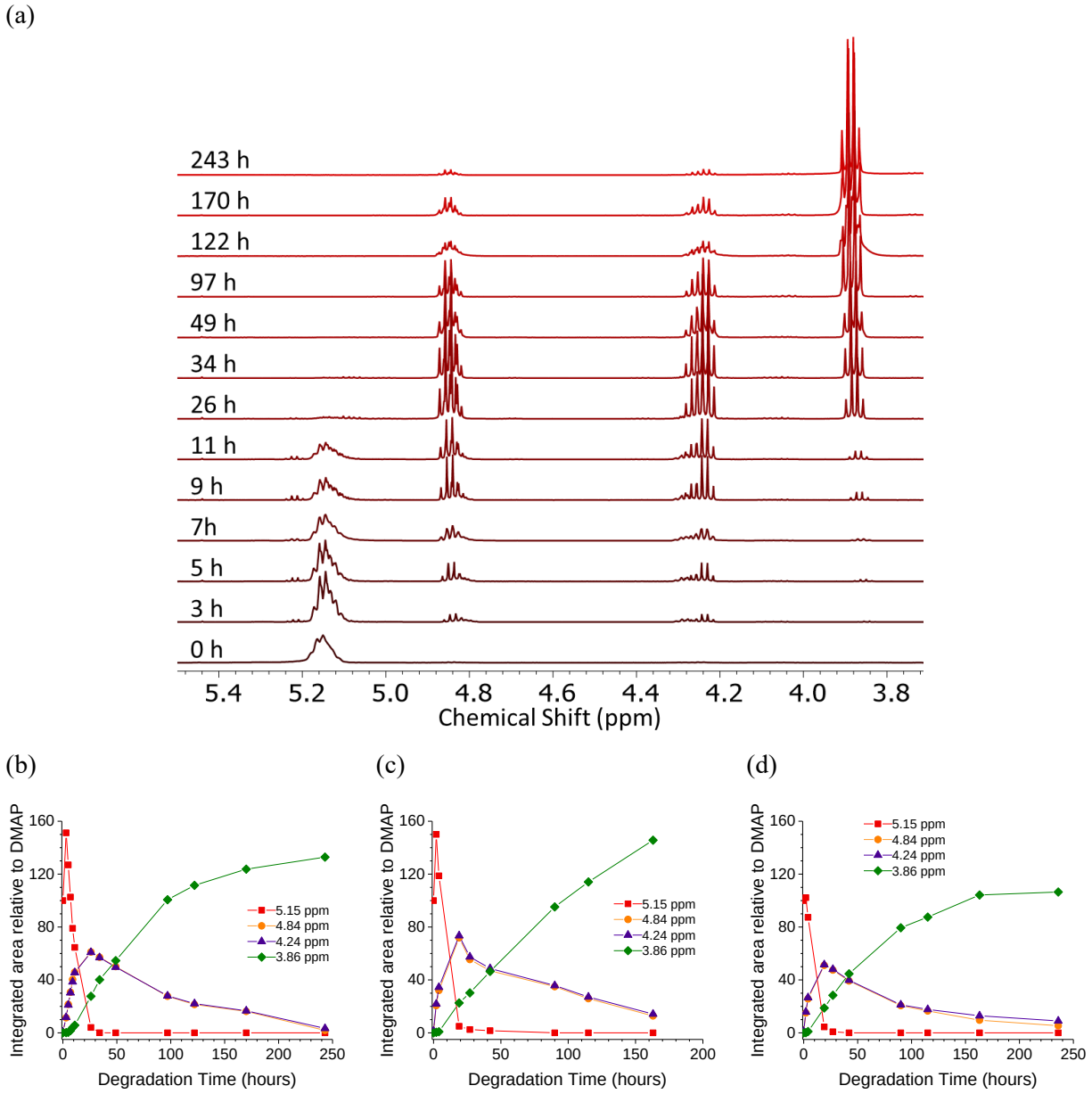

Figure 3.15. (a) The stacked ^{1}H NMR spectra of the degradation of PDLLAOH in acetonitrile-d3/D_2O (9:1), with DMAP, acquired over several days. The integrated area of the signals corresponding to methine of the internal polymer (5.15 ppm), the D- and L-methine end groups (4.84 and 4.24 ppm), and the methine of the lactic acid (3.86 ppm) of (b) PDLLAOH, (c) 50:50 PDLLAOTs/PBA-a, and (d) 50:50 PDLLAOH/PBA-a.

In the initial ^{1}H NMR (Figure 3.15a), the spectrum displays the characteristic peaks for the polymer at 5.15 and 1.49 ppm with smaller signals corresponding to the D and L end groups at 4.84 and 4.24 ppm. As the degradation progresses the internal polymer signals decrease and the end group signals increase as the end group to internal polymer ratio increases. The quartet from the methine hydrogen at 3.86 ppm begins to appear as well. The initial polymer increase between the first two points of data is likely from the polymer continuing to dissolve into solution. At about 20 hours the polymer signal has completely subsided and the spectrum is dominated by the signal from the end groups and lactic acid. At this point these end groups are likely not polymer but essentially a lactic acid dimer. At about 35 hours the end group signal has begun to diminish and the lactic acid continues to grow in. Finally at >200 hours all polymer and end group signals have waned and only lactic acid remains, resulting in the complete degradation of the polymer. The degradation of phases of PDLLAOH or PDLLAOTs should leave micro- or nano-pores that will lead to easier disposal or degradation by solvolysis of PBA-a. However, it is only in the blends of PDLLAOTs, where polymer grafting is possible, that molecular holes along the PBA-a backbone may appear after degradation of the PDLLA, exposing more of the PBA-a backbone.

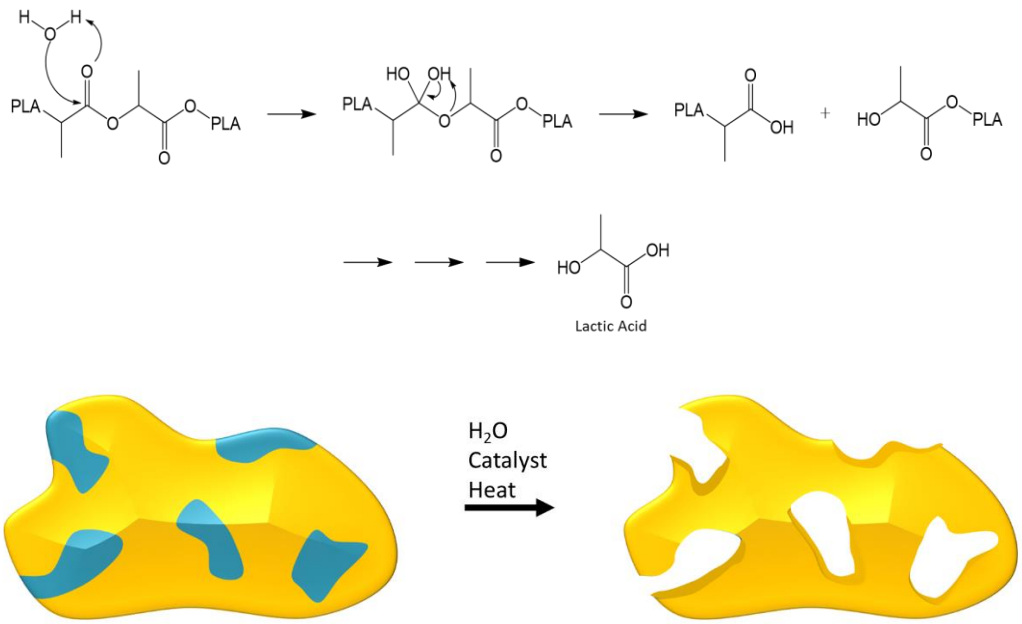

Scheme 3.3. Degradation of poly(lactic acid) via hydrolysis and the morphology after degradation in a polymerized blend.

3.4 Conclusions

In this chapter, the PEG system was further defined and three new systems were explored. From the mechanical analysis of the mPEGOTs system, the Gordon-Taylor relationship between benzoxazine and PEG was redefined and determined to have a *k* of near 1. The reduced curing temperature of benzoxazine blends was reaffirmed with two new tosylated polymers and tosylated silica. Compared to the previous PEG blends, the PSU blends did not achieve the same effect on the curing temperature of benzoxazine. At the same mass loading, the PSUOTs blends only reduced the curing temperature to 217-220 °C which is only slightly below the cure temperature of BA-a at about 230 °C. In comparison, the PSUOH had a much more dramatic effect on the blends than the mPEGOH system did, increasing the curing temperature to nearly 260 °C. The lessened effect of the tosylated PSU is likely due to the effect of the larger polymer size increasing the cure, offsetting the temperature of polymerization. The PSUOTs blends also resulted in a higher enthalpy of polymerization as the mPEGOTs blends did, therefore it is likely that the cured PSUOTs blends also possess a similarly unique grafted polymer network. The tosylated silica

and PDLLA had a more significant impact on the curing temperature, both decreasing the max exotherm temperature to about 190 °C, with the onset of cure for silica near 140 °C, the lowest achieved in this work. From the PSU blends thin films of benzoxazine were made and characterized with a load cell, the PSUOTs blends had a significantly lower error in its tensile modulus indicating better homogeneity over the PSUOH blends. A higher loading of silica particles than traditional was characterized by DMA at 20-40 wt % silica. The higher modulus of the SiOTs blends was determined to be due to the sulfonic acid and not the organic surface as a lower storage modulus was found in the SiPh blends. By SEM, the cured SiOTs blends displayed a different texture on the surface than the cured SiOH blends, most likely due to the instigation of the PBA-a cure at the surface of the particle. The curing temperature of the benzoxazine blends with PDLLA or PLGA benefitted from the degradation of the polymer, adding a carboxylic acid accelerant. The degradation of these blends to lactic acid was determined by a ^{1}H NMR time study with DMAP, water, and heat. Each of these blends further expands the scope of benzoxazine. Polysulfone aids in the process of making thin films from benzoxazine for applications such as fuel cell membranes. SiOTs blends offer a heightened modulus range for more durable materials. The PDLLAOTs blends offer the opportunity to degrade and remove components of the materials leaving a highly craterous and porous polybenzoxazine material that can easily be milled and repurposed as filler in other materials.

Chapter 4: Benzoxazine based surfactants for monomer processing

4.1 Introduction

As the scope of benzoxazine broadens, so too must its processing in order to achieve newer applications. Traditionally, benzoxazine materials are produced by melt or solvent casting with organic solutions. Water soluble benzoxazine surfactants provide a solution to solvent casting without organic solvents. Such surfactants are present in current research as benzoxazines gain more popularity.

Water soluble benzoxazine monomers are fairly uncommon, typically there are concerns surrounding water uptake of the final polybenzoxazine material as it becomes more hydroscopic. There are few water soluble benzoxazine monomers existing in the literature, such a monomer will typically require a large polar group.[69] Based on previous findings concerning blends of benzoxazine with non-curable components in literature as well as in the work presented in chapters 2 and 3 of this thesis, the addition of organic substituents to a benzoxazine unit results in an increased polymerization temperature and reduced mechanical properties. Surfactants can bypass this issue by suspending conventional benzoxazine monomer within water stable micellar structures and in principle would result in processed polybenzoxazine with properties closer to that of the conventional material.

In theory, a benzoxazine-based surfactant could co-polymerize with the hosted conventional monomer. The co-polymerization of these surfactants is a large benefit over commercial ones. Commercial surfactants like sodium dodecyl sulfate (SDS), cetyltrimethylammonium bromide (CTAB), or cetyltrimethylammonium p-toluenesulfonate (CTAT) will create non-polymer moieties or segments within the material. Mechanical failure of the material may occur at the interfaces between the polymer and surfactant.[230-234] A co-polymerizable surfactant will be molecularly integrated into the polybenzoxazine network and would be less likely to create these concentrated stress points within the fully cured polymeric material.

Benzoxazine monomer is best solubilized by the benzoxazine head group of the surfactant, this provides a bulky hydrophilic structure that must be further functionalized to improve its water solubility. A polymeric tail must be carefully selected to satisfy this need. A hydrophilic polyether such as poly(propylene glycol) or poly(ethylene glycol) is typically used. Such a surfactant structure with a hydrophilic tail and a hydrophobic head group is uncommon and should lead to a reverse micelle structure with the benzoxazines concentrated at its center.

Emulsions of monomer in benzoxazine surfactants are a fairly new area within the benzoxazine field. Taden et al. were the first to synthesize a polymerizable nonionic benzoxazine surfactant in 2010.[61] They were able to successfully load benzoxazine monomer in water at a 4:1 ratio by weight using a bis-benzoxazine surfactant with two hydrophilic tails (see structure I in Figure 4.1). In 2011 their group further established the concept by the synthesis and study of a main chain benzoxazine polymer surfactant with segments of hydrophobic and hydrophilic blocks capable of loading similar amounts of benzoxazine.[96] Finally, Taden with Ishida and Froimowicz developed a surfactant (structure IV in Figure 4.1) with a lower critical solution temperature that, upon heating, desolvated and precipitated in the form of a homogenous film.[235] In all three of these examples the surfactant was successfully co-polymerized with the suspended benzoxazine monomer.

These benzoxazine surfactants have also been utilized for stabilizing other non-benzoxazine-based monomers and materials. In 2014 and 2016, Krajnc et al. have successfully loaded water-stable benzoxazine micelles (structure I, III, and VI in Figure 4.1) with epoxy with a loading ratio of 9:1.[60,236] Wang et al. have recently used benzoxazine-based surfactants similar to those made by the Taden group to suspend graphene flakes and ultimately form graphene films with high strength and electrical conductivity after polymerization of the surfactant head group.[237] They have also improved their graphene exfoliation yield, surpassing commercial surfactants such as SDS and CTAB.[97,238]

Synthesis of these surfactants is possible due to the design flexibility of the benzoxazine monomer, typically using a linear polyether amine or a similar amine terminated hydrophilic polymer to fulfill the primary amine requirement of the oxazine ring.[61,236,238] This molecular design installs the tail directly onto the oxazine ring which can impede curing.[61,96] Ishida et al. synthesized a surfactant in which the hydrophilic tail is attached to the benzene ring (structure V in Figure 4.1) from the vanillin starting material (4-hydroxy-3-methoxybenzaldehyde) which resulted in a bimodal cure at high temperatures.[59]

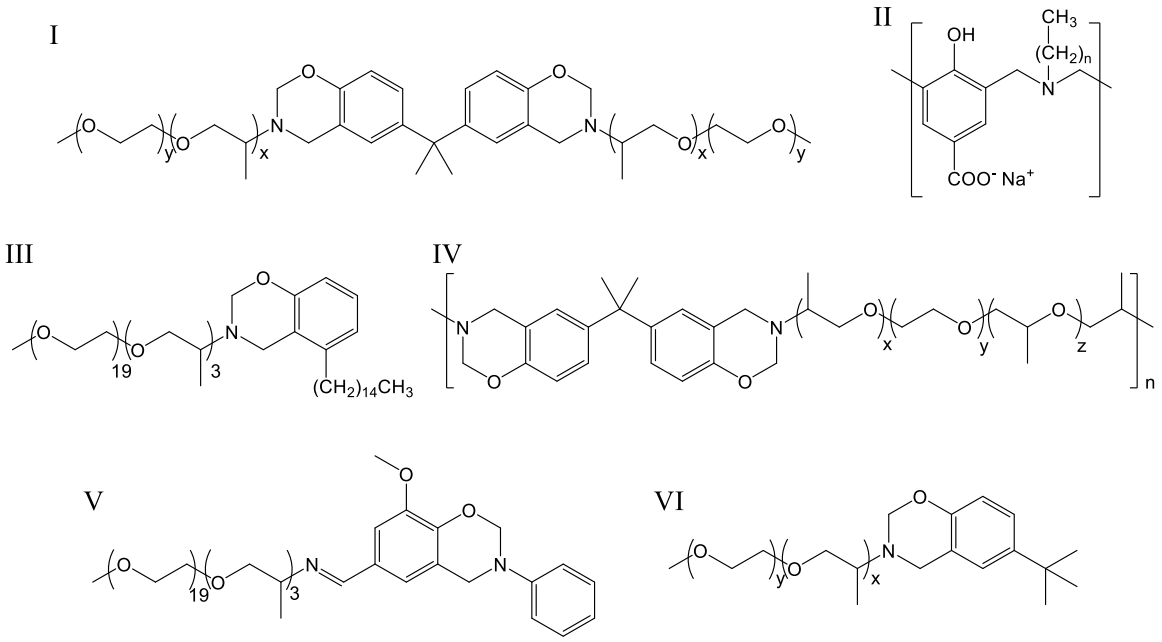

Figure 4.1. Examples of benzoxazine-based surfactants from literature.

I[60,61,97,237,238], II[239], III[236], IV[96], V[59], VI[60]

In this work, the synthesis of a benzoxazine surfactant by way of pegylation on the benzyl unit of a benzoxazine monomer is studied. The benzoxazine monomer bearing a hydroxy handle, *p*-hydroxy methylbenzoxazine (*p*HBA-a) is synthesized from *p*-hydroxybenzyl alcohol as described in literature.[56] An alternative synthesis by the polymerization of allyl glycidyl ether using *p*HBA-a as an initiator is also studied. This method allows for a more tunable tail length and possibly a more tunable surfactant geometry while also improving purity of the final product.

4.2 Experimental

4.2.1 Materials. The methoxypoly(ethylene glycol) tosylate ($mPEGOTs_{2000}$; M_n = 2000), methoxypoly(ethylene glycol) tosylate ($mPEGOTs_{900}$; M_n = 900), aniline (99.8% purity), allyl glycidyl ether (>99% purity), cetyltrimethylammonium bromide (99% purity), and cetyltrimethylammonium *p*-toluenesulfonate were acquired from Sigma Aldrich. Methylene chloride (99.9 % purity), ethylene acetate (99.9% purity), acetone (99.6% purity), methanol (99.9% purity), and sodium dodecyl sulfate were purchased from Fisher Scientific. Chloroform (99.8% purity), diethyl ether (99% purity), and anhydrous magnesium sulfate (99% purity) were received from J.T. Baker. Methoxypoly(ethylene glycol) ($mPEGOH_{500}$; M_w 500), *p*-toluenesulfonyl chloride (99% purity), paraformaldehyde (96% purity), pyridine (99% purity), 15-crown-5 (98% purity), and potassium in mineral oil (98% purity) were received from Acros Organics. Anhydrous sodium sulfate (99% purity), *p*-hydroxybenzyl alcohol (99% purity), and naphthalene (99% purity) were purchased from Alfa Aesar. Chloroform-d3 (>99% purity), methylene chloride-d2 (99.8% purity), acetonitrile-d3 (99.8% purity), and deuterium oxide (99.9% purity) were purchased from Cambridge Isotope Laboratories. Sodium chloride, toluene, sodium bicarbonate, tetrahydrofuran, and hexanes were purchased from Macron Fine Chemicals. Sodium hydride in paraffin (60% by mass) was purchased from Tokyo Chemical Industry.

4.2.2 Methods. A Bruker AVANCE-III, HD 500 MHz NMR spectrometer was used to collect all 1H NMR spectra. Matrix assisted laser desorption/ionization – time of flight (MALDI-TOF) spectra were collected with a Bruker AutoFlex II in positive ion mode. MALDI samples were prepared with a 2:1 matrix of α-cyano-4-hydroxycinnamic acid/2,5-dihydroxybenzoic acid. The sample solution was then spotted onto gold well plates. Micelle diameter was measured by dynamic light scattering (DLS) and was acquired with a Delsa Nano HC particle analyzer from Beckman Coulter equipped with a red laser (633 nm). Data for each sample was acquired in triplicate in glass cuvettes and particle size was determined with the CONTIN algorithm.

4.2.4 Thermal analysis. A TA Instruments Q100 differential scanning calorimetry (DSC) instrument was used for DSC-based cure studies on all samples. In hermetically sealed, aluminum DSC pans an average of 3 mg per sample were scanned. All DSC scans started with a 5 min isotherm at 25 °C then ramped to 300 °C, then to 25 °C and back to 300 °C at 10 °C/min.

4.2.5 Benzoxazine emulsions with surfactants. The surfactant was dissolved in nanopure water to a concentration of 20 mg/mL and filtered with a PTFE 0.45 µm syringe filter. The empty micelle solutions were then sonicated for 5 minutes with a Branson 450 Sonifier at 120 W for a 30 % time duration. The *p*HBA-a monomer was dissolved in THF at a 25 wt % and filtered with a 0.45 µm syringe filter. The monomer solution was then added dropwise to the micelle solution while being sonicated under the same conditions until solids began to form at which point the limit of loading was defined. The loaded micelle solution was then decanted from the solids and concentrated in vacuo to remove the THF solvent.

4.2.6 Preparation of blends. The following procedure is the general method for blend preparation. In a 10 mL round bottom flask the surfactant and *p*HBA-a were co-dissolved in acetone at a 1:4 ratio by mass. The blend was concentrated in vacuo and further dried over 12 h in a vacuum oven.

4.2.7 Lyophilization of blends. Micelle solutions were loaded at 75 % of their maximum and were prepared by lyophilization by freezing them with dry ice before removing the water with a Labconco FreeZone 2.5 L freeze dry system.

4.2.8 Synthesis.

Synthesis of (3-Phenyl-3,4-dihydro-2H-1,3-benzoxazin-6-yl)methanol (*p*HBA-a) To a 100 mL round bottom flask with a gas inlet aniline (2.00 mL, 21.5 mmol), *p*-hydroxybenzyl alcohol (2.50 g, 20.1 mmol), and paraformaldehyde (1.21 g, 40.3 mmol) were added. The solids were dissolved in toluene (30 mL) and stirred under nitrogen at 100 °C for 8 hours. The reaction mixture was then concentrated in vacuo after the solids were removed and dissolved in chloroform (30 mL). The solution was washed with $NaHCO_3$ (0.5 M, 3 x 30 mL) and deionized water (30 mL) before drying over Na_2SO_4. The product was allowed to

crystallize in the chloroform solution at 0 °C and collected as a white solid (95 %). ^{1}H NMR (500 MHz, DCM, ppm): δ 7.25 (2H, t, Ar-*H*), 7.10 (2H, d, Ar-*H*), 7.09 (1H, d, Ar-*H*), 7.05 (1H, s, Ar-*H*), 6.92 (1H, t, Ar-*H*), 6.76 (1H, d, Ar-*H*), 5.37 (2H, s, O-CH_2-N), 4.63 (2H, s, C-CH_2-N), 4.54 (2H, d, C-CH_2-OH), 1.64 (1H, t, O*H*).

Tosylation of methoxypoly(ethylene glycol) (mPEGOTs$_{500}$) To a 500 mL round bottom flask with a gas inlet mPEGOH$_{500}$ (6.00 g, 12.0 mmol) was dissolved in DCM (150 mL) was added. To the flask pyridine (20 mL, 0.253 mol) and *p*-toluenesulfonyl chloride (22.88 g, 120 mmol, 10 equiv) were added. The reaction was stirred under nitrogen at room temperature for 48 hours. The reaction mixture was concentrated in vacuo and dissolved in ether before being run through a column packed with neutralized alumina and subsequent additions of ether followed by chloroform. The chloroform eluent was then concentrated in vacuo and collected as a colorless oil (95 %). ^{1}H NMR (500 MHz, $CDCl_3$, ppm): δ 7.80 (d, Ar-*H*), 7.34 (d, Ar-*H*), 4.16 (t, O-C$_2$*H*$_4$-SO$_4$), 3.80-3.48 (m, C$_x$*H*$_{2x}$), 3.38 (s, O-C*H*$_3$), 2.45 (s, Ar-C*H*$_3$).

Synthesis of benzoxazine terminated poly(ethylene glycol) (mPEGpHBA-a) The following procedure represents the synthesis of all PEG-based surfactants in this work. To a 100 mL round bottom flask with a gas inlet *p*HBA-a (0.50 g, 2.0 mmol), potassium iodide (0.30 g, 1.8 mmol), 15-crown-5 (0.14 g, 0.64 mmol), and sodium hydride in paraffin (0.25 g, 6.3 mmol NaH) were added and dissolved in THF (10 mL). While the reaction was stirred under nitrogen mPEGOTs (0.63 mmol) in THF (5 mL) was added dropwise. The reaction mixture was allowed to stir under nitrogen for 4 days before being quenched with a few drops of methanol. The reaction mixture was concentrated in vacuo and dissolved in DCM before being washed with $NaHCO_3$ (2 x 50 mL) and brine (2 x 50 mL). The organic layer was dried over $MgSO_4$ and concentrated in vacuo. The product was then ran through a column packed with silica in ethyl acetate followed by THF. The THF eluent was concentrated in vacuo yielding a yellow oil. ^{1}H NMR (500 MHz, $CDCl_3$, ppm): δ 7.26 (t, Ar-*H*), 7.10 (d, Ar-*H*), 7.07 (d, Ar-*H*), 7.01 (s, Ar-*H*), 6.92 (t, Ar-*H*), 6.76 (d, Ar-*H*), 5.35 (s, O-CH_2-N), 4.62 (s, C-CH_2-N), 4.44 (d, C-CH_2-O), 3.80-3.48 (m, C$_x$*H*$_{2x}$), 3.38 (s, O-C*H*$_3$).

Synthesis of benzoxazine terminated poly(allyl glycidyl ether) (PAGEpHBA-a) In an inert environment the potassium in mineral oil was rinsed with hexanes and the oxidized layers were cut away. A 1 M solution of potassium in dry THF was prepared. A concentrated solution of *p*HBA-a (99.4 mg, 0.412 mmol) in THF was prepared and titrated with the potassium solution until a dark orange color. To the alkoxide solution, allyl glydyl ether (1.00 g, 8.76 mmol or 4.00 g, 35.0 mmol) was added and allowed to stir in the inert environment for 15 days. ^{1}H NMR (500 MHz, $CDCl_3$, ppm): δ 7.25 (t, Ar-*H*), 7.10 (d, Ar-*H*), 7.06 (d, Ar-*H*), 76.98 (s, Ar-*H*), 6.92 (t, Ar-*H*), 6.76 (d, Ar-*H*), 5.88 (m, CH_2=C*H*) 5.35 (s, O-CH_2-N), 5.25 and 5.15 (d, CH=CH_2), 4.62 (s, C-CH_2-N), 4.41 (d, C-CH_2-O), 3.98 (d, O-CH_2-CH), 3.70-3.40 (m, O-CH_2-CH and O-$C_xH_{1.5x}$).

4.3 Results and Discussion

4.3.1 Characterization of head group and surfactants. The synthesis of the benzoxazine head group of the surfactant molecule follows the conventional mechanism of the 1:1:2 reaction of phenol, aniline, and formaldehyde, respectively. The functionalization of the methyl alcohol on the phenol residue provides a handle for pegylation. At the benzoxazine synthesis stage, the aromatic alcohol will react during the monomer synthesis to form the oxazine ring. The hydroxy of the methylol substituent is deactivated by the methylene spacer and will not participate in any unwanted reaction.

Scheme 4.1. Synthesis of *p*HBA-a from formaldehyde, aniline, and *p*-hydroxybenzyl alcohol

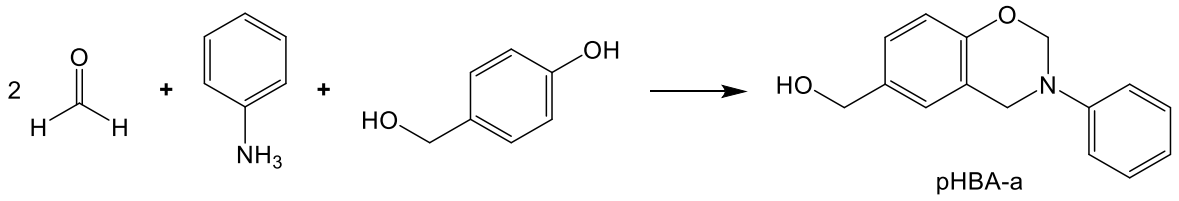

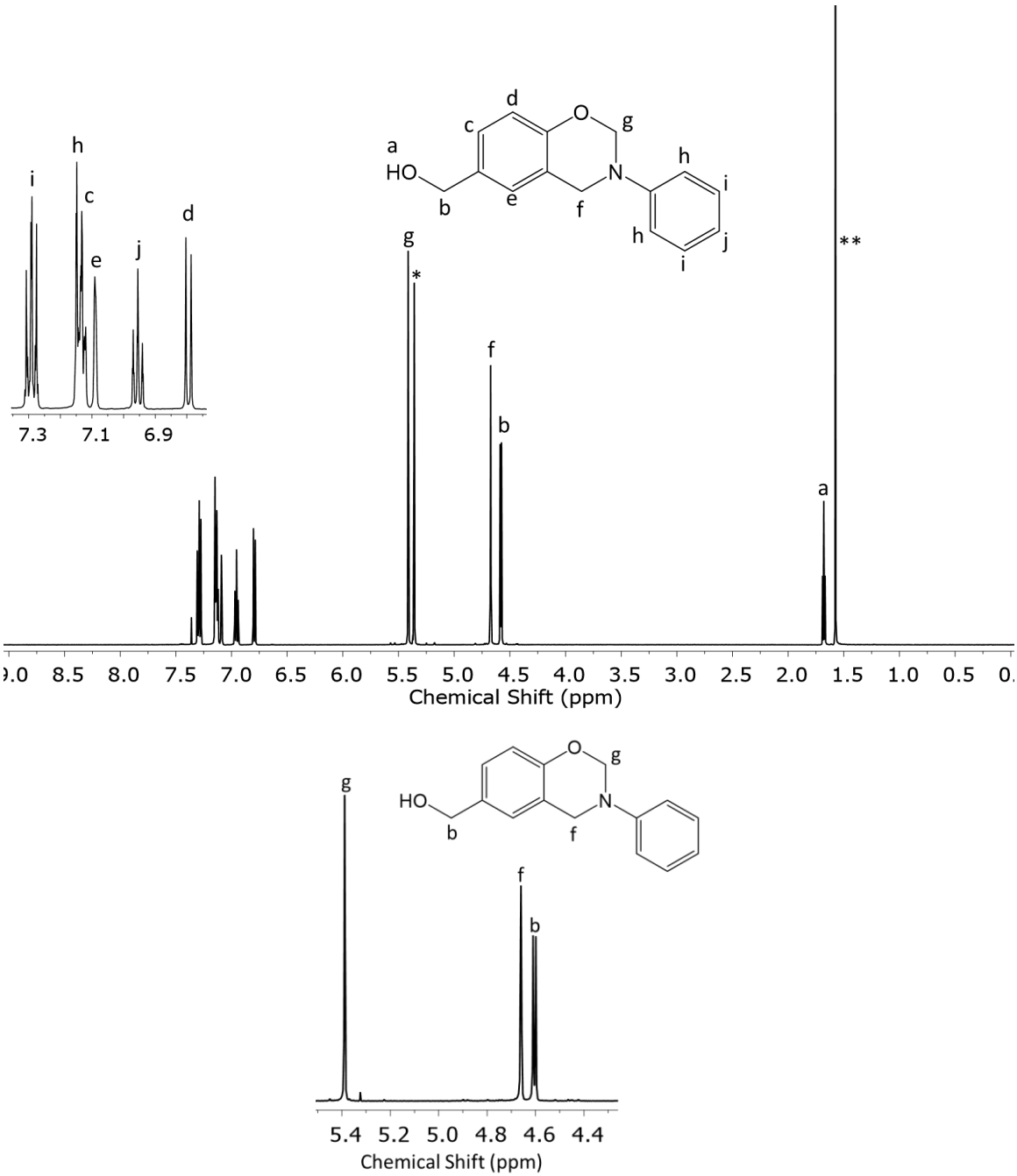

Figure 4.2. The ^{1}H NMR spectra (500 MHz) of *p*HBA-a in (a) DCM-d2 to provide characterization of the aromatic region and in (b) $CDCl_3$ to characterize the methylene groups. **Methylene chloride*; ***water*.

In the ^{1}H NMR spectrum of *p*HBA-a in Figure 4.2a, the aromatic region is resolved allowing for the assignment of the aromatic protons within the structure. The characteristic peaks of the oxazine ring are

also observable at 5.37 and 4.63 ppm (Figure 4.2b). The integral value of each signal has the expected value for 2 hydrogens. In this range, the methylene from the *p*-hydroxybenzyl alcohol is also present at 4.54 ppm and also integrates to 2 hydrogens. For these three signals, the 2:2:2 ratio confirms that the synthesis and purification/isolation of the *p*HBA-a proceeds without contamination by starting materials. Interestingly, this methylene has a doublet splitting pattern in both spectra and the adjacent hydroxy at 1.56 ppm (Figure 4.2a) displays a corresponding triplet pattern. Such a pattern is present in similar compounds.[240]

Scheme 4.2. The synthesis of $mPEGOTs_{500}$ from $mPEGOH_{500}$

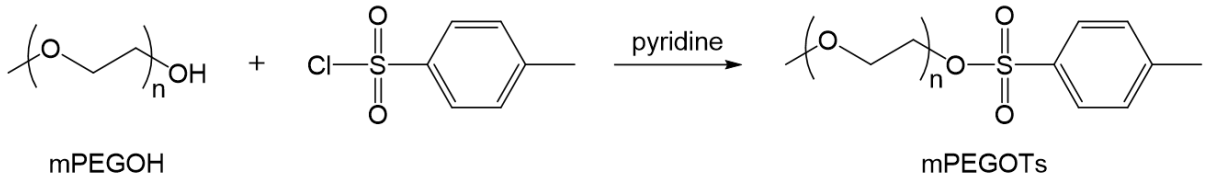

As in chapter 3, tosylation of the polymer proceeds in the presence of a weak base. Due to the chain length of these polymers, it is necessary to have the head group in a large molar excess. This excess of tosylate provides a challenge in its purification due to its two main contaminants present after the synthesis: the remaining unreacted *p*-toluenesulfonyl chloride, and the side production *p*-toluenesulfonic acid. The *p*-toluenesulonic acid (HOTs), as previously discussed, is a well-established accelerant for benzoxazine and should be absent in isolated material to avoid polymerizing the benzoxazine head group or the micellar structures.[20,21,24,25] Therefore the purification of the $mPEGOTs_{500}$ is critical in order to avoid the HOTs contaminant that may result in the curing of the *p*HBA-a during the synthesis of the surfactant.

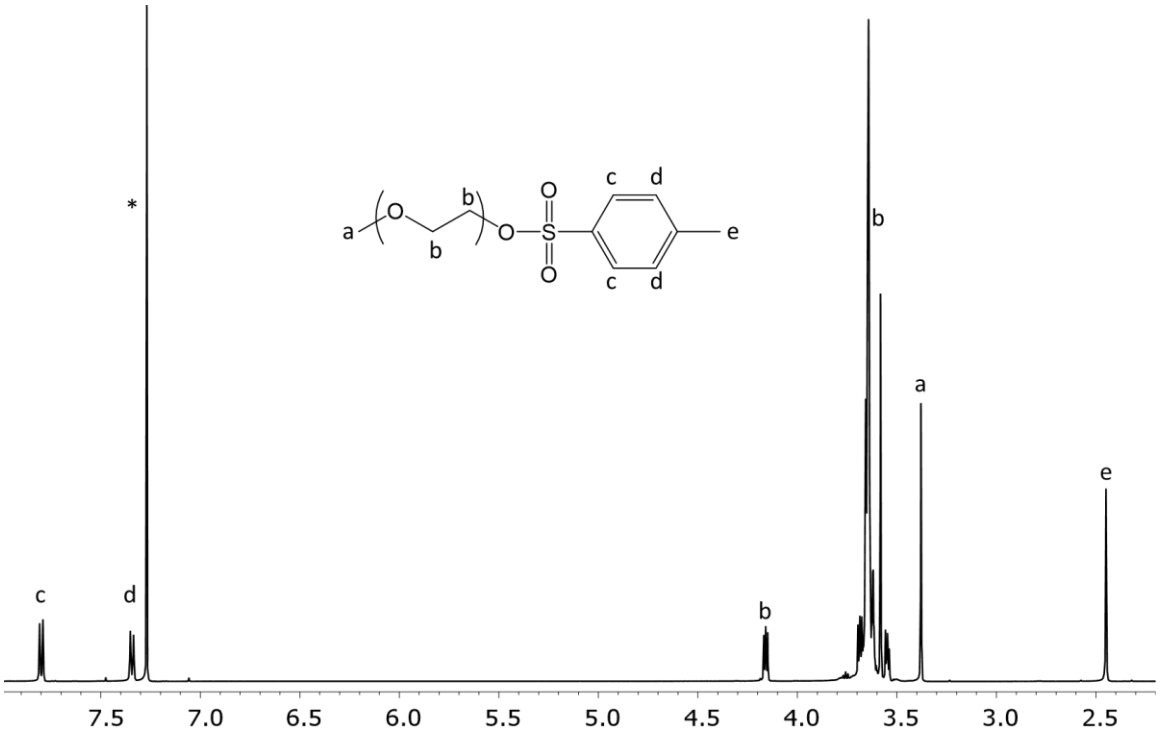

Figure 4.3. The ^{1}H NMR spectrum (500 MHz, $CDCl_3$) of mPEGOTs$_{500}$. **Chloroform*

In Figure 4.3, the spectrum of mPEGOTs$_{500}$ clearly shows the repeat unit ethylene oxide signals of PEG at 3.80-3.48 ppm, the peak labeled as *b* at 4.16 ppm corresponds to the ethylene oxide adjacent to the tosylate end group. The peaks in the aromatic region at 7.80 and 7.34 ppm, with a 2:2 integral ratio, confirms the presence of the product as the shift is similar to that of aklyl tosylates.[241] The *p*-toluenesulfonyl chloride typically has aromatic signals at 7.90 and 7.40 ppm, and equivalent signals from HOTs would appear at 7.80 and 7.30 ppm (See Appendix C, Figures C1 and C2). No such signals are found in the ^{1}H NMR spectrum of mPEGOTs$_{500}$. Furthermore, the signal for the methoxy end group, peak *a* at 3.38 ppm, integrates to 3 hydrogens, the 2:2:3 ratio of peaks *c*:*d*:*a* confirms there are no starting material contaminates from either the tosylate or the PEG.

Scheme 4.3. Reaction for mPEGpHBA-a from mPEGOTs and *p*HBA-a

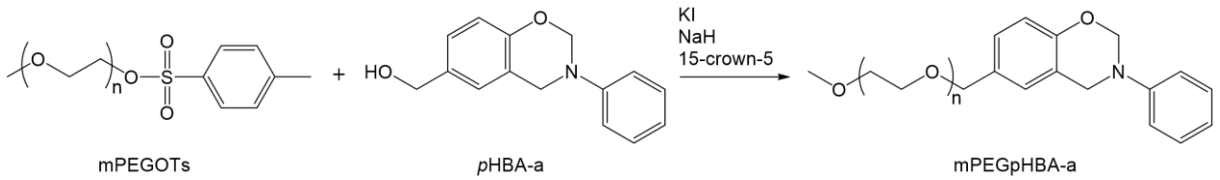

The replacement of the tosylate end group of PEG with *p*HBA-a required a specific set of reaction conditions. The presence of the of the strong NaH base, solubilized by 15-crown-5, helped to deprotonate the hydroxy of the *p*HBA-a in order to promote the nucleophilic attack of the alkoxide onto the *α* carbon to the tosylate of the mPEGOTs. The KI helped to detosylate the mPEGOTs via a Finkelstein reaction.[242-244]

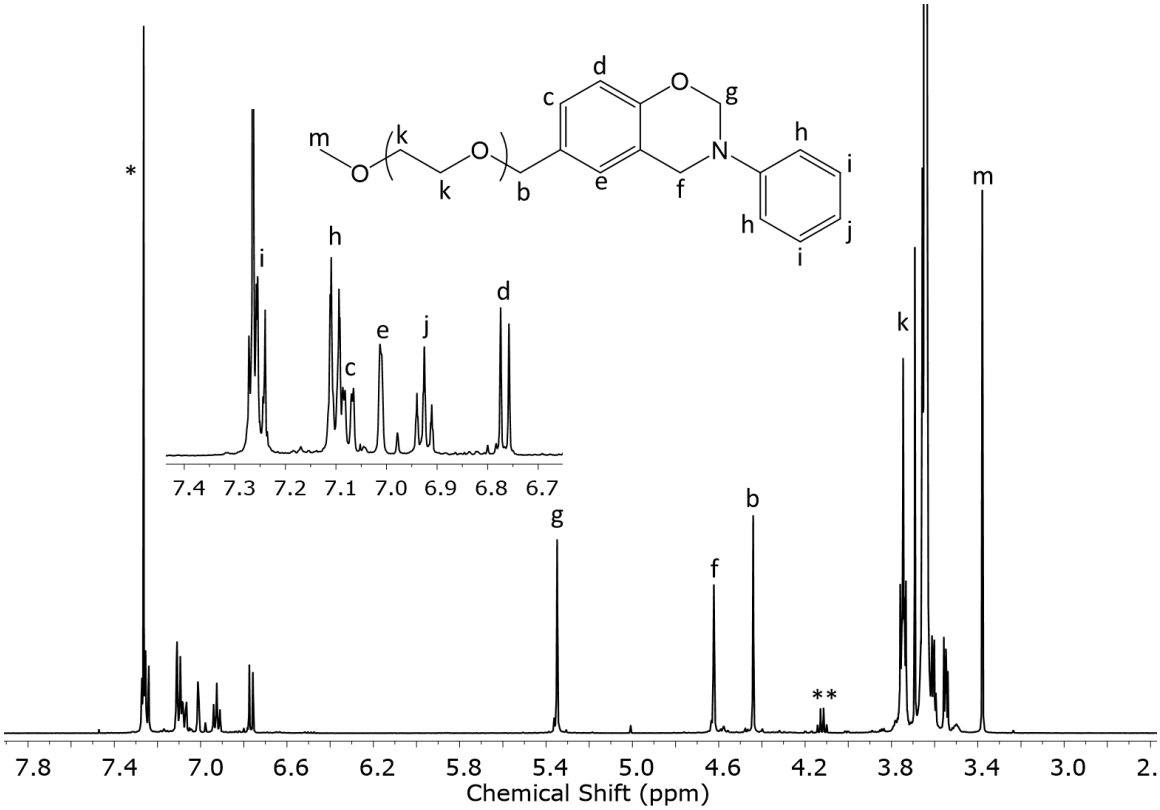

Figure 4.4. Representative ^{1}H NMR spectrum (500 MHz, $CDCl_3$) of the surfactant, mPEGpHBA-a_{900}. **Chloroform*; ***ethyl acetate*.

In Figure 4.4, the ^{1}H NMR spectrum displays all the signals for the PEG and the benzoxazine group. Most noticeable is the shift of peak *b*, the benzylic protons of the *p*HBA-a head group, from 4.54 to 4.44 ppm. This shift is present in all of the surfactant ^{1}H NMR spectra (Figures C3 and C4). After pegylation of the methylol, oxygen becomes less electron withdrawing and the methylene becomes more shielded and its signal shifts upfield. The integration of peaks *g*, *f*, *b*, and *m* have a ratio of 2:2:2:3, by ^{1}H NMR there are no starting material contaminant. There was a striking difference in purity by ^{1}H NMR of the three

surfactants. The mPEGpHBA-a_{900} was the most pure by ^{1}H NMR at 81 %, with purities of mPEGpHBA-a_{500} and mPEGpHBA-a_{2000} at about 75 %, mPEGpHBA-a_{2000} having excess head group impurities.

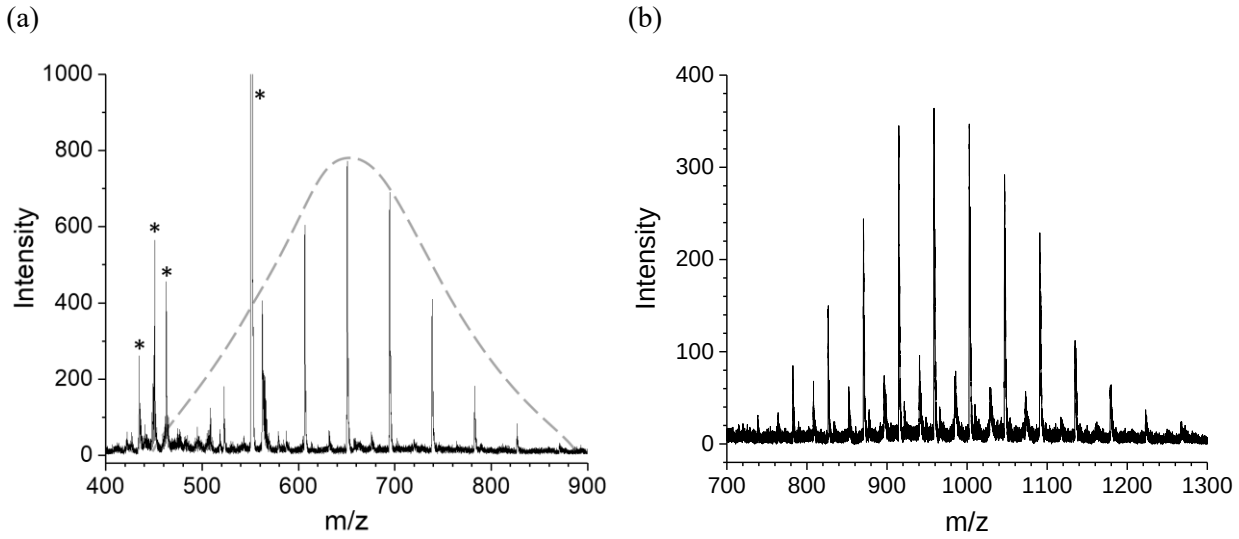

Figure 4.5. MALDI spectra of both (a) mPEGpHBA-a_{500} and (b) mPEGpHBA-a_{900}. In (a) the peaks belonging to the surfactant are outlined with the dashed line. *Artifacts from the α-cyano-4-hydroxycinnamic acid and 2,5-dihydroxybenzoic acid matrices at 650, 552, 462, 450, and 434 m/z.

The MALDI spectra in Figure 4.5 show a typical pattern for polymers with a peak distance of 44 m/z, the mass of the PEG repeat unit. In Figure 4.5a, the spectrum also contains signals from artifacts of the matrix at 552, 462, 450, and 434 m/z. The mPEGpHBA-a_{500} has its distribution centered at 650 m/z, in this case a mPEGpHBA-a with a degree of polymerization of 8 complexed with a Na^+ ion. The spectrum of mPEGpHBA-a_{900} shows two distributions within the 700-1300 m/z range, both have a 44 m/z peak distance indicating that both of these distributions are PEG polymers and are not from the polymerization of the benzoxazine head group. The distribution with a relatively higher intensity is centered at 958 m/z corresponding to a mPEGpHBA-a with a degree of polymerization of 15 complexed with a Na^+ ion. The relatively lower distribution is centered at 940 m/z which suggests the presence of a methoxypoly(ethylene glycol) contaminant that is likely a byproduct from the surfactant synthesis or a

contaminant in the starting material. By MALDI, the mPEGpHBA-a_{500} is significantly more pure than the mPEGpHBA-a_{900}.

4.3.2 Comparison of surfactant loading.

(a) (b)

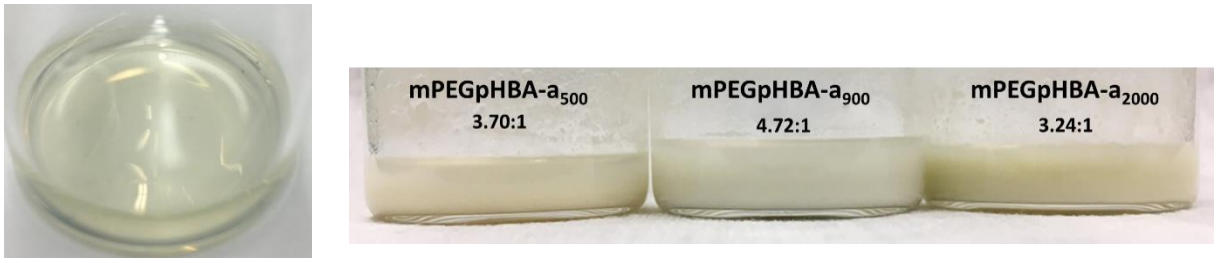

Figure 4.6. Pictures of (a) unloaded micelles of mPEGpHBA-a_{900} in nanopore water and (b) the loaded micelles of all three PEG-based surfactants with their monomer to surfactant mass loading ratios.

The solution containing the empty micelles exhibits minor scattering of light (Figure 4.6a), indicating the presence of small particles suspended in solution. After benzoxazine has been loaded into the solutions they turn cloudy white (Figure 4.6b), indicating much larger particles in suspension.

Table 4.1. The diameter, polydispersity index (PD), and mass loading of monomer of the three PEG-based surfactants determined by DLS.

	Unloaded Micelles		Loaded Micelles		
Surfactant	Diameter (nm)	PD	Diameter (nm)	PD	Monomer/surfactant by mass
mPEGpHBA-a_{500}	78.2	0.125	160.6	0.454	3.70
mPEGpHBA-a_{900}	108.0	0.187	1545.1	0.219	4.72
mPEGpHBA-a_{2000}	33.6	0.277	1813.6	0.731	3.24

In all surfactant solutions, the diameter of the micelles increases after loading with benzoxazine monomer. For mPEGpHBA-a_{2000}, the diameter ratio of the loaded to unloaded micelles is about 55 (Table

4.1). The diameter of the loaded micelles of the three surfactants increases with growing surfactant tail length despite the mPEGpHBA-a_{2000} having the smallest unloaded micelle diameter. It appears that larger loaded micelles result from surfactants with longer PEG tails. The longer tail of the mPEGpHBA-a_{2000} assumes a larger volume, resulting in a greater interfacial volume and a smaller internal diameter (Figure 4.7). The mPEGpHBA-a_{500} and mPEGpHBA-a_{900} have a similar tail length and a similar unloaded diameter. The larger diameter values of the loaded micelles favored by increased tail length may indicate that the large chain lengths are necessary to suspend larger particles. Loaded micellar particles assembled from smaller surfactants quickly destabilize and form precipitate.

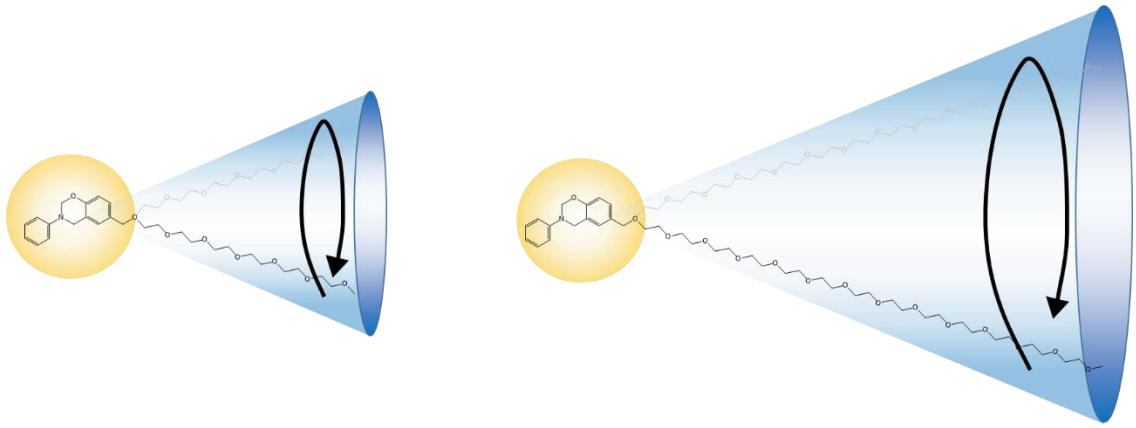

Figure 4.7. The difference in interfacial volume of surfactants with differing tail lengths.

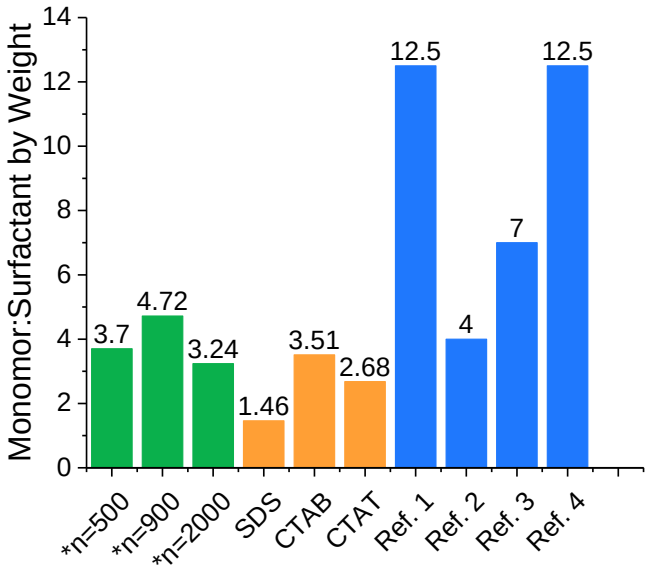

Figure 4.8. Performance of the synthesized surfactants in this work (green) compared to commercially available surfactants (orange) and benzoxazine-based surfactants from literature (blue). *mPEGpHBA-a_n

Ref 1. Sawaryn, C.; et al. *Macromolecules* **2011**, *44*, 5650-5658.[96]
Ref 2. Van, A.; et al. *Polymer* **2014**, *55*, 1443-1451.[59]
Ref 3. Ambrožič, R.; et al. *eXPRESS Polym. Letters* **2014**, *8*, 574-587.[60]
Ref 4. Chiou, K.; et al. *Macromolecules* **2014**, *47*, 3297-3305.[235]

The mPEGpHBA-a surfactants synthesized in this work load benzoxazine more effectively than commercial surfactants. All three outperformed SDS and CTAT, but only the mPEGpHBA-a_{900} and mPEGpHBA-a_{500}, the two most pure of the three, outperformed the CTAB. It is possible that the remaining head group impurities fill the formed micelles in mPEGpHBA-a_{2000} and interfere with further loading. All four literature examples had better monomer loading than the commercial surfactants and three performed better than all three mPEGpHBA-a surfactants. These surfactants all have poly(propylene oxide) (PPO) segment closest to the benzoxazine group. The PPO polymer is slightly more nonpolar compared to that of the PEG and may help with loading the monomer.[245]

(a)

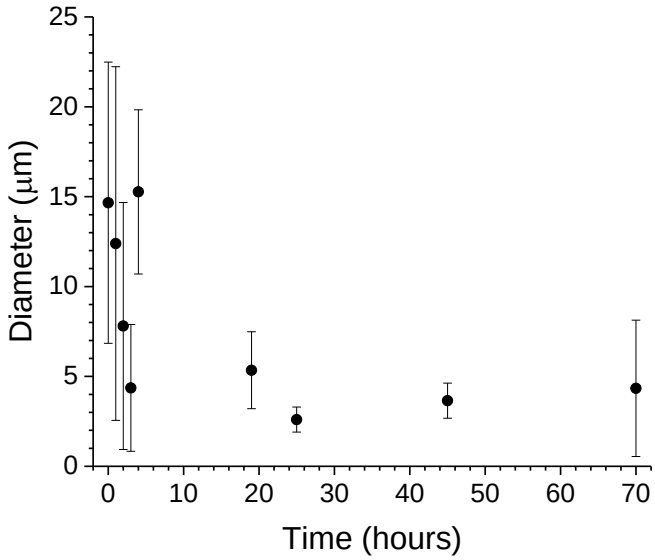

(b)

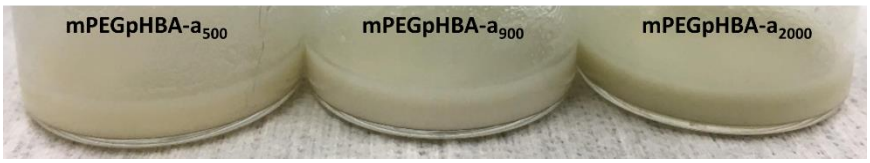

Figure 4.9. (a) Changing micelle diameter over time for the loaded mPEGpHBA-a_{900} micelle and the (b) micelle solutions at 100 hours, all solutions were loaded at a monomer to surfactant mass ratio of 1.5.

In Figure 4.9a the loaded micelle diameter starts very large, near 15 μm, but over the first few hours it decreases in size quickly to 4 μm. After the first 4 hours, it remains near constant for several days. The emulsions during this time remain white and turbid, displaying a suspension of large monomer particles in solution. The initial decrease in size is likely due to the release of excess monomer until the micelles reach their optimal size. It may also be due to the formation of larger precipitates, leaving only loaded micelles near 4 μm in suspension.

4.3.3 Co-polymerization of surfactants with monomer.

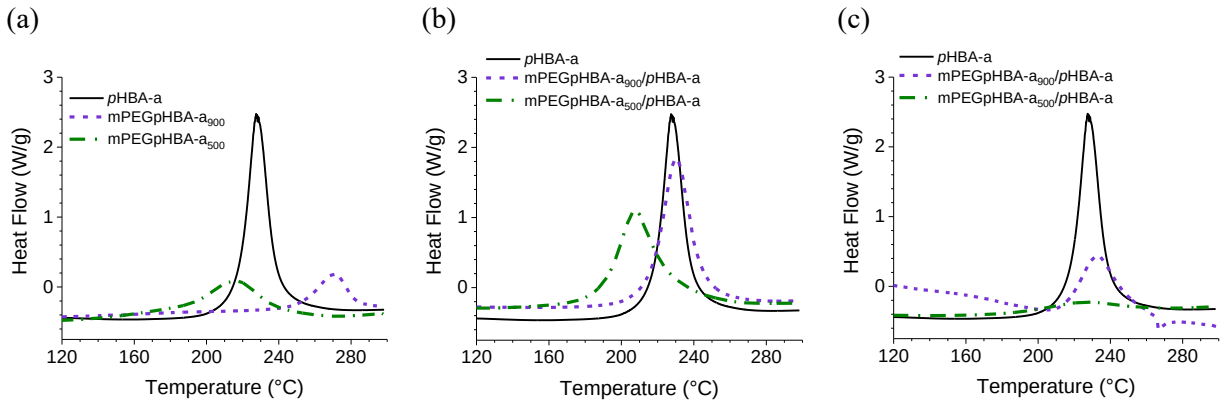

Figure 4.10. First heat scans from DSC of the (a) neat surfactants and *p*HBA-a, (b) surfactants blended with *p*HBA-a, and (c) lyophilized micelles of surfactants loaded with *p*HBA-a.

In each of the three DSC studies in Figure 4.10 the surfactants behave very differently. Both mPEGpHBA-a_{500} and mPEGpHBA-a_{900} cure at very different temperatures. The mPEGpHBA-a_{500} cures at a lower temperature than the mPEGpHBA-a_{900}. The neat mPEGpHBA-a_{500} has and onset and peak exotherm temperature of 181 and 216 °C, which is lower than pure *p*HBA-a which has an onset and peak cure exotherm temperature at 218 and 227 °C. The reduction in cure temperature may be from any small contaminants from the synthesis of the surfactant. The pure mPEGpHBA-a_{900} cures at the highest temperature of the three with an onset and peak temperature at 251 and 270 °C. The mPEGpHBA-a_{900} cures much higher likely due to the presence of more PEG and the possible PEG contaminant that would further impeded the cure as was discovered in chapter 2 with mPEGOH. The onset and peak exotherm temperature of both the blend and lyophilized micelles of mPEGpHBA-a_{500} are similar to those of the pure *p*HBA-a. This is likely due to the good miscibility of the two. These blends are also monomodal which is indication of co-polymerization of the surfactant with the loaded monomer. The blend of the mPEGpHBA-a_{500} with *p*HBA-a had a reduced temperature of cure compared to pure *p*HBA-a, with similar cure temperatures to that of pure mPEGpHBA-a_{500}. In both blends it seems the cure is initiated by the component with a lower curing temperature.

4.3.4 Alternative synthesis approach. The coupling of mPEGOTs to the *p*HBA-a head group synthesis suffers from impurities in the remaining product after running through a silica column. Such a purification process already impedes the ability to produce this surfactant at high volume for industry use. To increase the yield and reduce any need for rigorous purification, a second synthesis of the target molecule was studied. Instead of pursuing a coupling method, the hydrophilic polymer tail was grown from the head group with allyl glycidyl ether monomer.

Scheme 4.4. Polymerization of allyl glycidyl ether with *p*HBA-a

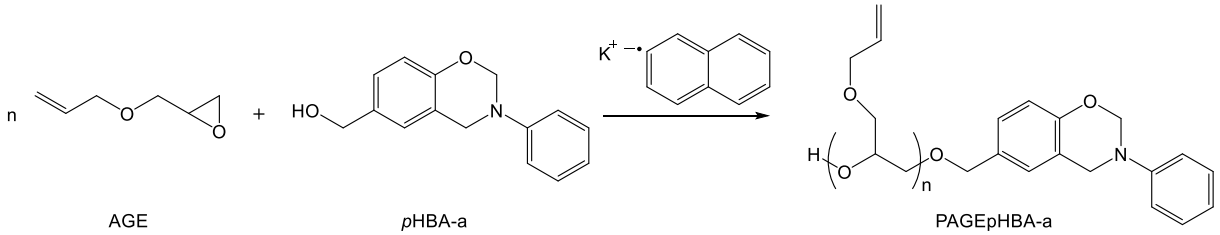

The epoxy of the allyl glycidyl ether (AGE) can undergo a ring opening polymerization (ROP) similarly to benzoxazine. Typically the polymerization of AGE into poly(allyl glycidyl ether) (PAGE) at room temperature will be initiated by an alkoxide.[245] The deprotonation of the an alcohol initiator can be promoted by a strong nucleophile such as potassium naphthalenide or cesium hydroxide.[246,247] However, epoxy has been co-polymerized with benzoxazine,[248,249] this polymerization is done at room temperature which should avoid any ROP of the benzoxazine head group. The ROP of epoxy in this reaction is an anionic ROP unlike benzoxazine which polymerizes through a cationic ROP, this also reduces the prospect of co-polymerization of the *p*HBA-a head group.

(a)

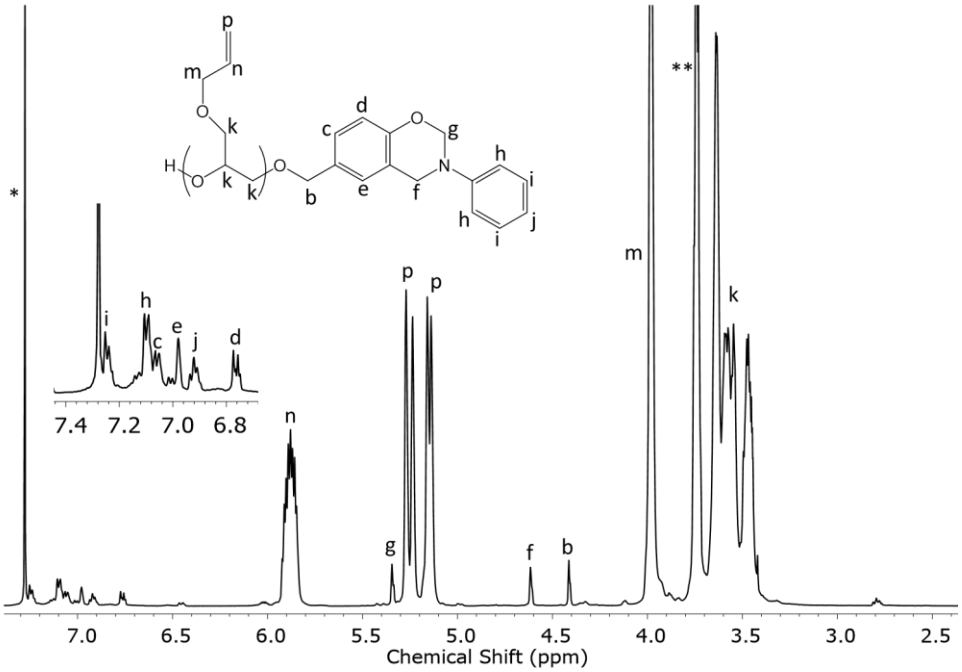

(b)

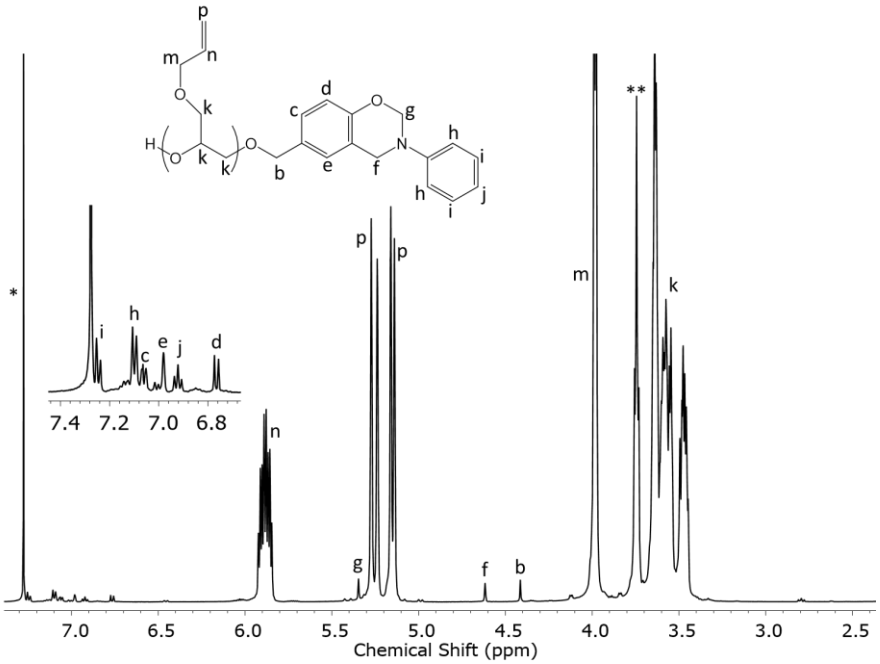

Figure 4.11. ^{1}H NMR (500 MHZ, $CDCl_3$) of PAGE surfactant with the addition of (a) 1 g of AGE or (b) 4 g of AGE during the synthesis. **Chloroform*; ***tetrahydrofuran*.

In both the spectra in Figure 4.11 the signals for PAGE and *p*HBA-a are apparent. Again there is a shift of peak *b*, the methylene of the *p*HBA-a, from 4.54 to 4.41 ppm, confirming the presence of the PAGEpHBA-a product. There is a noticeably higher ratio of PAGE signal to *p*HBA-a signal in the spectra from the product of the synthesis with 4 g of AGE. The increased AGE content should correlate to a larger PAGE tail. By ^{1}H NMR, the doublets corresponding to the primary alkene in the repeat unit of PAGE at 5.25 and 5.15 ppm (peak *p*) compared to the isolated methylenes of the *p*HBA-a head group (peaks *f* and *b*) should yield an estimation of the length of the PAGE tail. In Figure 4.11a, the PAGEpHBA-a product has a degree of polymerization of about 41. In Figure 4.11b, by the same comparison yields a degree of polymerization of 115.

Unfortunately, the PAGE polymer has a low affinity to water and is unable to host any *p*HBA-a monomer. However, the chemistry of an epoxy ROP with a *p*HBA-a initiator has been established without any polybenzoxazine side products. The same reaction can be repeated with an alternative epoxy monomer with a higher hydrophilicity. Many small epoxy monomers are typically gases or very reactive, making them difficult to work with. However, glycidyl methyl ether (GME) (Scheme 4.5) is proposed as a promising alternative to the AGE. Like AGE, GME is also a liquid at room temperature, is commercially available, and can feasibly be handled. The polymer of GME will have less alkyl content and will have better water solubility.[250]

Scheme 4.5. Polymerization of glycidyl methyl ether with *p*HBA-a

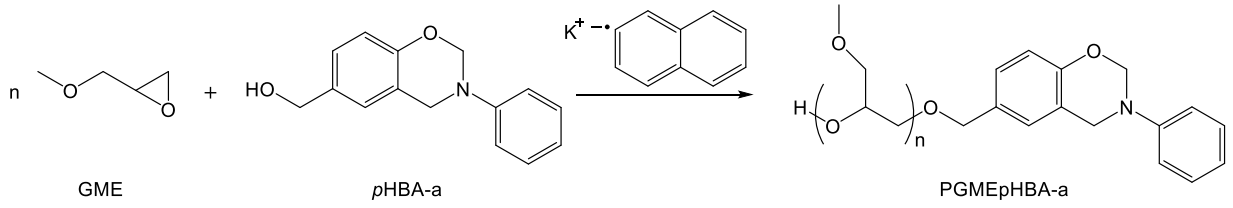

4.4 Conclusions

Within this chapter the successful synthesis of a benzoxazine/PEG-based surfactant is described from the coupling of tosylated PEG onto *p*-hyrdoxybenzyl alcohol based benzoxazine monomer. The benzoxazine termination of PEG was confirmed with ^{1}H NMR and MALDI. The surfactants had comparable benzoxazine loading values to other literatures surfactants with up to 4.72 g of monomer per 1 g of surfactant in the case of the mPEGpHBA-a_{900}. This loading also exceeded that of commercial surfactants prepared with the same method. Micelle diameter was observed to increase with increased length of the PEG tail as expected. This tunable micelle size is beneficial to the resin infiltration into woven fiber composites. The loaded micelles had a long shelf life up to several days, retaining decent monomer loading and enlarged micelle diameter of about 50x the diameter of the unloaded micelle. An alternative synthesis approach was studied to access similar surfactants with higher yields. This surfactant was synthesized from the initiation of the polymerization of allyl glycidyl ether with a benzoxazine monomer without formation of polybenzoxazine. This polymerization widens the scope of *p*HBA-a and synthesis of surfactants with the potential to initiate glycidyl methyl ether for a more hydrophilic surfactant.

Chapter 5: Conclusions

Benzoxazines are a rapidly growing area in thermoset research and offer a wide scope of applications and chemistries. While previous research has characterized many thermoplastic or polymer blends with benzoxazine and polybenzoxazine, this work expands the versatility of these blends by defining and confirming the concept for generating novel polymer grafted polybenzoxazine and composite hybrids from end group functionalized polymer. The effects of tosylated blend components was explored with a range of additives with differing mechanical, thermal, and FST (flame, smoke, toxicity) properties, each imparting unique features onto the polymerized material. Three tosylated polymers and one particle were either purchased or synthesized; PEG, PSU, PDLLA, and amorphous silica microparticles. All tosylated series showed reduced polymerization temperatures by DSC and good homogeneity in all tosylated polymer blends. The applications and processing of benzoxazines are further developed with the synthesis of water-soluble benzoxazine-based surfactants capable of stabilizing a benzoxazine monomer in aqueous emulsions.

Blends of BA-a with methoxypoly(ethylene glycol) (mPEG) with either hydroxy or tosylate terminals were investigated. Materials from each of these blend series had distinctly different thermal and mechanical properties. Miscibility of BA-a in PEG was determined by quantifying the percent crystallinity in phase separated mPEG. By DSC, the mPEGOH blends were found to be miscible up to 40 wt % PEG and the mPEGOTs were miscible up to 50 or 60 wt %. The molecular weight effects were thought to be the cause of decreased miscibility in the $mPEGOTs_{2000}$ blends from the $mPEGOTs_{900}$ blends. From the same DSC scans, there was also a noticeable reduction in the curing temperature in the mPEGOTs blends from the evolution of the tosylate end group, the acid of which is a known BA-a cure accelerant. The onset of cure in the $mPEGOTs_{900}$ blends was found to be as low as 151 °C at 80 wt % PEG. However the addition of non-polymerizable content to the BA-a did not benefit the cure of BA-a in the mPEGOH blends. While the onset of cure for the mPEGOH remained near constant, the peak cure temperature increased by nearly 20 °C at the same weight loading of PEG. Furthermore, the enthalpy of

the exotherm of the mPEGOTs blends was much higher than predicted for the enthalpy of cure of the content of BA-a in each blend. The mPEGOH blends followed the expected trend in enthalpy from BA-a content. The increased enthalpy, as well as the greater miscibility of the cured mPEGOTs blends determined from FTIR, XRD, and the Gordon-Taylor trending glass transition temperature, confirms the formation of a grafted network denoted as P(BA-a)-*graft*-mPEGOTs. This grafted material was investigated by scanning electron microscopy. After a solvent extraction, voids were found in the cured mPEGOH blend samples, where unbound mPEG was once located. The mPEGOTs analogues show a noticeable shift to a material free of voids with a smoother surface. This characteristic dominated blends at the miscibility threshold of 50 wt %. This smooth surface was the result of grafted mPEG that was unable to be extracted.

While the PEG improves the handling of BA-a, two alternative polymers were selected, one more chemically sensitive and one more robust with good FST properties, PDLLA and PSU. Tosylated silica was also studied to represent the more extreme scenario of chemical and mechanical stability. All three series of tosylated additives had a reduced curing temperature, SiOTs of which had the lowest curing temperatures near 135 °C. The PSUOH blends were the only blend to increase the curing temperature which had a much more significant effect than the mPEGOH blends. Neither SiOH nor PDLLAOH increased the curing temperature. The PDLLAOH blends had a similarly reduced cure to their PDLLAOTs analogues, this was likely from the cleavage at the ester in PDLLA at the elevated temperature resulting in the exposure of the carboxylic acid to the BA-a phase. Carboxylic acids, like adipic acid, are known accelerants for benzoxazine polymerization and are the likely cause of the reduced polymerization temperature in the PDLLA blends.[172]

There was an excess of enthalpy of the PSUOTs blends as was seen in the mPEGOTs blends. This increased enthalpy during the cure is also likely due to the grafting of the polymer onto the polybenzoxazine network, which was possible on both terminals of PSU. This grafting mechanism is supported by the improved homogeneity of the PSUOTs blend films from the PSUOH blend films. Free-

standing films of cured PSUOTs and PBA-a with a ratio of 80:20 exhibited higher modulus as a result of the increased crosslinking/bonding between the PBA-a and PSU. Additionally, there was a smaller error in the tensile modulus measurements in the PSUOTs films which is likely a consequence of increased homogeneity throughout the films.

All three of the polymer blends with BA-a offer new applications for benzoxazine. The films of the PSUOTs blends benefit from the addition of the benzoxazine monomer, showing a greater tensile modulus at the 80 wt % PSU than that of pure PSUOTs. This novel grafted material with improved modulus could serve multiple applications including fuel cell membranes as PSU becomes more widely used in this area.[251-253] The degradation of PDLLA in benzoxazine can improve the disposal and reduce waste of composite materials, but may also improve the recyclability of benzoxazine as they become easier to mill and use as additives in other materials.

Despite the tosylate on the silica being attached by the phenyl, which would negate any grafting of PBA-a to the silica, there was a noticeably unique morphology between the SiOTs and SiOH blends observed by SEM analysis. The SiOTs particles were better integrated and less distinguishable from the PBA-a phase, this was likely due to the immobilized tolylsulfonate groups located at the surface of the SiOTs particles, which act as local cure accelerants for BA-a. This results in a PBA-a shell, likely rich in the thermodynamic phenolic PBA-a structure, forming tightly around the particle. The shell of PBA-a may better compatibilize the surrounding PBA-a material. Both blends of SiOTs and SiOH microparticles showed decently improved modulus at high mass loading, both more than doubling the storage modulus at 30 °C relative to pure PBA-a. The SiOTs blends also had a wider compositional range for materials exhibiting improved storage modulus.

Benzoxazine based surfactants for creating water-based formulations were synthesized from the pegylation of the benzene ring of *p*HBA-a. This synthesis was also successful with mPEG of three different molecular weights. The mPEGpHBA-a_{2000} had minor head group impurities determined by ^{1}H

NMR and the mPEGpHBA-a_{900} had $mPEGOH_{900}$ impurities determined by MALDI. The further purification of these surfactants may be accomplished by dialysis. The termination of the mPEG by *p*HBA-a was confirmed by both ^{1}H NMR in all three and MALDI in the two lower molecular weight surfactants. All three had high monomer loading values, the mPEGpHBA-a_{900} had the highest loading capacity of 4.72 monomer/surfactant by mass. Both mPEGpHBA-a_{900} and mPEGpHBA-a_{500} also had better loading of benzoxazine monomer than other commercial surfactants (CTAB, CTAT, or SDS). We hypothesize that the enthalpy of mixing of BA-a into a micelle with a benzoxazine core is beneficial for loading and stability. The mPEGpHBA-a_{900} emulsion was very stable up to several days determined by DLS. When either the mPEGpHBA-a_{500} or mPEGpHBA-a_{900} were cured with benzoxazine monomer, their exothermic profile in the DSC scan assumed a similar shape and polymerization temperature to that of the pure monomer. These exotherms were monomodal in both cases suggesting a complete co-polymerization of the surfactant with monomer. Not only do these surfactants improve the environmental impact benzoxazine processing has, but similar benzoxazine-based surfactants have already been used for xerogels, films, and coatings with benzoxazine monomer.[60,96,235,236,254]

In an effort to establish a larger scale route to similar benzoxazine-based surfactants, the initiation of the polymerization of allyl glycidyl ether by a benzoxazine monomer, *p*HBA-a, was demonstrated. The attachment of the *p*HBA-a head group onto the polymer was determined by ^{1}H NMR. The signals at 5.35 and 4.62 ppm from the still intact oxazine were present and there were no signals corresponding to the ROP products of benzoxazine, therefore there was no co-polymerization between the epoxy and the benzoxazine. Such chemistry can be applied to the polymerization of a more hydrophilic epoxy based polymers such as glycidyl methyl ether or ethylene oxide. This polymerization route to benzoxazine-based surfactants should yield pure, easily tunable, and water-soluble benzoxazine-based surfactants in high quantities that are relevant to industrial processes.

Works Cited

1. Holly, F. W.; Cope, A. C. Condensation Products of Aldehydes and Ketones with o-Aminobenzyl Alcohol and o-Hydroxybenzylamine. *J. Am. Chem. Soc.* **1944**, *66*, 1875-1879.
2. Higginbottom, H. P. Polymerizable compositions comprising polyamines and poly(dihydrobenzoxazines). 4,501,864, Feb. 26, 1985.
3. Ning, X.; Ishida, H. Phenolic materials via ring-opening polymerization: Synthesis and characterization of bisphenol-A based benzoxazines and their polymers. *J. Polym. Sci., Part A: Polym. Chem.* **1994**, *32*, 1121-1129.
4. Ishida, H. In *Handbook of Benzoxazine Resins*; Ishida, H., Agag, T., Eds.; Elsevier: Amsterdam, 2011, p 3-81.
5. Benzoxazines www.huntsman.com (August 6, 2018).
6. Alhwaige, A. A.; Ishida, H.; Qutubuddin, S. Carbon Aerogels with Excellent CO_2 Adsorption Capacity Synthesized from Clay-Reinforced Biobased Chitosan-Polybenzoxazine Nanocomposites. *ACS Sustainable Chem. Eng.* **2016**, *4*, 1286-1295.
7. Schäfer, H.; Hartwig, A.; Koschek, K. The nature of bonding matters: Benzoxazine based shape memory polymers. *Polymer* **2018**, *135*, 285-294.
8. Bălănucă, B.; Raicopol, M.; Maljusch, A.; Garea, S.; Hanganu, A.; Schuhmann, W.; Andronescu, C. Phenolated Oleic Acid Based Polybenzoxazine Derivatives as Corrosion Protection Layers. *ChemPlusChem* **2015**, *80*, 1170-1177.
9. Arslan, M.; Kiskan, B.; Yagci, Y. Benzoxazine-Based Thermosets with Autonomous Self-Healing Ability. *Macromolecules* **2015**, *48*, 1329-1334.
10. Arslan, M.; Kiskan, B.; Yagci, Y. Recycling and self-healing of polybenzoxazines with dynamic sulfide linkages. *Sci. Rep.* **2017**, *7*, 5207.
11. Arslan, M.; Motallebzadeh, A.; Kiskan, B.; Demirel, A. L.; Kumbaraci, I. V.; Yagci, Y. Combining benzoxazine and ketene chemistries for self-healing of high performance thermoset surfaces. *Polym. Chem.* **2018**, 2031-2039.
12. Kiskan, B. Adapting benzoxazine chemistry for unconventional applications. *React. Funct. Polym.* **2017**.
13. Brunovska, Z.; Liu, J. P.; Ishida, H. 1,3,5-Triphenylhexahydro-1,3,5-triazine-active intermediate and precursor in the novel synthesis of benzoxazine monomers and oligomers. *Macromol. Chem. Phys.* **1999**, *200*, 1745-1752.
14. Chen, W.; He, J.; Li, L. Characterization of polybenzoxazine and its electrochemical polymerization mechanism. *Front. Chem. China* **2009**, *4*, 390.
15. Chutayothin, P.; Ishida, H. Cationic Ring-Opening Polymerization of 1,3-Benzoxazines: Mechanistic Study Using Model Compounds. *Macromolecules* **2010**, *43*, 4562-4572.
16. Wang, Y. X.; Ishida, H. Cationic ring-opening polymerization of benzoxazines. *Polymer* **1999**, *40*, 4563-4570.
17. Andreu, R.; Reina, J. A.; Ronda, J. C. Studies on the thermal polymerization of substituted benzoxazine monomers: Electronic effects. *J. Polym. Sci., Part A: Polym. Chem.* **2008**, *46*, 3353-3366.
18. Liu, C.; Chen, Q. Y. In *Advanced and Emerging Polybenzoxazine Science and Technology*; Froimowicz, P., Ed.; Elsevier: Amsterdam, 2017, p 9-21.
19. Oie, H.; Mori, A.; Sudo, A.; Endo, T. Synthesis of networked polymer based on ring-opening addition reaction of 1,3-benzoxazine with resorcinol. *J. Polym. Sci., Part A: Polym. Chem.* **2012**, *50*, 4756-4761.

20. Liu, C.; Shen, D.; Sebastián, R. M.; Marquet, J.; Schönfeld, R. Catalyst effects on the ring-opening polymerization of 1,3-benzoxazine and on the polymer structure. *Polymer* **2013**, *54*, 2873-2878.
21. Sudo, A.; Kudoh, R.; Nakayama, H.; Arima, K.; Endo, T. Selective Formation of Poly(N,O-acetal) by Polymerization of 1,3-Benzoxazine and Its Main Chain Rearrangement. *Macromolecules* **2008**, *41*, 9030-9034.
22. Soto, M.; Hiller, M.; Oschkinat, H.; Koschek, K. Multifunctional Benzoxazines Feature Low Polymerization Temperature and Diverse Polymer Structures. *Polymers* **2016**, *8*, 278.
23. Ishida, H.; Rodriguez, Y. Catalyzing the curing reaction of a new benzoxazine-based phenolic resin. *J. Appl. Polym. Sci.* **1995**, *58*, 1751–1760.
24. Sudo, A.; Hirayama, S.; Endo, T. Highly efficient catalysts-acetylacetonato complexes of transition metals in the 4th period for ring-opening polymerization of 1,3-benzoxazine. *J. Polym. Sci., Part A: Polym. Chem.* **2010**, *48*, 479-484.
25. Sudo, A.; Yamashita, H.; Endo, T. Ring-opening polymerization of 1,3-benzoxazines by p-toluenesulfonates as thermally latent initiators. *J. Polym. Sci., Part A: Polym. Chem.* **2011**, *49*, 3631-3636.
26. Sun, J.; Wei, W.; Xu, Y.; Qu, J.; Liu, X.; Endo, T. A curing system of benzoxazine with amine: reactivity, reaction mechanism and material properties. *RSC Adv.* **2015**, *5*, 19048-19057.
27. Sharma, P.; Srivastava, M.; Lochab, B.; Kumar, D.; Ramanan, A.; Roy, P. K. Metal-Organic Frameworks as curing accelerators for benzoxazines. *ChemistrySelect* **2016**, *1*, 3924-3932.
28. Rucigaj, A.; Alic, B.; Krajnc, M.; Sebenik, U. Curing of bisphenol A-aniline based benzoxazine using phenolic, amino and mercapto accelerators. *Polym. Lett.* **2015**, *9*, 647-657.
29. Liu, C.; Shen, D.; Sebastián, R. M.; Marquet, J.; Schönfeld, R. Mechanistic Studies on Ring-Opening Polymerization of Benzoxazines: A Mechanistically Based Catalyst Design. *Macromolecules* **2011**, *44*, 4616-4622.
30. Yei, D. R.; Fu, H. K.; Chen, W. Y.; Chang, F. C. Synthesis of a novel benzoxazine monomer-intercalated montmorillonite and the curing kinetics of polybenzoxazine/clay hybrid nanocomposites. *J. Polym. Sci., Part B: Polym. Phys.* **2006**, *44*, 347-358.
31. Saeed, R.; Schlegel, J.; Castano Giraldo, C.; Sawafta, R. Uncertainty of Thermal Characterization of Phase Change Material by Differential Scanning Calorimetry Analysis. *Int. J. Eng. Res. Technol.* **2016**, *5*, 405-412.
32. Wang, Y.-X.; Ishida, H. Synthesis and Properties of New Thermoplastic Polymers from Substituted 3,4-Dihydro-2H-1,3-benzoxazines. *Macromolecules* **2000**, *33*, 2839-2847.
33. Dumas, L.; Bonnaud, L.; Olivier, M.; Poorteman, M.; Dubois, P. High performance bio-based benzoxazine networks from resorcinol and hydroquinone. *Eur. Polym. J.* **2016**, *75*, 486-494.
34. Sini, N. K.; Bijwe, J.; Varma, I. K. Thermal behaviour of bis-benzoxazines derived from renewable feed stock 'vanillin'. *Polym. Degrad. Stab.* **2014**, *109*, 270-277.
35. Shamim Rishwana, S.; Mahendran, A.; Vijayakumar, C. T. Studies on structurally different benzoxazines based on diphenols and diamines: Kinetics of thermal degradation and TG-FTIR studies. *Thermochim. Acta* **2015**, *618*, 74-87.
36. Kim, H. J.; Brunovska, Z.; Ishida, H. Dynamic mechanical analysis on highly thermally stable polybenzoxazines with an acetylene functional group. *J. Appl. Polym. Sci.* **1999**, *73*, 857-862.

37. Hamerton, I.; Howlin, B.; L. Mitchell, A.; T. McNamara, L.; Takeda, S. Systematic examination of thermal, mechanical and dielectrical properties of aromatic polybenzoxazines. *React. Funct. Polym.* **2012**, *72*, 736–744.
38. Kolanadiyil, S. N.; Azechi, M.; Endo, T. Synthesis of novel tri‐benzoxazine and effect of phenolic nucleophiles on its ring-opening polymerization. *J. Polym. Sci., Part A: Polym. Chem.* **2016**, *54*, 2811-2819.
39. Xu, G.-m.; Shi, T.; Liu, J.; Wang, Q. Preparation of a liquid benzoxazine based on cardanol and the thermal stability of its graphene oxide composites. *J. Appl. Polym. Sci.* **2014**, *131*, 40353.
40. Xu, G.-m.; Shi, T.; Wang, Q.; Liu, J.; Yi, Y. A facile way to prepare two novel DOPO-containing liquid benzoxazines and their graphene oxide composites. *J. Appl. Polym. Sci.* **2015**, *132*, 41634.
41. Shukla, S.; Mahata, A.; Pathak, B.; Lochab, B. Cardanol benzoxazines - interplay of oxazine functionality (mono to tetra) and properties. *RSC Adv.* **2015**, *5*, 78071-78080.
42. Minigher, A.; Benedetti, E.; De Giacomo, O.; Campaner, P.; Aroulmoji, V. Synthesis and Characterization of Novel Cardanol Based Benzoxazines. *Nat. Prod. Commun.* **2009**, *4*, 521-528.
43. Agag, T.; Takeichi, T. Synthesis and Characterization of Novel Benzoxazine Monomers Containing Allyl Groups and Their High Performance Thermosets. *Macromolecules* **2003**, *36*, 6010-6017.
44. Shen, S. B.; Ishida, H. Development and characterization of high-performance polybenzoxazine composites. *Polym. Compos.* **1996**, *17*, 710-719.
45. Kiskan, B.; Yagci, Y. Synthetic Strategies to Combine High Performance Benzoxazine Thermosets with Polymers. *Macromol. Symp.* **2010**, *298*, 145-153.
46. Kotzebue, L. R. V.; de Oliveira, J. R.; da Silva, J. B.; Mazzetto, S. E.; Ishida, H.; Lomonaco, D. Development of Fully Biobased High-Performance Bis-Benzoxazine under Environmentally Friendly Conditions. *ACS Sustainable Chem. Eng.* **2018**, *6*, 5485-5494.
47. Zhang, K.; Han, L.; Froimowicz, P.; Ishida, H. A Smart Latent Catalyst Containing o-Trifluoroacetamide Functional Benzoxazine: Precursor for Low Temperature Formation of Very High Performance Polybenzoxazole with Low Dielectric Constant and High Thermal Stability. *Macromolecules* **2017**, *50*, 6552-6560.
48. Ren, S.; Yang, X.; Zhao, X.; Zhang, Y.; Huang, W. An m-phenylenediamine-based benzoxazine with favorable processability and its high-performance thermoset. *J. Appl. Polym. Sci.* **2016**, *133*.
49. Ishida, H.; Low, H. Y. Synthesis of benzoxazine functional silane and adhesion properties of glass-fiber-reinforced polybenzoxazine composites. *J. Appl. Polym. Sci.* **1998**, *69*, 2559-2567.
50. Qu, L.; Xin, Z. Preparation and Surface Properties of Novel Low Surface Free Energy Fluorinated Silane-Functional Polybenzoxazine Films. *Langmuir* **2011**, *27*, 8365-8370.
51. Liu, J.; Lu, X.; Xin, Z.; Zhou, C. Synthesis and Surface Properties of Low Surface Free Energy Silane-Functional Polybenzoxazine Films. *Langmuir* **2013**, *29*, 411-416.
52. Yee Low, H.; Ishida, H. Structural effects of phenols on the thermal and thermo-oxidative degradation of polybenzoxazines. *Polymer* **1999**, *40*, 4365-4376.
53. Chang, C. W.; Lin, C. H.; Lin, H. T.; Huang, H. J.; Hwang, K. Y.; Tu, A. P. Development of an aromatic triamine-based flame-retardant benzoxazine and its high-performance copolybenzoxazines. *Eur. Polym. J.* **2009**, *45*, 680-689.

54. Zhang, W.; Gao, X.; Yu, L.; Ren, Y.; Xu, H.; Liu, B.; Wang, Y.; Fang, X.; Xu, Y.; Ding, T. Silane-functional benzoxazine: synthesis, polymerization kinetics and thermal stability. *Polym. Int.* **2017**, *66*, 908-915.
55. Zhang, K.; Froimowicz, P.; Han, L.; Ishida, H. Hydrogen-bonding characteristics and unique ring-opening polymerization behavior of Ortho-methylol functional benzoxazine. *J. Polym. Sci., Part A: Polym. Chem.* **2016**, *54*, 3635-3642.
56. Baqar, M.; Agag, T.; Huang, R.; Maia, J.; Qutubuddin, S.; Ishida, H. Mechanistic Pathways for the Polymerization of Methylol-Functional Benzoxazine Monomers. *Macromolecules* **2012**, *45*, 8119-8125.
57. Chiou, K.; Hollanger, E.; Agag, T.; Ishida, H. Highly improved thermal properties of hydroxyl-containing polymers via modification by benzoxazine groups. *Macromol. Chem. Phys.* **2013**, *214*, 1629-1635.
58. Hu, W.-H.; Huang, K.-W.; Kuo, S.-W. Heteronucleobase-functionalized benzoxazine: synthesis, thermal properties, and self-assembled structure formed through multiple hydrogen bonding interactions. *Polym. Chem.* **2012**, *3*, 1546-1554.
59. Van, A.; Chiou, K.; Ishida, H. Use of renewable resource vanillin for the preparation of benzoxazine resin and reactive monomeric surfactant containing oxazine ring. *Polymer* **2014**, *55*, 1443-1451.
60. Ambrožič, R.; Šebenik, U.; Krajnc, M. Novel epoxy-benzoxazine water-based emulsions with reactive benzoxazine surfactants for coatings. *Express Polym. Lett.* **2014**, *8*, 574-587.
61. Sawaryn, C.; Landfester, K.; Taden, A. Benzoxazine Miniemulsions Stabilized with Polymerizable Nonionic Benzoxazine Surfactants. *Macromolecules* **2010**, *43*, 8933-8941.
62. Choi, S.-W.; Ohba, S.; Brunovska, Z.; Hemvichian, K.; Ishida, H. Synthesis, characterization and thermal degradation of functional benzoxazine monomers and polymers containing phenylphosphine oxide. *Polym. Degrad. Stab.* **2006**, *91*, 1166-1178.
63. Baqar, M.; Agag, T.; Ishida, H.; Qutubuddin, S. Polymerization behavior of methylol-functional benzoxazine monomer. *React. Funct. Polym.* **2013**, *73*, 360-368.
64. Takeichi, T.; Kano, T.; Agag, T. Synthesis and thermal cure of high molecular weight polybenzoxazine precursors and the properties of the thermosets. *Polymer* **2005**, *46*, 12172-12180.
65. Agag, T.; Takeichi, T. High-molecular-weight AB-type benzoxazines as new precursors for high-performance thermosets. *J. Polym. Sci., Part A: Polym. Chem.* **2007**, *45*, 1878-1888.
66. Chernykh, A.; Agag, T.; Ishida, H. Effect of Polymerizing Diacetylene Groups on the Lowering of Polymerization Temperature of Benzoxazine Groups in the Highly Thermally Stable, Main-Chain-Type Polybenzoxazines. *Macromolecules* **2009**, *42*, 5121-5127.
67. Santhosh Kumar, K. S.; Reghunadhan Nair, C. P.; Radhakrishnan, T. S.; Ninan, K. N. Bis allyl benzoxazine: Synthesis, polymerisation and polymer properties. *Eur. Polym. J.* **2007**, *43*, 2504-2514.
68. Oliveira, J. R.; Kotzebue, L. R. V.; Ribeiro, F. W. M.; Mota, B. C.; Zampieri, D.; Mazzetto, S. E.; Ishida, H.; Lomonaco, D. Microwave-assisted solvent-free synthesis of novel benzoxazines: A faster and environmentally friendly route to the development of bio-based thermosetting resins. *J. Polym. Sci., Part A: Polym. Chem.* **2017**, *55*, 3534-3544.
69. Dumas, L.; Bonnaud, L.; Olivier, M.; Poorteman, M.; Dubois, P. Arbutin-based benzoxazine: en route to an intrinsic water soluble biobased resin. *Green Chem.* **2016**, *18*, 4954-4960.

70. Thirukumaran, P.; Sathiyamoorthi, R.; Parveen, A. S.; Sarojadevi, M. New benzoxazines from renewable resources for green composite applications. *Polym. Compos.* **2016**, *37*, 573-582.
71. Calo, E.; Maffezzoli, A.; Mele, G.; Martina, F.; Mazzetto, S. E.; Tarzia, A.; Stifani, C. Synthesis of a novel cardanol-based benzoxazine monomer and environmentally sustainable production of polymers and bio-composites. *Green Chem.* **2007**, *9*, 754-759.
72. Rao, B. S.; Palanisamy, A. Monofunctional benzoxazine from cardanol for bio-composite applications. *React. Funct. Polym.* **2011**, *71*, 148-154.
73. Wang, Y. X.; Ishida, H. Development of low-viscosity benzoxazine resins and their polymers. *J. Appl. Polym. Sci.* **2002**, *86*, 2953-2966.
74. Kudoh, R.; Sudo, A.; Endo, T. A Highly Reactive Benzoxazine Monomer, 1-(2-Hydroxyethyl)-1,3-Benzoxazine: Activation of Benzoxazine by Neighboring Group Participation of Hydroxyl Group. *Macromolecules* **2010**, *43*, 1185-1187.
75. Chernykh, A.; Agag, T.; Ishida, H. Novel benzoxazine monomer containing diacetylene linkage: An approach to benzoxazine thermosets with low polymerization temperature without added initiators or catalysts. *Polymer* **2009**, *50*, 3153-3157.
76. Wang, X.; Chen, F.; Gu, Y. Influence of electronic effects from bridging groups on synthetic reaction and thermally activated polymerization of bisphenol-based benzoxazines. *J. Polym. Sci., Part A: Polym. Chem.* **2011**, *49*, 1443-1452.
77. Periyasamy, T.; Asrafali, S. P.; Muthusamy, S.; Kim, S.-C. Replacing bisphenol-A with bisguaiacol-F to synthesize polybenzoxazines for a pollution-free environment. *New Journal of Chemistry* **2016**, *40*, 9313-9319.
78. Zúñiga, C.; Bonnaud, L.; Lligadas, G.; Ronda, J. C.; Galià, M.; Cádiz, V.; Dubois, P. Convenient and solventless preparation of pure carbon nanotube/polybenzoxazine nanocomposites with low percolation threshold and improved thermal and fire properties. *Journal of Materials Chemistry A* **2014**, *2*, 6814-6822.
79. Sesigur, F.; Sakar, D.; Yazici, O.; Cakar, F.; Cankurtaran, O.; Karaman, F. Dispersive Surface Energy and Acid-Base Parameters of Tosylate Functionalized Poly(ethylene glycol) via Inverse Gas Chromatography. *J. Chem.* **2014**, *2014*.
80. Huber, S.; Hutter, N.; Jordan, R. Effect of end group polarity upon the lower critical solution temperature of poly(2-isopropyl-2-oxazoline). *Colloid. Polym. Sci.* **2008**, *286*, 1653-1661.
81. Imran-ul-haq, M.; Tiersch, B.; Beuermann, S. Influence of Polymer End Groups on Crystallization and Morphology of Poly(vinylidene fluoride) Synthesized in Homogeneous Phase with Supercritical Carbon Dioxide. *Macromolecules* **2008**, *41*, 7453-7462.
82. Trejo-Machin, A.; Verge, P.; Puchot, L.; Quintana, R. Phloretic acid as an alternative to the phenolation of aliphatic hydroxyls for the elaboration of polybenzoxazine. *Green Chem.* **2017**, *19*, 5065-5073.
83. Lü, H.; Zheng, S. Miscibility and phase behavior in thermosetting blends of polybenzoxazine and poly(ethylene oxide). *Polymer* **2003**, *44*, 4689-4698.
84. Huang, J.-M.; Kuo, S.-W.; Lee, Y.-J.; Chang, F.-C. Synthesis and characterization of a vinyl-terminated benzoxazine monomer and its blends with poly(ethylene oxide). *J. Polym. Sci., Part B: Polym. Phys.* **2007**, *45*, 644-653.
85. Ishida, H.; Lee, Y.-H. Infrared and thermal analyses of polybenzoxazine and polycarbonate blends. *J. Appl. Polym. Sci.* **2001**, *81*, 1021-1034.

86. Zheng, S.; Lü, H.; Guo, Q. Thermosetting Blends of Polybenzoxazine and Poly(ε -caprolactone): Phase Behavior and Intermolecular Specific Interactions. *Macromol. Chem. Phys.* **2004**, *205*, 1547-1558.
87. Ishida, H.; Lee, Y.-H. Synergism observed in polybenzoxazine and poly (ε-caprolactone) blends by dynamic mechanical and thermogravimetric analysis. *Polymer* **2001**, *42*, 6971-6979.
88. Xia, Y.; Yang, P.; Miao, Y.; Zhang, C.; Gu, Y. Blends of sulfonated polysulfone/polysulfone/4,4'-diaminodiphenyl methane-based benzoxazine: multiphase structures and properties. *Polym. Int.* **2015**, *64*, 118-125.
89. Zhao, P.; Liang, X.; Chen, J.; Ran, Q.; Gu, Y. Poly(ether imide)-modified benzoxazine blends: Influences of phase separation and hydrogen bonding interactions on the curing reaction. *J. Appl. Polym. Sci.* **2013**, *128*, 2865-2874.
90. Takeichi, T.; Agag, T.; Zeidam, R. Preparation and properties of polybenzoxazine/poly(imide-siloxane) alloys: In situ ring-opening polymerization of benzoxazine in the presence of soluble poly(imide-siloxane)s. *J. Polym. Sci., Part A: Polym. Chem.* **2001**, *39*, 2633-2641.
91. Chen, W.; Lei, Y.; Liu, X. High Performance Composites of Polybenzoxazine and Polyarylene Ether Nitriles (PEN). *Polym. Polym. Compos.* **2012**, *20*, 73-76.
92. Su, Y.-C.; Kuo, S.-W.; Yei, D.-R.; Xu, H.; Chang, F.-C. Thermal properties and hydrogen bonding in polymer blend of polybenzoxazine/poly(N-vinyl-2-pyrrolidone). *Polymer* **2003**, *44*, 2187-2191.
93. Tiptipakorn, S.; Damrongsakkul, S.; Ando, S.; Hemvichian, K.; Rimdusit, S. Thermal degradation behaviors of polybenzoxazine and silicon-containing polyimide blends. *Polym. Degrad. Stab.* **2007**, *92*, 1265-1278.
94. Kuo, S.-W.; Wu, Y.-C.; Wang, C.-F.; Jeong, K.-U. Preparing Low-Surface-Energy Polymer Materials by Minimizing Intermolecular Hydrogen-Bonding Interactions. *J. Phys. Chem. C* **2009**, *113*, 20666-20673.
95. Burke, W. J.; Stephens, C. W. Monomeric Products from the Condensation of Phenol with Formaldehyde and Primary Amines. *J. Am. Chem. Soc.* **1952**, *74*, 1518-1520.
96. Sawaryn, C.; Landfester, K.; Taden, A. Benzoxazine Miniemulsions Stabilized with Multifunctional Main-chain Benzoxazine Protective Colloids. *Macromolecules* **2011**, *44*, 5650-5658.
97. Wang, T.; Quinn, M. D. J.; Notley, S. M. A benzoxazine surfactant exchange for atomic force microscopy characterization of two dimensional materials exfoliated in aqueous surfactant solutions. *RSC Adv.* **2017**, *7*, 3222-3228.
98. Jönsson, B.; Lindman, B.; Holmberg, K.; Kronberg, B. *Surfactants and Polymers in Aqueous Solution*; John Wiley & Sons: England, 2000.
99. Oliveux, G.; Le Gal La Salle, E.; Bailleul, J.-L. Recycling by solvolysis thermosetting composite materials of sustainable surface transport. *AIP Conf. Proc.* **2011**, *1315*, 209-214.
100. Prinçaud, M.; Aymonier, C.; Loppinet-Serani, A.; Perry, N.; Sonnemann, G. Environmental feasibility of the recycling of carbon fibers from CFRPs by solvolysis using supercritical water. *ACS Sustainable Chem. Eng.* **2014**, *2*, 1498-1502.
101. Vallee, M.; Tersac, G.; Destais-Orvoen, N.; Durand, G. Chemical recycling of class A surface quality sheet-molding composites. *Ind. Eng. Chem. Res.* **2004**, *43*, 6317-6324.

102. Das, M.; Varughese, S. A Novel Sonochemical Approach for Enhanced Recovery of Carbon Fiber from CFRP Waste Using Mild Acid–Peroxide Mixture. *ACS Sustainable Chem. Eng.* **2016**, *4*, 2080-2087.
103. Wang, J.; Xu, Y. Z.; Fu, Y. F.; Liu, X. D. Latent curing systems stabilized by reaction equilibrium in homogeneous mixtures of benzoxazine and amine. *Sci. Rep.* **2016**, *6*, 38584.
104. Kawaguchi, A. W.; Sudo, A.; Endo, T. Polymerization–Depolymerization System Based on Reversible Addition-Dissociation Reaction of 1,3-Benzoxazine with Thiol. *ACS Macro Lett.* **2013**, *2*, 1-4.
105. Lo, J. N.; Nutt, S. R.; Williams, T. J. Recycling benzoxazine–epoxy composites via catalytic oxidation. *ACS Sustainable Chem. Eng.* **2018**, *6*, 7227-7231.
106. Lu, H.; Madbouly, S. A.; Schrader, J. A.; Srinivasan, G.; McCabe, K. G.; Grewell, D.; Kessler, M. R.; Graves, W. R. Biodegradation behavior of poly(lactic acid) (PLA)/distiller's dried grains with solubles (DDGS) composites. *ACS Sustainable Chem. Eng.* **2014**, *2*, 2699-2706.
107. Li, S. M.; Rashkov, I.; Espartero, J. L.; Manolova, N.; Vert, M. Synthesis, Characterization, and Hydrolytic Degradation of PLA/PEO/PLA Triblock Copolymers with Long Poly(l-lactic acid) Blocks. *Macromolecules* **1996**, *29*, 57-62.
108. Takeichi, T.; Kawauchi, T.; Agag, T. High Performance Polybenzoxazines as a Novel Type of Phenolic Resin. *Polym. J.* **2008**, *40*, 1121-1131.
109. Kiskan, B.; Yagci, Y.; Ishida, H. Synthesis, characterization, and properties of new thermally curable polyetheresters containing benzoxazine moieties in the main chain. *J. Polym. Sci., Part A: Polym. Chem.* **2008**, *46*, 414-420.
110. Ishida, H.; Ohba, S. Synthesis and characterization of maleimide and norbornene functionalized benzoxazines. *Polymer* **2005**, *46*, 5588-5595.
111. Agag, T.; Takeichi, T. Novel Benzoxazine Monomers Containing p-Phenyl Propargyl Ether: Polymerization of Monomers and Properties of Polybenzoxazines. *Macromolecules* **2001**, *34*, 7257-7263.
112. Andreu, R.; Reina, J. A.; Ronda, J. C. Carboxylic acid-containing benzoxazines as efficient catalysts in the thermal polymerization of benzoxazines. *J. Polym. Sci., Part A: Polym. Chem.* **2008**, *46*, 6091-6101.
113. Allen, D. J.; Ishida, H. Physical and mechanical properties of flexible polybenzoxazine resins: Effect of aliphatic diamine chain length. *J. Appl. Polym Sci.* **2006**, *101*, 2798-2809.
114. Baranek, A. D.; Kendrick, L. L.; Narayanan, J.; Tyson, G. E.; Wand, S.; Patton, D. L. Flexible aliphatic-bridged bisphenol-based polybenzoxazines. *Polym. Chem.* **2012**, *3*, 2892-2900.
115. Demir, K. D.; Kiskan, B.; Aydogan, B.; Yagci, Y. Thermally curable main-chain benzoxazine prepolymers via polycondensation route. *React. Funct. Polym.* **2013**, *73*, 346-359.
116. Lin, C. H.; Chang, S. L.; Shen, T. Y.; Shih, Y. S.; Lin, H. T.; Wang, C. F. Flexible polybenzoxazine thermosets with high glass transition temperatures and low surface free energies. *Polym. Chem.* **2012**, *3*, 935-945.
117. Kawaguchi, A. W.; Sudo, A.; Endo, T. Synthesis of highly polymerizable 1,3-benzoxazine assisted by phenyl thio ether and hydroxyl moieties. *J. Polym. Sci., Part A: Polym. Chem.* **2012**, *50*, 1457-1461.

118. Beyazkilic, Z.; Kahveci, M. U.; Aydogan, B.; Kiskan, B.; Yagci, Y. Synthesis of polybenzoxazine precursors using thiols: Simultaneous thiol–ene and ring-opening reactions. *J. Polym. Sci., Part A: Polym. Chem.* **2012**, *50*, 4029-4036.
119. Kasapoglu, F.; Cianga, I.; Yagci, Y.; Takeichi, T. Photoinitiated Cationic Polymerization of Monofunctional Benzoxazine. *J. Polym. Sci., Part A: Polym. Chem.* **2003**, *41*, 3320 –3328.
120. Rimdusit, S.; Jubsilp, C.; Tiptipakorn, S. *Alloys and composites of polybenzoxazines: properties and applications*; Springer Science & Business Media: Singapore, 2013.
121. Ergin, M.; Kiskan, B.; Gacal, B.; Yagci, Y. Thermally Curable Polystyrene via Click Chemistry. *Macromolecules* **2007**, *40*, 4724-4727.
122. Tuzun, A.; Kiskan, B.; Alemdar, N.; Erciyes, A. T.; Yagci, Y. Benzoxazine containing polyester thermosets with improved adhesion and flexibility. *J. Polym. Sci., Part A: Polym. Chem.* **2010**, *48*, 4279-4284.
123. Koz, B.; Kiskan, B.; Yagci, Y. A novel benzoxazine monomer with methacrylate functionality and its thermally curable (co)polymers. *Polym. Bull.* **2011**, *66*, 165-174.
124. Demir, K. D.; Kiskan, B.; Latthe, S. S.; Demirel, A. L.; Yagci, Y. Thermally curable fluorinated main chain benzoxazine polyethers via Ullmann coupling. *Polym. Chem.* **2013**, *4*, 2106-2114.
125. Altinkok, C.; Kiskan, B.; Yagci, Y. Synthesis and characterization of sulfone containing main chain oligobenzoxazine precursors. *J. Polym. Sci., Part A: Polym. Chem.* **2011**, *49*, 2445-2450.
126. Kiskan, B.; Yagci, Y. Synthesis and characterization of naphthoxazine functional poly(ε-caprolactone). *Polymer* **2005**, *46*, 11690-11697.
127. Aydogan, B.; Sureka, D.; Kiskan, B.; Yagci, Y. Polysiloxane-containing benzoxazine moieties in the main chain. *J. Polym. Sci., Part A: Polym. Chem.* **2010**, *48*, 5156-5162.
128. Kiskan, B.; Aydogan, B.; Yagci, Y. Synthesis, characterization, and thermally activated curing of oligosiloxanes containing benzoxazine moieties in the main chain. *J. Polym. Sci., Part A: Polym. Chem.* **2009**, *47*, 804-811.
129. Kiskan, B.; Yagci, Y. Synthesis and characterization of thermally curable polyacetylenes by polymerization of propargyl benzoxazine using rhodium catalyst. *Polymer* **2008**, *49*, 2455-2460.
130. Zhang, K.; Zhuang, Q.; Liu, X.; Yang, G.; Cai, R.; Han, Z. A New Benzoxazine Containing Benzoxazole-Functionalized Polyhedral Oligomeric Silsesquioxane and the Corresponding Polybenzoxazine Nanocomposites. *Macromolecules* **2013**, *46*, 2696-2704.
131. Mohamed, M.; Kuo, S.-W. Polybenzoxazine/Polyhedral Oligomeric Silsesquioxane (POSS) Nanocomposites. *Polymers* **2016**, *8*, 225.
132. Selvi, M.; Devaraju, S.; Vengatesan, M.; Alagar, M. Development of polybenzoxazine–silica–titania (PBZ–SiO2–TiO2) hybrid nanomaterials with high surface free energy. *J. Sol-Gel Sci. Technol.* **2014**, *3*, 518-526.
133. Selvi, M.; Devaraju, S.; Sethuraman, K.; Alagar, M. Carbon black–polybenzoxazine nanocomposites for high K dielectric applications. *Polym. Compos.* **2014**, *35*, 2121-2128.
134. Nour-Eddine, E. M.; Yuan, Q.; Huang, F. Investigation of curing and thermal behavior of benzoxazine and lignin mixtures. *J. Appl. Polym. Sci.* **2012**, *125*, 1773-1781.
135. Bandeira, C. F.; Pereira, A. C.; Botelho, E. C.; Costa, M. L. Benzoxazine resin and their nanostructured composites cure kinetic by DSC. *J. Mater. Res.* **2013**, *28*, 3094-3099.
136. Jain, R.; Narula, A. K.; Choudhary, V. Studies on curing and thermal behavior of diglycidyl ether of bisphenol-A and benzoxazine mixtures. *J. Appl. Polym. Sci.* **2007**, *106*, 3327-3334.

137. Jin, Q.; Misasi, J. M.; Wiggins, J. S.; Morgan, S. E. Simultaneous reinforcement and toughness improvement in an aromatic epoxy network with an aliphatic hyperbranched epoxy modifier. *Polymer* **2015**, *73*, 174-182.
138. De France, K. J.; Chan, K. J. W. W.; Cranston, E. D.; Hoare, T. R. Enhanced Mechanical Properties in Cellulose Nanocrystal-Poly(oligo Ethylene Glycol Methacrylate) Injectable Nanocomposite Hydrogels through Control of Physical and Chemical Cross-Linking. *Biomacromolecules* **2016**, *17*, 649–660.
139. Lü, H.; Zheng, S. X.; Tian, G. H. Poly(hydroxyether sulfone) and its blends with poly(ethylene oxide): miscibility, phase behavior and hydrogen bonding interactions. *Polymer* **2004**, *45*, 2897-2909.
140. Rimdusit, S.; Jubsilp, C.; Tiptipakorn, S. *Introduction to Commercial Benzoxazine and Their Unique Properties*; Springer Science & Business Media: Singapore, 2013.
141. Hackler, R. A.; Hollcraft, A. T.; Kirkness, T. A.; Larson, N. S.; Hoekstra, N. L.; Rider, D. A. Relief of Cure Stress in Prepreg Composites with Engineered Voids: A Solution to Warping in Composite Phenolic Resin/Fiberglass Laminates. *Ind. Eng. Chem. Res.* **2016**, *55*, 3568-3578.
142. Meng, Q.; Hu, J. A poly (ethylene glycol)-based smart phase change material. *Sol. Energ. Mater. Sol. Cells* **2008**, *92*, 1260-1268.
143. Wei, T.; Zheng, B.; Yi, H.; Gao, Y.; Guo, W. Thermal analysis and non-isothermal kinetics of poly(ethylene glycol) with different molecular weight. *Polym. Eng. Sci.* **2014**, *54*, 2872-2876.
144. Damle, R.; Kulkarni, P. N.; Bhat, S. V. Study of effect of composition, irradiation and quenching on ionic conductivity in (PEG) x : NH4NO3 solid polymer electrolyte. *Bull. Mater. Sci.* **2008**, *31*, 869-876.
145. Stanescu, P. O.; Cursaru, B.; Teodorescu, M. Thermal Properties of Networks Prepared from α,ω-Diepoxy Terminated Poly(ethylene glycol)s and Aliphatic Polyamines. *Mater. Plast.* **2009**, *46*, 419-425.
146. Sánchez-Soto, P. J.; Ginés, J. M.; Arias, M. J.; Novák, C.; Ruiz-Conde, A. Effect of Molecular Mass on the Melting Temperature, Enthalpy and Entropy of Hydroxy-Terminated PEO. *J. Therm. Anal. Calorim.* **2002**, *67*, 189-197.
147. Costagliola, M.; Greco, R.; Martuscelli, E. Melt viscosity and thermal properties of poly(ethylene oxide) fractions and blends. *Polymer* **1978**, *19*, 860-862.
148. Vidotto, G.; Levy, D.; Kovacs, A. J. Crystallisation et fusion des polymeres autoensemences. I. Polybutene-1, polyethylene et polyoxyethylene de haute mass moleculaire. *Kolloid Z.Z. Polym.* **1969**, *230*, 289-305.
149. Van Krevelen, D. W. In *Properties of Polymers*; 3rd ed.; Elsevier: Amsterdam, 1990, p 794-795.
150. Floudas, G.; Tsitsilianis, C. Crystallization kinetics of poly(ethylene oxide) in poly(ethylene oxide)−polystyrene−poly(ethylene oxide) triblock copolymers. *Macromolecules* **1997**, *30*, 4381-4390.
151. Buzarovska, A. Crystallization of polymers (2nd edition) Volume 2: Kinetics and mechanisms. Edited by Leo Mandelkern. Cambridge University Press, Cambridge, 2004. ISBN 0 521 81682 3. pp 478. *Polym. Int.* **2005**, *54*, 1466-1467.
152. Ishida, H.; Rodriguez, Y. Curing kinetics of a new benzoxazine-based phenolic resin by differential scanning calorimetry. *Polymer* **1995**, *36*, 3151-3158.

153. Vijayakumar, C. T.; Shamim Rishwana, S.; Surender, R.; David Mathan, N.; Vinayagamoorthi, S.; Alam, S. Structurally diverse benzoxazines: synthesis, polymerization, and thermal stability. *Des. Monomers Polym.* **2014**, *17*, 47-57.
154. Lin, Y.; Stone, C. A.; Shaw, S. J.; Song, M. Preparation and characterization of benzoxazine based nanocomposites: Comprehensive study in curing kinetics and enhanced thermal stabilities. *J. Appl. Polym. Sci.* **2015**, *132*, 41903.
155. Escobar, J.; Poorteman, M.; Dumas, L.; Bonnaud, L.; Dubois, P.; Olivier, M.-G. Thermal curing study of bisphenol A benzoxazine for barrier coating applications on 1050 aluminum alloy. *Prog. Org. Coat.* **2015**, *79*, 53-61.
156. Gordon, M.; Taylor, J. S. Ideal copolymers and the second-order transitions of synthetic rubbers. i. non-crystalline copolymers. *J. Appl. Chem.* **1952**, *2*, 493-500.
157. Belorgey, G.; Prud'homme, R. E. Miscibility of polycaprolactone/chlorinated polyethylene blends. *J. Polym. Sci., Part B: Polym. Phys.* **1982**, *20*, 191-203.
158. Belorgey, G.; Aubin, M.; Prud'homme, R. E. Studies of Polyester-chlorinated poly(vinyl chloride) blends. *Polymer* **1982**, *23*, 1051-1056.
159. Yan, C.; Fan, X.; Li, J.; Shen, S. Z. Synthesis and characterization of bisphenol a diphthalimide bisbenzoxazine monomers and the properties of their polybenzoxazines. *J. Appl. Polym Sci.* **2011**, *121*, 2778-2787.
160. Ishida, H.; Lee, Y.-H. Study of hydrogen bonding and thermal properties of polybenzoxazine and poly-(ε-caprolactone) blends. *J. Polym. Sci., Part B: Polym. Phys.* **2001**, *39*, 736-749.
161. Štirn, Ž.; Ručigaj, A.; Krajnc, M. Innovative approach using aminomaleimide for unlocking phenolic diversity in high-performance maleimidobenzoxazine resins. *Polymer* **2017**, *120*, 129-140.
162. Miwa, Y. Novel and Accurate Method for Determination of Glass Transition Temperature of Spin-Labeled Polymer by ESR Microwave Power Saturation. *Macromolecules* **2009**, *42*, 6141-6146.
163. Törmälä, P. Determination of glass transition temperature of poly(ethylene glycol) by spin probe technique. *Eur. Polym. J.* **1974**, *10*, 519-521.
164. Kozlowska, M.; Goclon, J.; Rodziewicz, P. Intramolecular hydrogen bonds in low-molecular-weight polyethylene glycol. *ChemPhysChem* **2016**, *17*, 1143-1153.
165. Silverstein, R. M.; Webster, F. X.; Kiemle, D. J. *Spectrometric Identification of Organic Compounds*; 7th ed.; John Wiley and Sons: Hoboken, NJ, 2005.
166. Burton, G. *Chemical Ideas*; Heinemann Educational, 2000.
167. Kuo, S. W.; Chang, F. C. Miscibility Behavior and Specific Interaction of Phenolic Resin with Poly(acetoxystyrene) Blends. *Macromol. Chem. Phys.* **2002**, *203*, 868-878.
168. Espinosa, M. A.; Cádiz, V.; Galià, M. Synthesis and characterization of benzoxazine-based phenolic resins: Crosslinking study. *J. Appl. Polym. Sci.* **2003**, *90*, 470-481.
169. Barroso-Bujans, F.; Alegría, A.; Pomposo, J. A.; Colmenero, J. Thermal Stability of Polymers Confined in Graphite Oxide. *Macromolecules* **2013**, *46*, 1890-1898.
170. Douglas, P.; Albadarin, A. B.; Sajjia, M.; Mangwandi, C.; Kuhs, M.; Collins, M. N.; Walker, G. M. Effect of poly ethylene glycol on the mechanical and thermal properties of bioactive poly(ε-caprolactone) melt extrudates for pharmaceutical applications. *Int. J. Pharm.* **2016**, *500*, 179-186.
171. Spectral Database for Organic Compounds (SDBS); mass spectrum; SDBS No. 23565; RN 4124-41-8; http://riodb01.ibase.aist.go.jp/sdbs/ (accessed June 7, 2017).

172. Dunkers, J.; Ishida, H. Reaction of benzoxazine-based phenolic resins with strong and weak carboxylic acids and phenols as catalysts. *J. Polym. Sci., Part A: Polym. Chem.* **1999**, *37*, 1913-1921.
173. Riess, G.; Schwob, J. M.; Guth, G.; Roche, M.; Laude, B. In *Adv. Polym. Synth.*; Culbertson, B. M., McGrath, J. E., Eds.; Springer US: Boston, MA, 1985, p 27-49.
174. Corey, E. J.; Posner, G. H.; Atkinson, R. F.; Wingard, A. K.; Halloran, D. J.; Radzik, D. M.; Nash, J. J. Formation of olefins via pyrolysis of sulfonate esters. *J. Org. Chem.* **1989**, *54*, 389-393.
175. Kishore, V. C.; Dhanya, R.; Sreekumar, K.; Rani, J.; Kartha, C. S. In *2007 International Workshop on Physics of Semiconductor Devices* 2007, p 586-589.
176. Rajaei, M.; Wang, D.-Y.; Bhattacharyya, D. Combined effects of ammonium polyphosphate and talc on the fire and mechanical properties of epoxy/glass fabric composites. *Composites Part B* **2017**, *113*, 381-390.
177. Yousef, J.; Morteza, E. The rheological modification of talc-filled polypropylene by epoxy-polyester hybrid resin and its effect on morphology, crystallinity, and mechanical properties. *Polym. Eng. Sci.* **2009**, *49*, 619-629.
178. Agag, T.; Takeichi, T. In *Materials Science Forum*; Trans Tech Publ: 2004; Vol. 449, p 1157-1160.
179. T. Huang, M.; Ishida, H. Investigation of the boron nitride/polybenzoxazine interphase. *J. Polym. Sci., Part B: Polym. Phys.* **1999**, *37*, 2360-2372.
180. Su, W.-C.; Kuo, S.-W. Reversible Surface Properties of Polybenzoxazine/Silica Nanocomposites Thin Films. *J. Nanomater.* **2013**, 453623.
181. Shi, Z.; Yu, D. S.; Wang, Y.; Xu, R. Investigation of isothermal curing behaviour during the synthesis of polybenzoxazine-layered silicate nanocomposites via cyclic monomer. *Eur. Polym. J.* **2002**, *38*, 727-733.
182. Rimdusit, S.; Punson, K.; Dueramae, I.; Somwangthanaroj, A.; Tiptipakorn, S. Rheological and Thermomechanical Characterizations of Fumed Silica-Filled Polybenzoxazine Nanocomposites. *Eng. J.* **2011**, *15*, 27-38.
183. Huang, P.; Zheng, S.; Huang, J.; Guo, Q.; Zhu, W. Miscibility and mechanical properties of epoxy resin/polysulfone blends. *Polymer* **1997**, *38*, 5565-5571.
184. Kim, S.; Chen, L.; Johnson, J. K.; Marand, E. Polysulfone and functionalized carbon nanotube mixed matrix membranes for gas separation: Theory and experiment. *J. Membr. Sci.* **2007**, *294*, 147-158.
185. Linares, A.; Benavente, R. Effect of Sulfonation on Thermal, Mechanical, and Electrical Properties of Blends Based on Polysulfones. *Polym. J.* **2009**, *41*, 407-415.
186. Chen, Z.; Lin, Y.; Sun, D.; Han, Y. Direct synthesis of triphenylamine-containing polyarylsulfones from commercially available aniline: Polymerization via N-C coupling reactions. *High Perform. Polym.* **2015**, *28*, 868-878.
187. B., G. L.; Boettner, E. A. Volatile combustion products of polycarbonate and polysulfone. *J. Appl. Polym. Sci.* **1972**, *16*, 855-863.
188. Imhof, L. G.; Stueben, K. C. Evaluation of the smoke and flammability characteristics of polymer systems. *Polym. Eng. Sci.* **1973**, *13*, 146-152.
189. El-Hibri, J.; Weinberg, S. A. In *Encyclopedia of Polymer Science and Technology*; Mark, H. F., Ed.; John Wiley and Sons: Mishawaka, 2006; Vol. 4.

190. ASTM D2843-16, Standard Test Method for Density of Smoke from the Burning or Decomposition of Plastics, ASTM International, West Conshohocken, PA, 2016, www.astm.org.
191. Dahe, G. J.; Kadam, S. S.; Sabale, S. S.; Kadam, D. P.; Sarkate, L. B.; Bellare, J. R. In Vivo Evaluation of the Biocompatibility of Surface Modified Hemodialysis Polysulfone Hollow Fibers in Rat. *PLOS ONE* **2011**, *6*, e25236.
192. Stosovic, M.; Stanojevic, M.; Radović, M.; Ogrizovic, S.; Lezaic, V.; Naumovic, R.; Jovanović, D.; Ristic, G.; Djukanović, L.; Marinkovic, J. Hemodialysis Modality, Percentage of Body Fat, and Patient Survival. *Int. J. Artif. Organs* **2009**, *32*, 20-30.
193. Hafiz, A. M.; Hilmi, M.; Maizatul, S. S.; Mohd, R. O.; Thanabalan, M. Polysulfone/poly(ether sulfone) blended membranes for CO2 separation. *J. Appl. Polym. Sci.* **2016**, *133*.
194. Segărceanu, M.; Grosu, A.; Lica, C.; Oprea, O.; Abbas, A.; Kadhim, K.; Rikabi, A.; Vaireanu, D.-I. Comparative Study of Polysulfone Matrix Based Composite Membranes Designed for Fuel Cells. *Rev. Chim.* **2018**, *69*, 772-776.
195. Dhandayuthanpani, B.; Yoshida, Y.; Maekawa, T.; Kumar, D. S. Polymeric Scaffolds in Tissue Engineering Application: A Review. *Int. J. Polym. Sci.* **2011**, *2011*, 290602.
196. Kucharczyk, P.; Pavelková, A.; Stloukal, P.; Sedlarík, V. Degradation behaviour of PLA-based polyesterurethanes under abiotic and biotic environments. *Polym. Degrad. Stab.* **2016**, *129*, 222-230.
197. Ho, K.-L. G.; Pometto, A. L.; Gadea-Rivas, A.; Briceño, J. A.; Rojas, A. Degradation of Polylactic Acid (PLA) Plastic in Costa Rican Soil and Iowa State University Compost Rows. *J. Environ. Polym. Degrad.* **1999**, *7*, 173-177.
198. Mukul, A.; Koelling, K. W.; Chalmers, J. J. Characterization of the Degradation of Polylactic Acid Polymer in a Solid Substrate Environment. *Biotechnol. Progr.* **1998**, *14*, 517-526.
199. Ndazi, B. S.; Karlsson, S. Characterization of hydrolytic degradation of polylactic acid/rice hulls composites in water at different temperatures. *Polym. Lett.* **2011**, *5*, 119-131.
200. Kwiecien, I.; Adamus, G.; Jiang, G.; Radecka, I.; Baldwin, T. C.; Khan, H. R.; Johnston, B.; Pennetta, V.; Hill, D.; Bretz, I.; Kowalczuk, M. Biodegradable PBAT/PLA Blend with Bioactive MCPA-PHBV Conjugate Suppresses Weed Growth. *Biomacromolecules* **2018**, *19*, 511-520.
201. Kenry; Liu, B. Recent Advances in Biodegradable Conducting Polymers and Their Biomedical Applications. *Biomacromolecules* **2018**, *19*, 1783-1803.
202. Makadia, H. K.; Siegel, S. J. Poly Lactic-co-Glycolic Acid (PLGA) as Biodegradable Controlled Drug Delivery Carrier. *Polymers* **2011**, *3*, 1377.
203. Anderson, J. M.; Shive, M. S. Biodegradation and biocompatibility of PLA and PLGA microspheres. *Adv. Drug Deliv. Rev.* **2012**, *64*, 5-24.
204. Rydz, J.; Sikorska, W.; Kyulavska, M.; Christova, D. Polyester-Based (Bio)degradable Polymers as Environmentally Friendly Materials for Sustainable Development. *Int. J. Mol. Sci.* **2015**, *16*, 564-596.
205. Vey, E.; Rodger, C.; Meehan, L.; Booth, J.; Claybourn, M.; Miller, A.; Saiani, A. The impact of chemical composition on the degradation kinetics of poly(lactic-co-glycolic) acid copolymers cast films in phosphate buffer solution. *Polym. Degrad. Stab.* **2012**, *97*, 358-365.

206. Majid, J.; Arab, T. E.; Muhammad, I.; Muriel, J.; Stéphane, D. Poly-Lactic Acid: Production, Applications, Nanocomposites, and Release Studies. *Compr. Rev. Food Sci. Food Saf.* **2010**, *9*, 552-571.
207. Hamad, K.; Kaseem, M.; Yang, H. W.; Deri, F.; Ko, Y. G. Properties and medical applications of polylactic acid: A review. *Express Polym. Lett.* **2015**, *9*, 435–455.
208. Lasprilla, A. J. R.; Martinez, G. A. R.; Lunelli, B. H.; Jardini, A. L.; Filho, R. M. Poly-lactic acid synthesis for application in biomedical devices — A review. *Biotechnol. Adv.* **2012**, *30*, 321-328.
209. Shih, C. A Graphical Method for the Determination of the Mode of Hydrolysis of Biodegradable Polymers. *Pharm. Res.* **1995**, *12*, 2036-2040.
210. Erbetta, C.; Alves, R. J.; Resende, J. M.; de Souza Freitas, R. F.; de Sousa, R. G. Synthesis and Characterization of Poly(D,L-Lactide-co-Glycolide) Copolymer. *J. Biomater. Nanobiotechnol.* **2012**, *3*, 208-225.
211. Michaelidou, S. S.; Koutentis, P. A. Detosylation of 3-amino-1-tosylindole-2-carbonitriles using DBU and thiophenol. *Tetrahedron* **2010**, *66*, 3016-3023.
212. Suzuki, Y. Ph.D. Dissertation, Johannes Gutenberg-Universität in Mainz, 2015.
213. Pulst, M.; Samiullah, M. H.; Baumeister, U.; Prehm, M.; Balko, J.; Thurn-Albrecht, T.; Busse, K.; Golitsyn, Y.; Reichert, D.; Kressler, J. Crystallization of Poly(ethylene oxide) with a Well-Defined Point Defect in the Middle of the Polymer Chain. *Macromolecules* **2016**, *49*, 6609-6620.
214. Chen, C.-H.; Lee, K.-W.; Lin, C.-H.; Juang, T.-Y. Low-Dissipation Thermosets Derived from Oligo(2,6-Dimethyl Phenylene Oxide)-Containing Benzoxazines. *Polymers* **2018**, *10*, 411.
215. Taskin, O. S.; Kiskan, B.; Yagci, Y. Polybenzoxazine Precursors As Self-Healing Agents for Polysulfones. *Macromolecules* **2013**, *46*, 8773-8778.
216. Lee, S. H.; Kim, K. S.; Shim, J. H.; Ahn, C.-H. High-Performance Printed Circuit Board Materials Based on Benzoxazine and Epoxy Blend System. *Macromol. Res.* **2018**, *26*, 388-393.
217. Lin, J.; Tarek, A.; Hatsuo, I. Use of allyl-functional benzoxazine monomers as replacement for styrene in vinyl ester resins. *Polym. Int.* **2013**, *62*, 71-78.
218. Shiao-Wei, K.; Wei-Chen, L. Synthesis and characterization of a cured epoxy resin with a benzoxazine monomer containing allyl groups. *J. Appl. Polym. Sci.* **2010**, *117*, 3121-3127.
219. Wang, H.; Yang, P.; Zhu, R.; Gu, Y. Preparation and characterization of novel multi-branched polymers in situ cured from benzoxazine/epoxy resin/primary amines blends. *RSC Adv.* **2016**, *6*, 15271-15278.
220. Haque, H. M. E.; Islam, Z.; Kawauchi, T.; Takeichi, T. Preparation and Properties of Polybenzoxazine/Lignin Alloy. *Appl. Mech. Mater.* **2012**, *217-219*, 571-577.
221. Zhang, C.; Luo, X.; Zhu, R.; Ling, H.; Gu, Y. Thermal and dielectric properties of epoxy/DDS/CTBN adhesive modified by cardanol-based benzoxazine. *J. Adhes. Sci. Technol.* **2015**, *29*, 767-777.
222. Su, Y.-C.; Chen, W.-C.; Ou, K.-l.; Chang, F.-C. Study of the morphologies and dielectric constants of nanoporous materials derived from benzoxazine-terminated poly(ε-caprolactone)/polybenzoxazine co-polymers. *Polymer* **2005**, *46*, 3758-3766.
223. Bai, J.; Shi, Z.; Yin, J.; Tian, M. Tailoring the Morphologies and Mechanical Properties of Styrene–Butadiene–Styrene Triblock Copolymers by the Incorporation of Thiol Functionalized Benzoxazine. *Macromolecules* **2014**, *47*, 2964-2973.

224. Feng, T.; Wang, J.; Pan, L.; Derradji, M.; Ramdani, N.; Liu, W.; Zhou, H. Tunable properties of novel tetra-functional fluorene-based benzoxazines from mixed amines: Synthesis, characterization and curing kinetics. *Thermochim. Acta* **2016**, *633*, 1-11.
225. Sahre, K.; Hoffmann, T.; Pospiech, D.; Eichhorn, K.-J.; Fischer, D.; Voit, B. Monitoring of the polycondensation reaction of bisphenol A and 4,4'-dichlorodiphenylsulfone towards polysulfone (PSU) by real-time ATR‐FTIR spectroscopy. *Eur. Polym. J.* **2006**, *42*, 2292-2301.
226. Jubsilp, C.; Taewattana, R.; Takeichi, T.; Rimdusit, S. Investigation on Rubber-Modified Polybenzoxazine Composites for Lubricating Material Applications. *J. Mater. Eng. Perform.* **2015**, *24*, 3958-3968.
227. Tiptipakorn, S.; Punuch, W.; Okhawilai, M.; Rimdusit, S. Property enhancement of polybenzoxazine modified with monoanhydrides and dianhydrides. *J. Polym. Res.* **2015**, *22*, 132.
228. Omura, M.; Tsukegi, T.; Shirai, Y.; Nishida, H.; Endo, T. Thermal Degradation Behavior of Poly(Lactic Acid) in a Blend with Polyethylene. *Ind. Eng. Chem. Res.* **2006**, *45*, 2949-2953.
229. Signori, F.; Coltelli, M.-B.; Bronco, S. Thermal degradation of poly(lactic acid) (PLA) and poly(butylene adipate-co-terephthalate) (PBAT) and their blends upon melt processing. *Polym. Degrad. Stab.* **2009**, *94*, 74-82.
230. Yue, W.; Zhipeng, H.; Qiong, L.; He, H. Synthesis and characterization of polymerizable epoxy resin surfactants. *J. Appl. Polym. Sci.* **2015**, *132*.
231. Asua, J. M.; Schoonbrood, H. A. S. Reactive surfactants in heterophase polymerization. *Acta Polym.* **1998**, *49*, 671-686.
232. Lam, S.; Hellgren, A. C.; Sjöberg, M.; Holmberg, K.; Schoonbrood, H. A. S.; Unzué, M. J.; Asua, J. M.; Tauer, K.; Sherrington, D. C.; Goni, A. M. Surfactants in heterophase polymerization: A study of film formation using force microscopy. *J. Appl. Polym. Sci.* **1997**, *66*, 187-198.
233. Du, C. A.; Bettina, G.; Günter, L. The Segregation of Surfactant upon Film Formation of Latex Dispersions: an Investigation by Energy Filtering Transmission Electron Microscopy. *Polym. Int.* **1997**, *43*, 187-196.
234. Holmberg, K. Polymerizable surfactants. *Progress in Organic Coatings* **1992**, *20*, 325-337.
235. Chiou, K.; Froimowicz, P.; Landfester, K.; Taden, A.; Ishida, H. Triggered Precision Benzoxazine Film Formation by Thermally Induced Destabilization of Benzoxazine Nanodroplets Using a LCST-Bearing Surfactant. *Macromolecules* **2014**, *47*, 3297-3305.
236. Ambrožič, R.; Šebenik, U.; Krajnc, M. Epoxy emulsions stabilized with reactive bio-benzoxazine surfactant from epoxidized cardanol for coatings. *Eur. Polym. J.* **2016**, *81*, 138-151.
237. Wang, T.; Quinn, M. D. J.; Nguyen, S. H. T.; Yu, A.; Notley, S. M. Graphene Films Using a Thermally Curable Surfactant. *Adv. Mater. Interfaces* **2016**, *3*, 1600182.
238. Wang, T.; Quinn, M. D. J.; Notley, S. M. Enhanced electrical, mechanical and thermal properties by exfoliating graphene platelets of larger lateral dimensions. *Carbon* **2018**, *129*, 191-198.
239. Mahfud, R.; Agag, T.; Ishida, H.; Shaikh, S.; Qutubuddin, S. Synthesis and evaluation of novel anionic polymeric surfactants based on polybenzoxazines. *J. Colloid Interface Sci.* **2013**, *407*, 339-347.

240. Zhang, K.; Froimowicz, P.; Han, L.; Ishida, H. Hydrogen-bonding characteristics and unique ring-opening polymerization behavior of Ortho-methylol functional benzoxazine. *J. Polym. Sci., Part A: Polym. Chem.* **2016**, *54*, 3635-3642.
241. Spectral Database for Organic Compounds (SDBS); H-NMR; SDBS No. 781; RN 80-40-0; http://riodb01.ibase.aist.go.jp/sdbs/ (accessed July 17, 2018).
242. Abdel-Rahman, M. A.; Al-Abd, A. M. Thermoresponsive dendrimers based on oligoethylene glycols: Design, synthesis and cytotoxic activity against MCF-7 breast cancer cells. *Eur. J. Med. Chem.* **2013**, *69*, 848-854.
243. Reber, K. P.; Tilley, S. D.; Carson, C. A.; Sorensen, E. J. Toward a Synthesis of Hirsutellone B by the Concept of Double Cyclization. *The Journal of Organic Chemistry* **2013**, *78*, 9584-9607.
244. Kim, D.; Lee, J.; Shim, P. J.; Lim, J. I.; Jo, H.; Kim, S. Asymmetric Total Synthesis of (+)-Brefeldin A from (S)-Lactate by Triple Chirality Transfer Process and Nitrile Oxide Cycloaddition,1. *The Journal of Organic Chemistry* **2002**, *67*, 764-771.
245. Herzberger, J.; Niederer, K.; Pohlit, H.; Seiwert, J.; Worm, M.; Wurm, F. R.; Frey, H. Polymerization of Ethylene Oxide, Propylene Oxide, and Other Alkylene Oxides: Synthesis, Novel Polymer Architectures, and Bioconjugation. *Chem. Rev.* **2016**, *116*, 2170-2243.
246. Lee, B. F.; Kade, M. J.; Chute, J. A.; Gupta, N.; Campos, L. M.; Fredrickson, G. H.; Kramer, E. J.; Lynd, N. A.; Hawker, C. J. Poly(allyl glycidyl ether)-A versatile and functional polyether platform. *J. Polym. Sci., Part A: Polym. Chem.* **2011**, *49*, 4498-4504.
247. Obermeier, B.; Frey, H. Poly(ethylene glycol-co-allyl glycidyl ether)s: A PEG-Based Modular Synthetic Platform for Multiple Bioconjugation. *Bioconjugate Chem.* **2011**, *22*, 436-444.
248. Jubsilp, C.; Punson, K.; Takeichi, T.; Rimdusit, S. Curing kinetics of Benzoxazine–epoxy copolymer investigated by non-isothermal differential scanning calorimetry. *Polym. Degrad. Stab.* **2010**, *95*, 918-924.
249. Kimura, H.; Matsumoto, A.; Hasegawa, K.; Ohtsuka, K.; Fukuda, A. Epoxy resin cured by bisphenol A based benzoxazine. *J. Appl. Polym. Sci.* **1998**, *68*, 1903-1910.
250. Isono, T.; Miyachi, K.; Satoh, Y.; Sato, S.-i.; Kakuchi, T.; Satoh, T. Design and synthesis of thermoresponsive aliphatic polyethers with a tunable phase transition temperature. *Polym. Chem.* **2017**, *8*, 5698-5707.
251. Karlsson, L. E.; Jannasch, P. Polysulfone ionomers for proton-conducting fuel cell membranes: sulfoalkylated polysulfones. *J. Membr. Sci.* **2004**, *230*, 61-70.
252. Iojoiu, C.; Sanchez, J.-Y. Polysulfone-based Ionomers for Fuel Cell Applications. *High Perform. Polym.* **2009**, *21*, 673-692.
253. Lufrano, F.; Gatto, I.; Staiti, P.; Antonucci, V.; Passalacqua, E. Sulfonated polysulfone ionomer membranes for fuel cells. *Solid State Ionics* **2001**, *145*, 47-51.
254. Thubsuang, U.; Ishida, H.; Wongkasemjit, S.; Chaisuwan, T. Advanced and economical ambient drying method for controlled mesopore polybenzoxazine-based carbon xerogels: Effects of non-ionic and cationic surfactant on porous structure. *J. Colloid Interface Sci.* **2015**, *459*, 241-249.

Appendix A

Table A1. Equilibrium melting points for BA-a/mPEGOH and BA-a/mPEGOTs blends.

BA-a:PEG ratio	BA-a/mPEGOH$_{2000}$ (°C)	BA-a/mPEGOTs$_{2000}$ (°C)	BA-a/mPEGOTs$_{900}$ (°C)
0:100	50.79	50.1	24.77
10:90	50.34	47.86	25.56
20:80	47.06	45.81	24.56
30:70	46.18	45.14	22.99
40:60	45.77	39.27	21.23
50:50	41.92	38.93	None
60:40	42.67	38.68	22
80:20	None	None	None
100:0	None	None	None

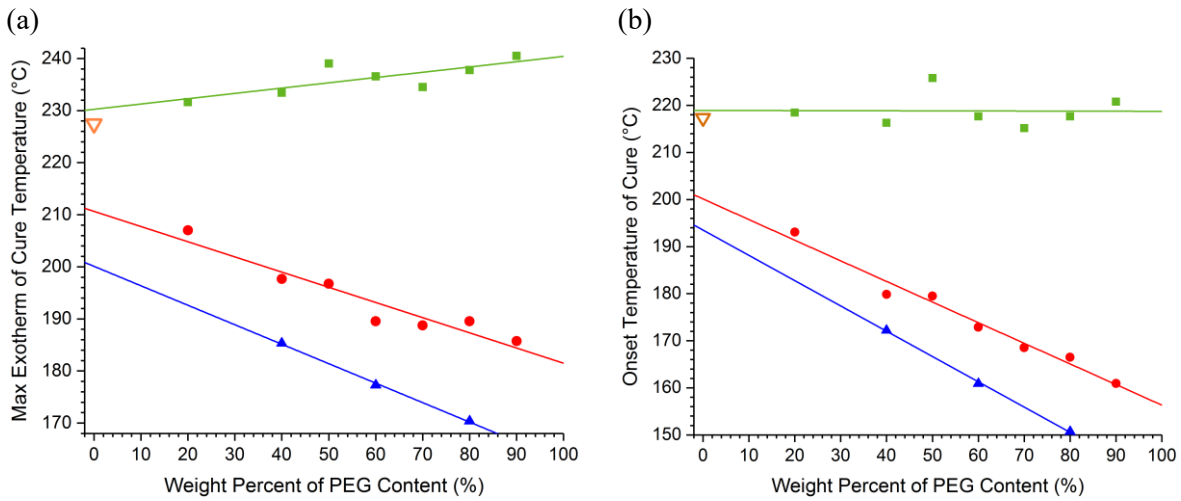

Figure A1. (a) Plots for the peak exotherm temperature of cure of BA-a in blends with mPEGOH$_{2000}$ (■), mPEGOTs$_{2000}$ (●), and mPEGOTs$_{900}$ (▲) as a function of PEG wt %. (b) Plots for the onset temperature for cure of BA-a in blends with mPEGOH$_{2000}$ (■), mPEGOTs$_{2000}$ (●), and mPEGOTs$_{900}$ (▲) as a function of PEG wt %. Empty triangles (▽) are used to identify the onset and max cure temperatures of pure BA-a monomer.

Table A2. Enthalpy of benzoxazine cure exotherms for BA-a/mPEGOH and BA-a/mPEGOTs blends.

BA-a:PEG ratio	BA-a/mPEGOH$_{2000}$ (J/g)	BA-a/mPEGOTs$_{2000}$ (J/g)	BA-a/mPEGOTs$_{900}$ (J/g)
0:100	0	0	0
10:90	26.89	50.52	-
20:80	33.01	76.84	91.35
30:70	81.85	89.91	-
40:60	94.84	142.1	195.7
50:50	146.25	165.8	-
60:40	132.03	185.3	206.9
80:20	144.92	255.7	-
100:0	242.18	286.8	286.8

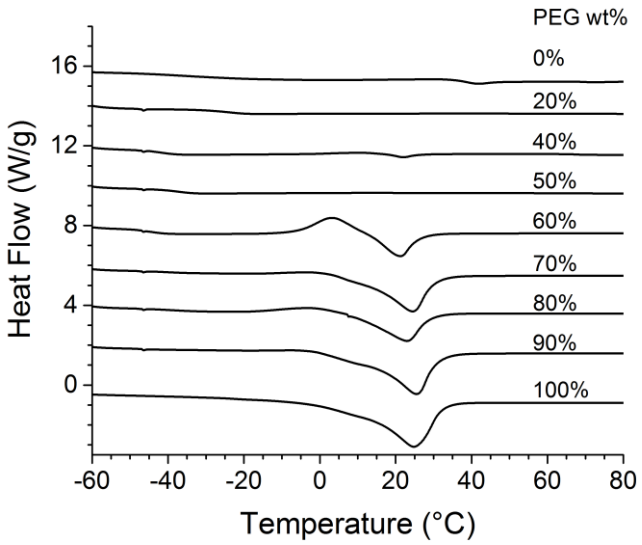

Figure A2. DSC curves of BA-a/mPEGOTs$_{900}$ from the first heat after liquid nitrogen quench. The wt % of PEG in each sample is listed above the data curve. The y-axis is correlated to the curve of the pure mPEGOTs, all other curves have been offset for clarity.

Table A3. Enthalpy of melting for PEG in BA-a/mPEGOH, BA-a/mPEGOTs, PBA-a/mPEGOH and PBA-a/mPEGOTs blends.

BA-a:PEG ratio	Heat Cycle 1		Heat Cycle 2	
	BA-a/mPEGOH$_{2000}$ (J/g)	BA-a/mPEGOTs$_{2000}$ (J/g)	PBA-a/mPEGOH$_{2000}$ (J/g)	PBA-a/mPEGOTs$_{2000}$ (J/g)
0:100	148.8	164.8	142.2	105.9
10:90	125.5	134.2	125.2	106.4
20:80	95.32	116	98.7	103.6
30:70	98.23	103	92.88	88.82
40:60	86.05	74.55	75.26	18.89
50:50	59.12	48.05	55.55	0
60:40	9.082	3.188	43.52	0
80:20	0	0	0	0
100:0	0	0	0	0

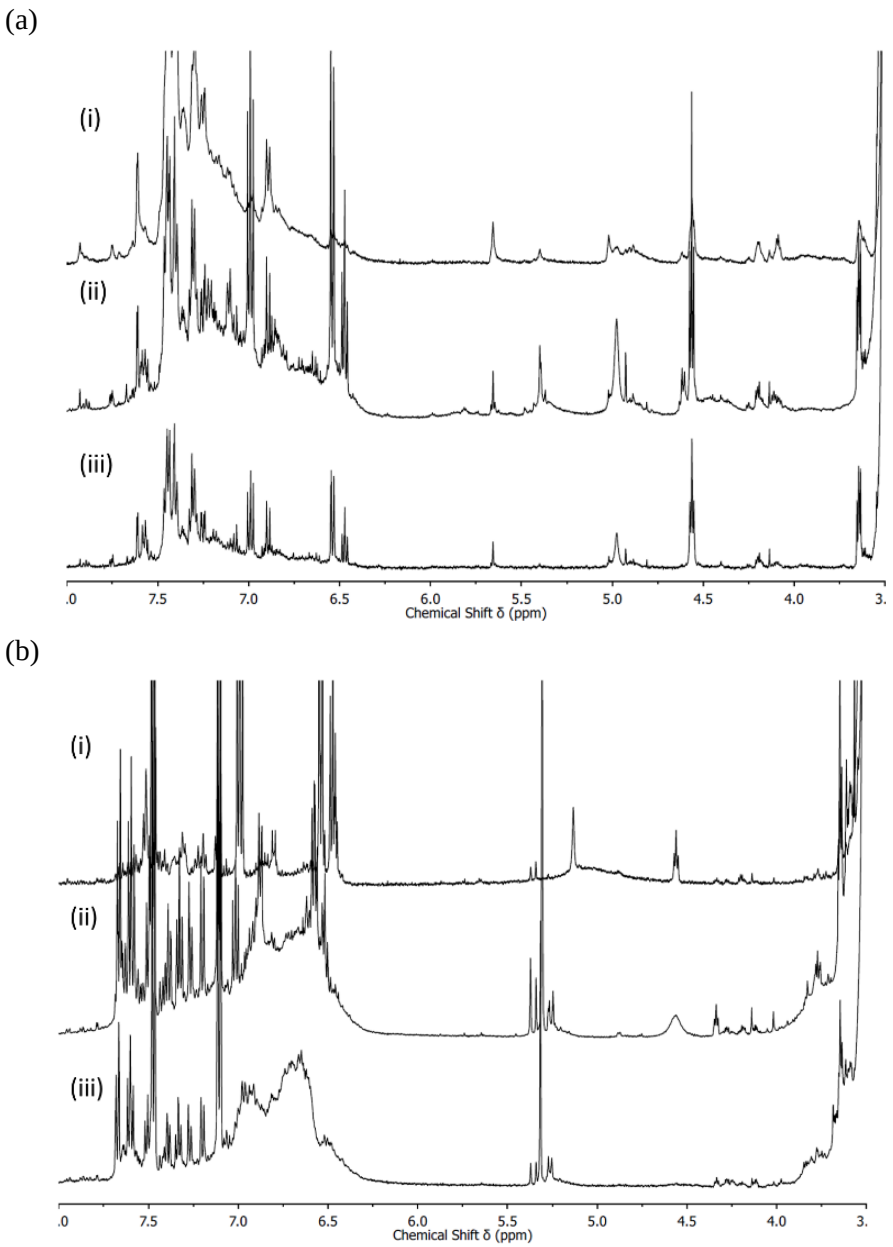

Figure A3. ^{1}H NMR spectra (500 MHz in D6-DMSO) of extractable polymer from cured (a) $mPEGOH_{2000}$ blends and (b) $mPEGOTs_{2000}$ blends. The original content of PEG in (a) and (b) are 20, 40, and 50 wt % (i-iii).

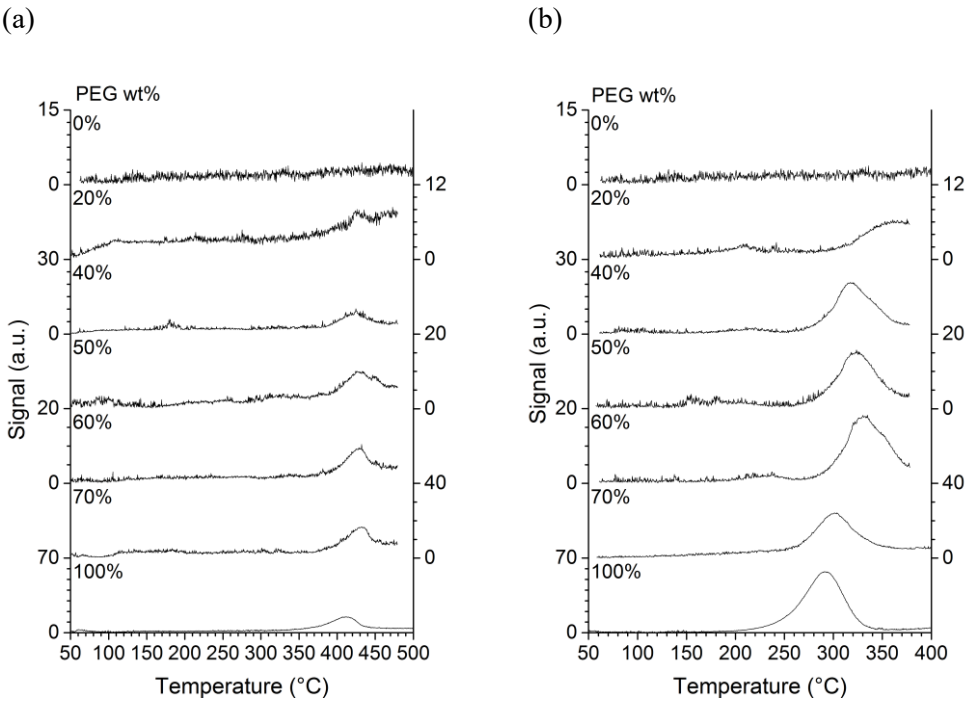

Figure A4. FTIR tracer plots for sp^3 ν_{CH} stretching at 2973 cm^{-1} from the effluent of PBA-a blends with (a) $mPEGOH_{900}$ and (b) $mPEGOTs_{900}$ from TGA.

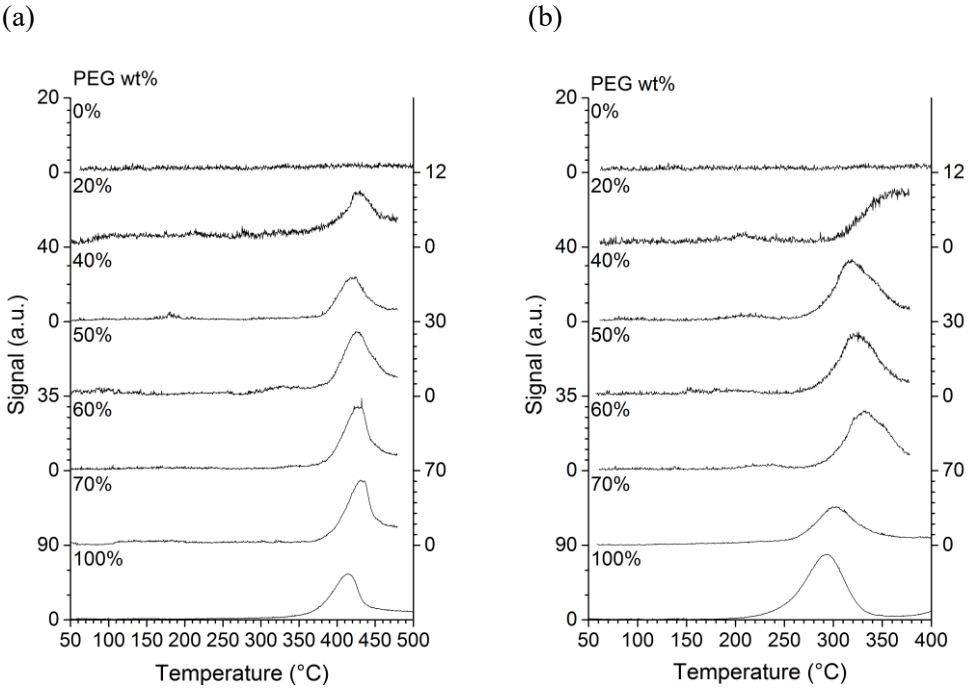

Figure A5. FTIR tracer plots for ν_{CO} ether stretch at 1136 cm^{-1} from the effluent of PBA-a blends with (a) $mPEGOH_{900}$ and (b) $mPEGOTs_{900}$ from TGA.

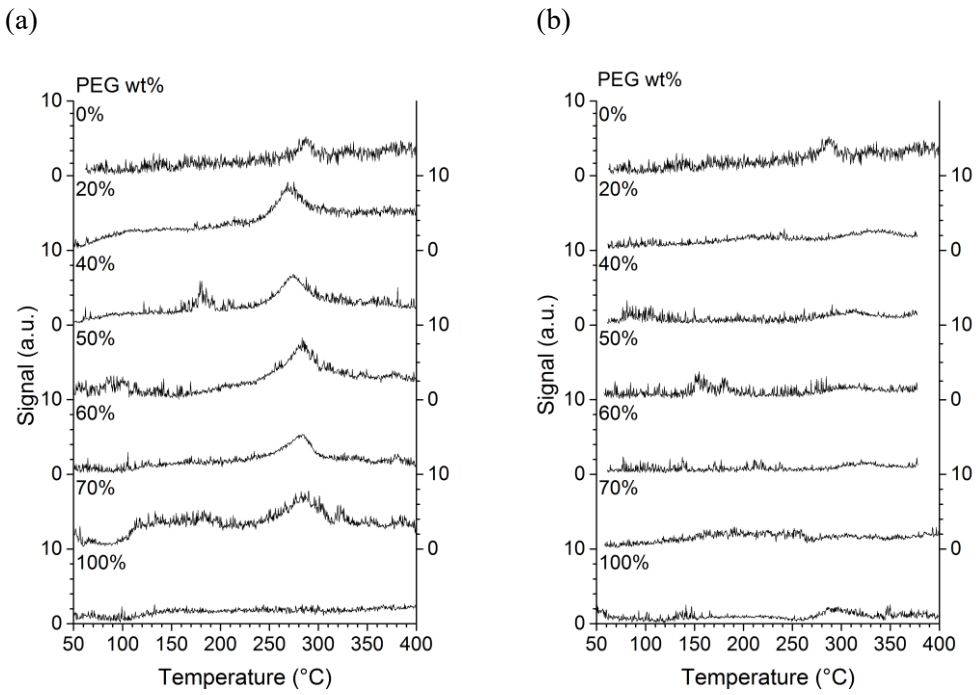

Figure A6. FTIR tracer plots for sp^2 ν_{CH} stretch at 3048 cm^{-1} from the effluent of PBA-a blends with (a) $mPEGOH_{900}$ and (b) $mPEGOTs_{900}$ from TGA.

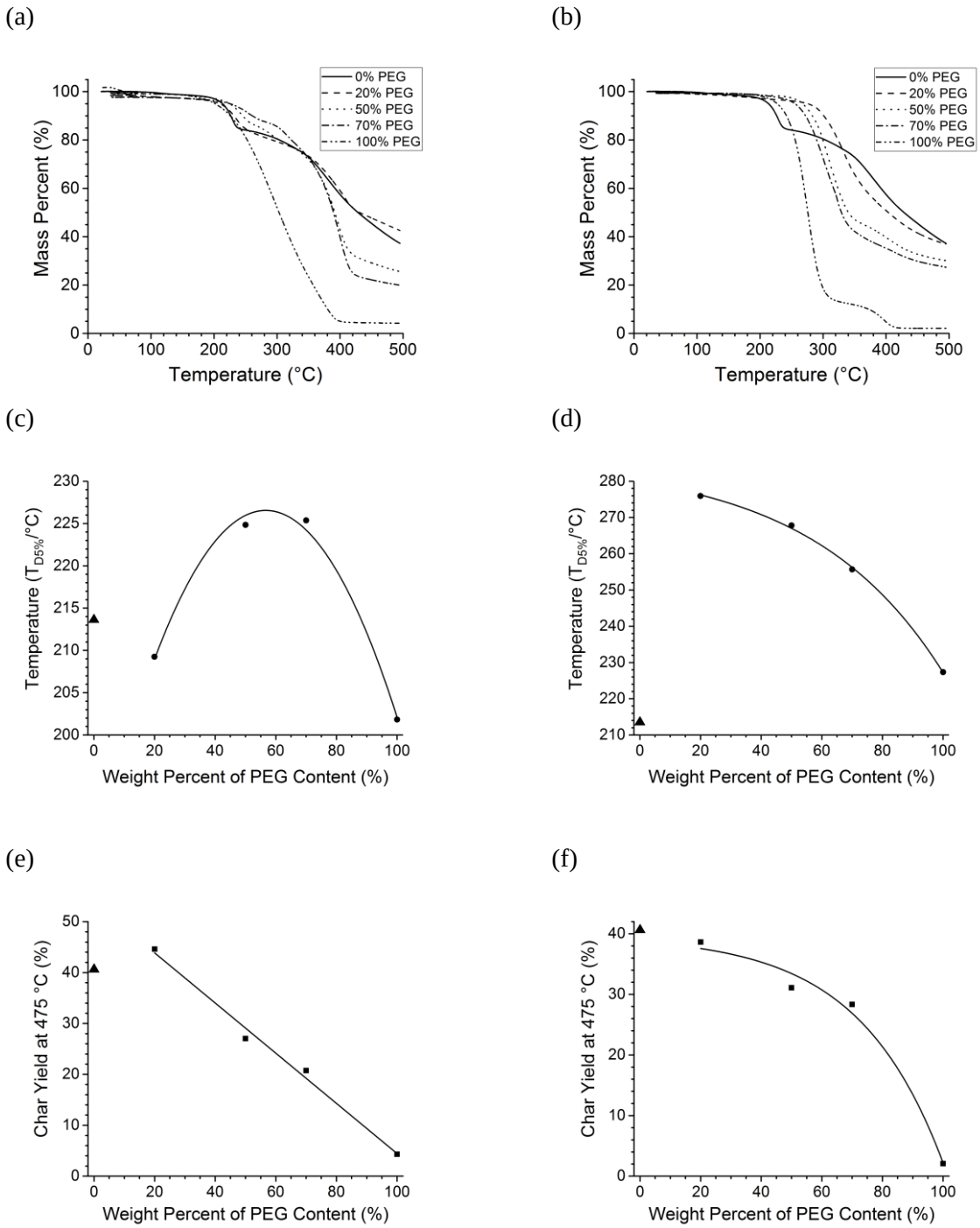

Figure A7. The TGA thermograms for PBA-a blends with (a) $mPEGOH_{900}$ and (b) $mPEGOTs_{900}$. The $T_{D5\%}$ and the char yield at 475 °C of (c, e) $mPEGOH_{900}$ and (d, f) $mPEGOTs_{900}$ blends were determined from the thermograms. Triangles (▲) are used to identify the $T_{D5\%}$ and char yield at 475 °C of pure BA-a monomer in (c-f).

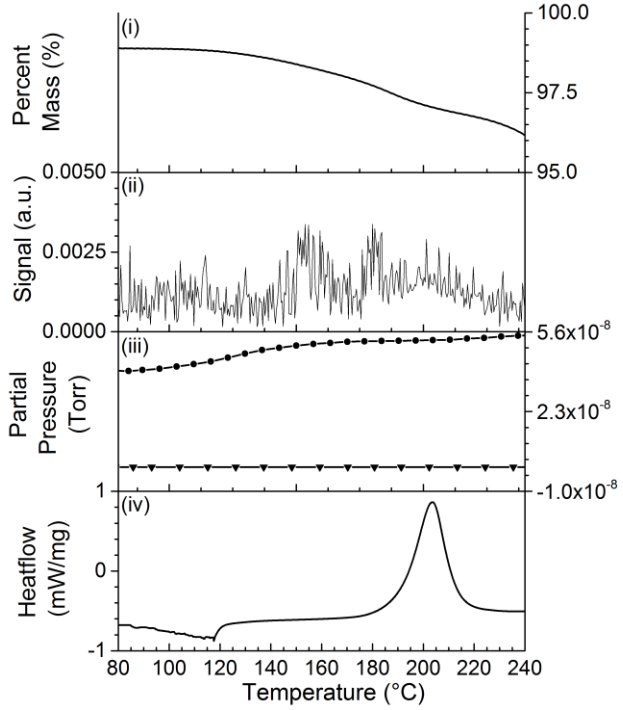

Figure A8. The generation of the *p*-TSA fragment with increasing temperature as determined with (i) TGA thermogram, (ii) FTIR tracer plot of the signal at 885 cm^{-1} from the TGA effluent, (iii) TGA-MS spectrum scan for m/z 91 of the blend sample (●) and pure BA-a (▼), and (iv) a DSC thermogram of the 1:1 BA-a:mPEGOTs$_{900}$ blend.

(a)

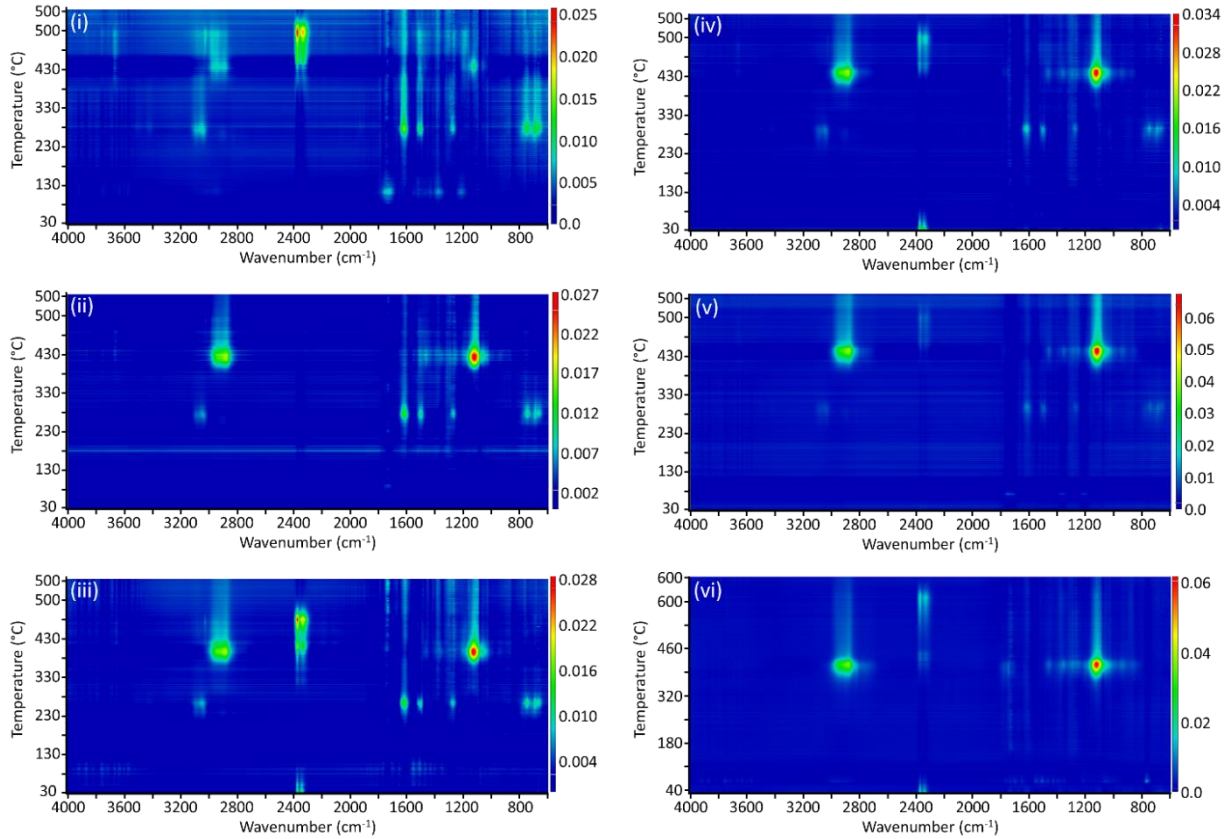

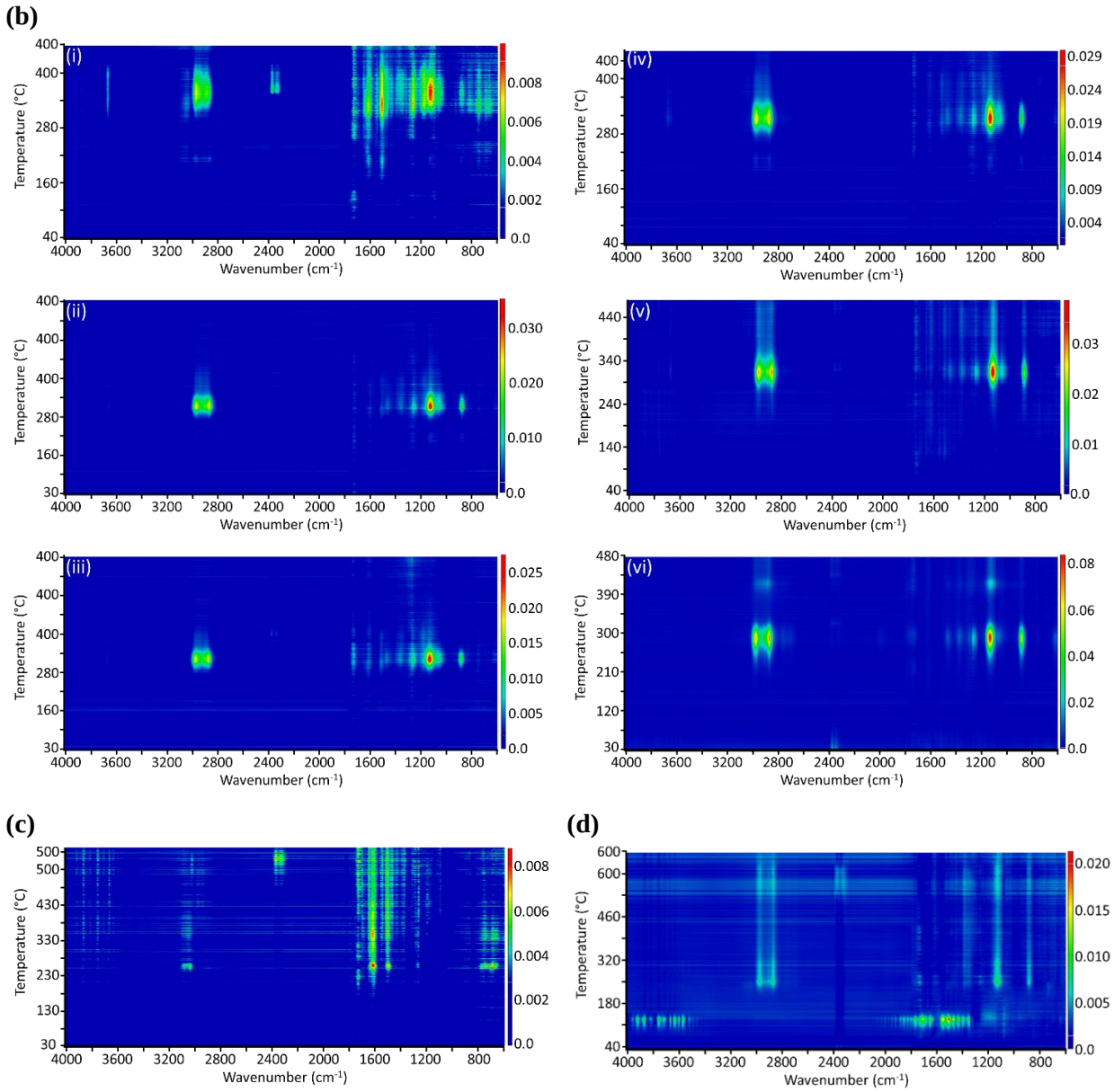

Figure A9. TGA-FTIR absorbance maps of blends composed of BA-a with (a) $mPEGOH_{900}$ and (b) $mPEGOTs_{900}$ with PEG wt % content of 20, 40, 50, 60, 70, and 100 % (i-vi). TGA-FTIR absorbance maps of pure PBA-a (c) and pure *p*-toluene sulfonic acid (d). For datasets i-vi in (a), i-iv in (b), and those in (c-d), the FTIR absorbance data for the final isotherm is included in the maps. The absorbance scale is shown as a colored intensity bar beside each map.

Appendix B

(a) (b)

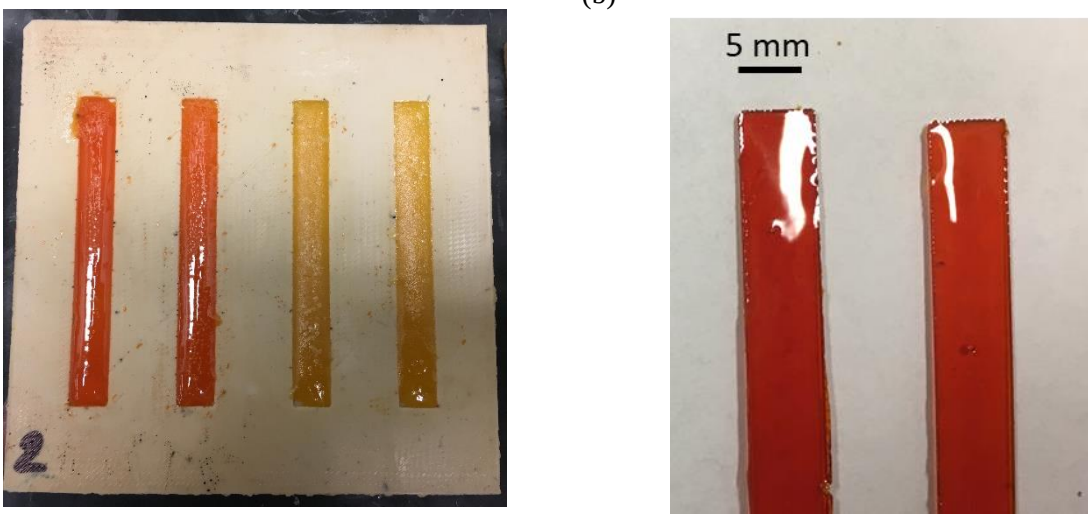

Figure B1. (a) Silicon molds filled with silica blends for DMA sample preparation prior to cure, and (b) the cured samples.

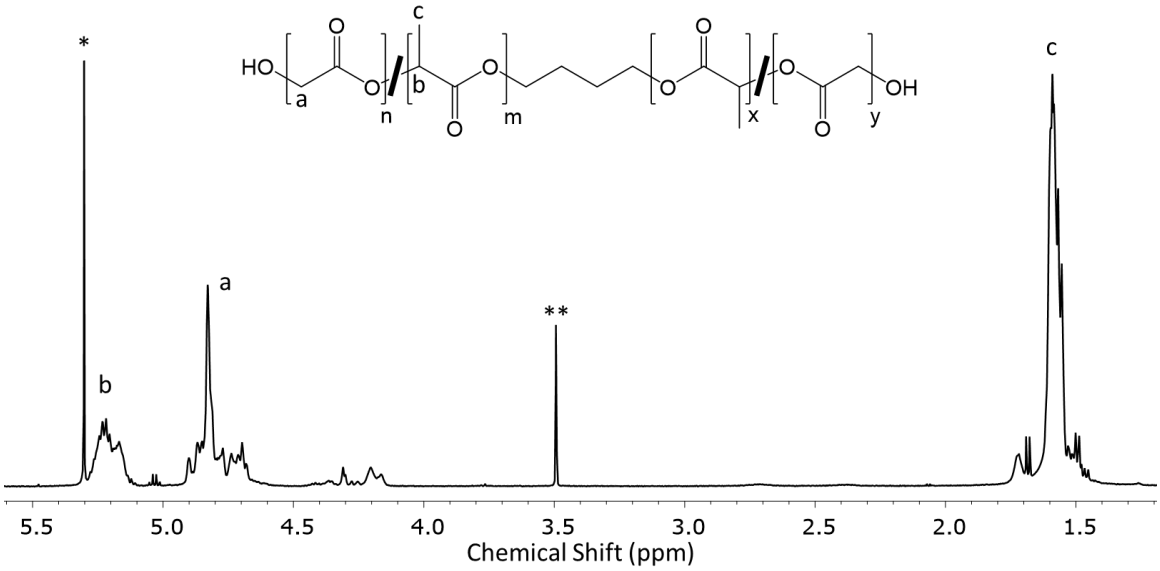

Figure B2. ^{1}H NMR of 50:50 poly(lactic-*co*-glycolic acid) in $CDCl_3$. **Methylene chloride*, ***Methanol*

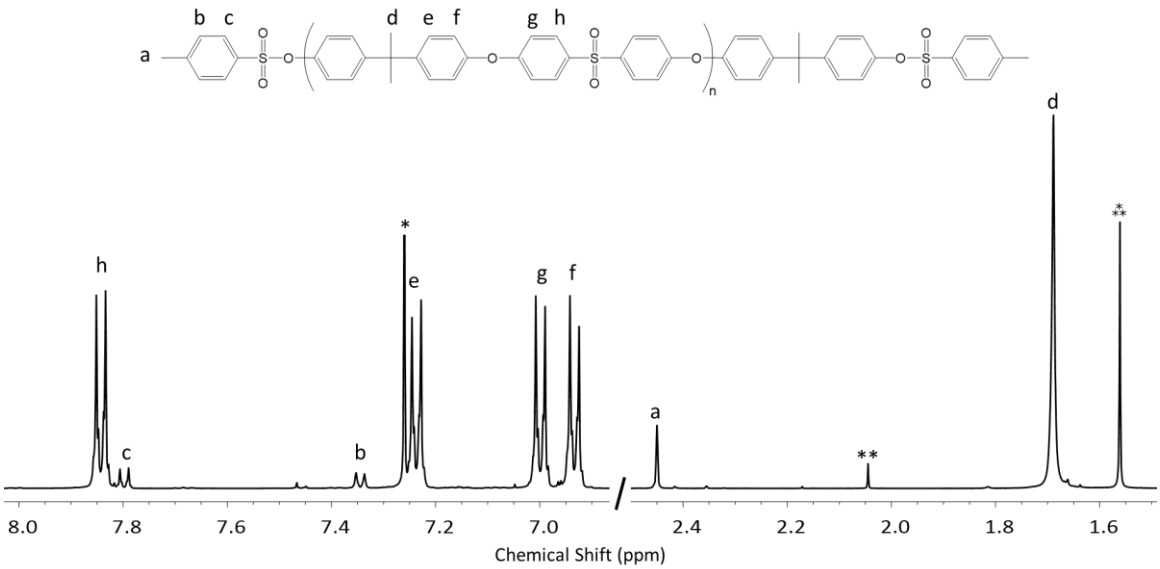

Figure B3. ^{1}H NMR spectrum of *α,ω*-bistosylated polysulfone in $CDCl_3$. **Chloroform*, ***ethyl acetate*, ***Water*

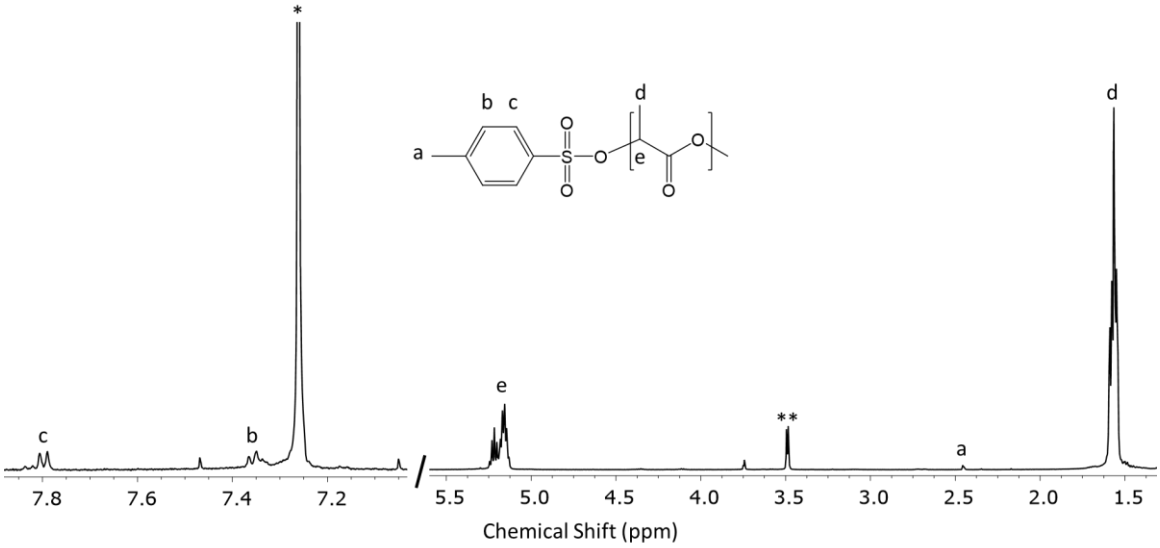

Figure B4. ^{1}H NMR of tosylated poly(D,L-lactic acid) in $CDCl_3$. **Chloroform*, ***Methanol*

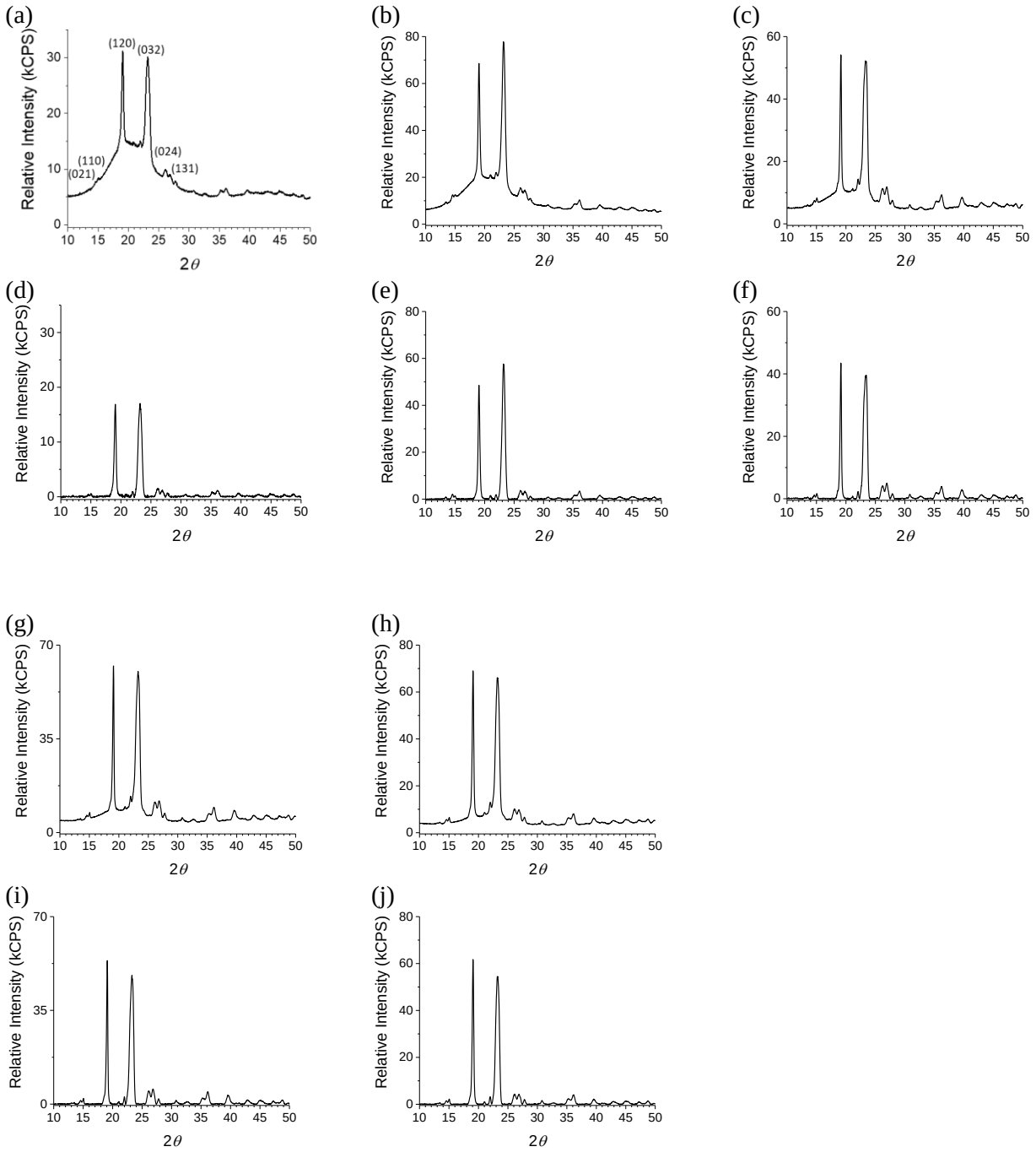

Figure B5. X-ray diffraction patterns of blends of BA-a with $mPEGOH_{2000}$ at (a,d) 40, (b,e) 50, (c,f) 60, (g,i) 70, and (h,j) 80 wt %. The baseline corrected plots are directly below the uncorrected pattern.

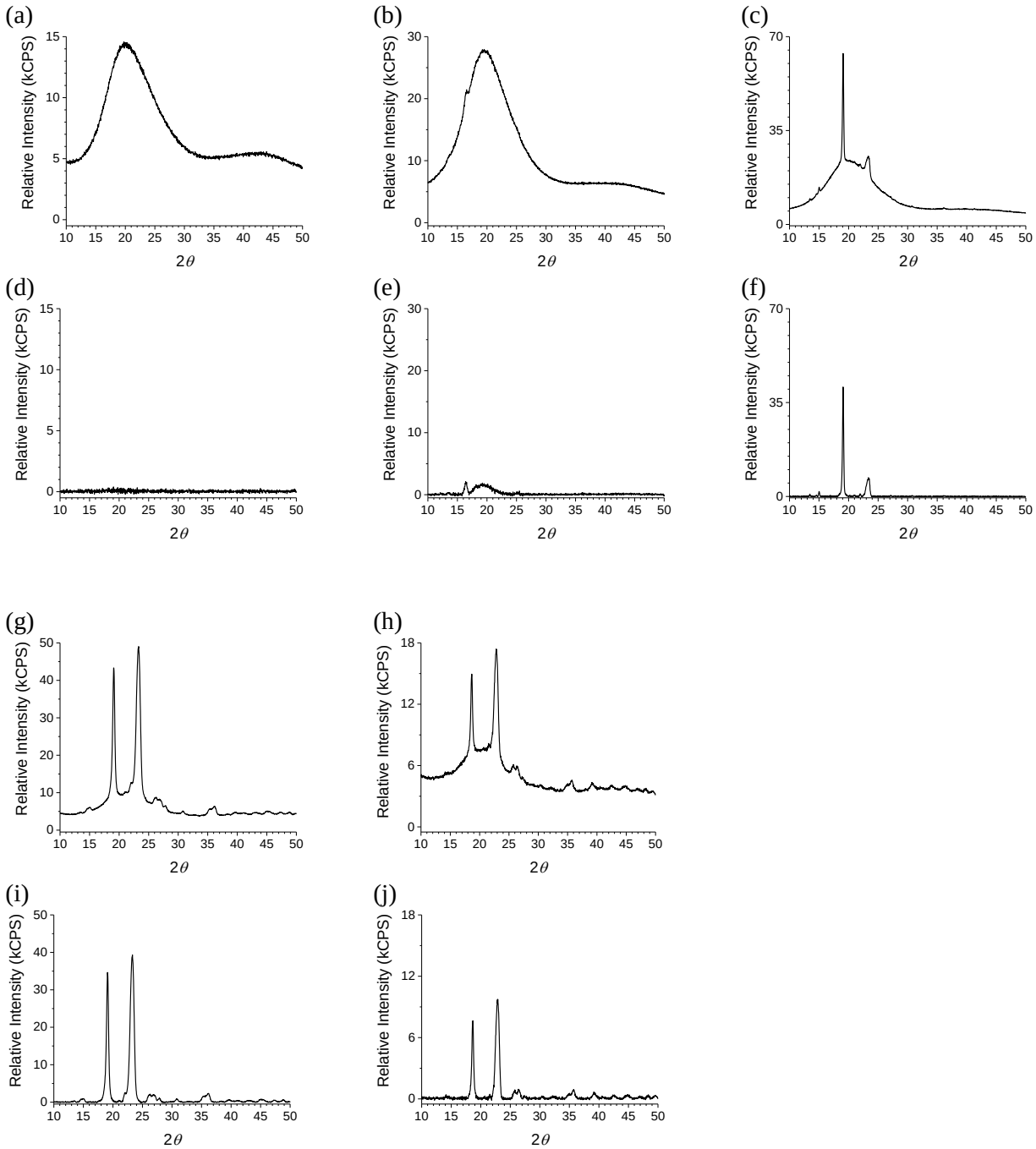

Figure B6. X-ray diffraction patterns of blends of BA-a with $mPEGOTs_{2000}$ at (a,d) 40, (b,e) 50, (c,f) 60, (g,i) 70, and (h,j) 80 wt %. The baseline corrected plots are directly below the uncorrected pattern.

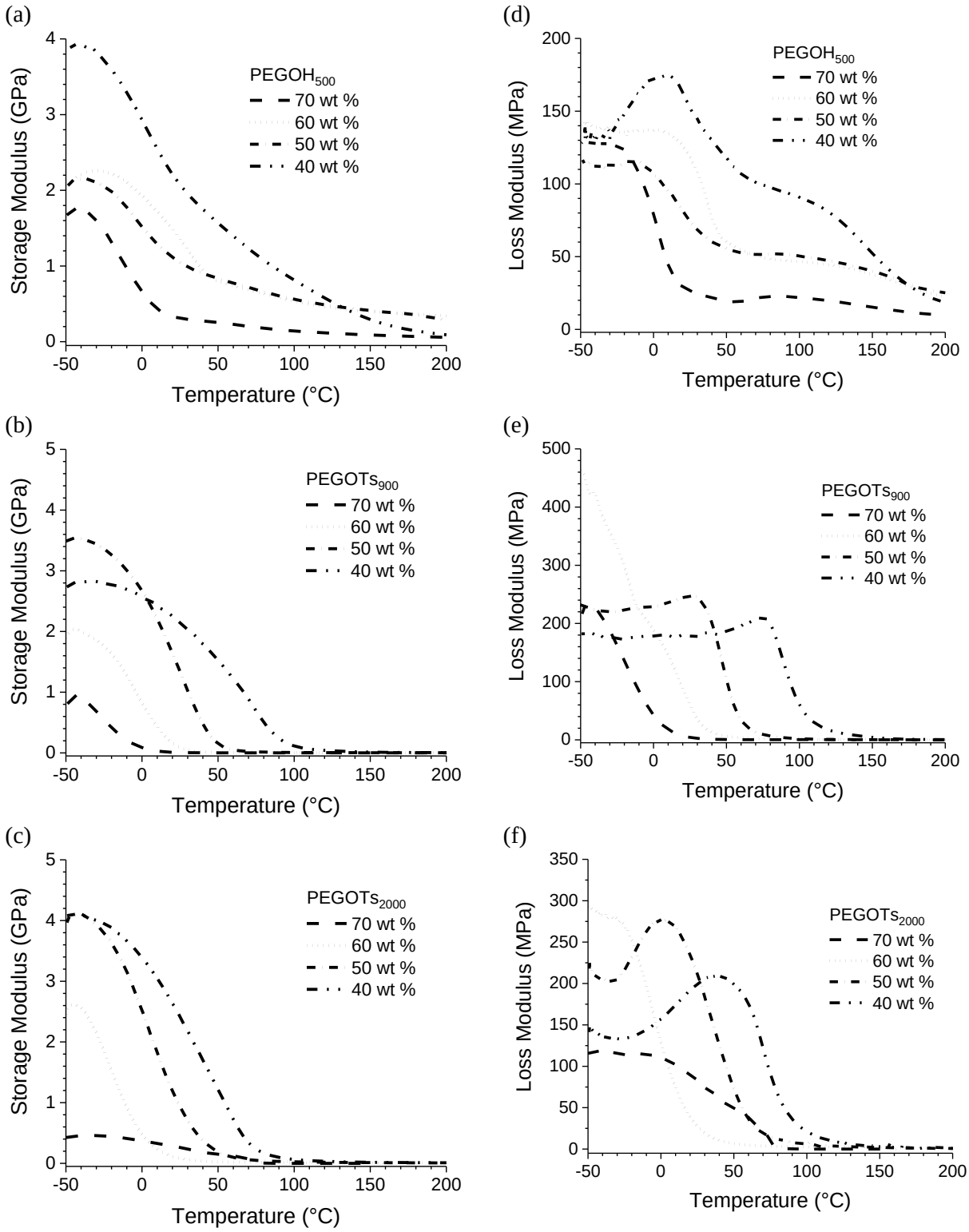

Figure B7. Storage modulus (a-c) and loss modulus (d-f) of PBA-a blends with $mPEGOH_{500}$, $mPEGOTs_{900}$, $mPEGOTs_{2000}$ at varying weight loading.

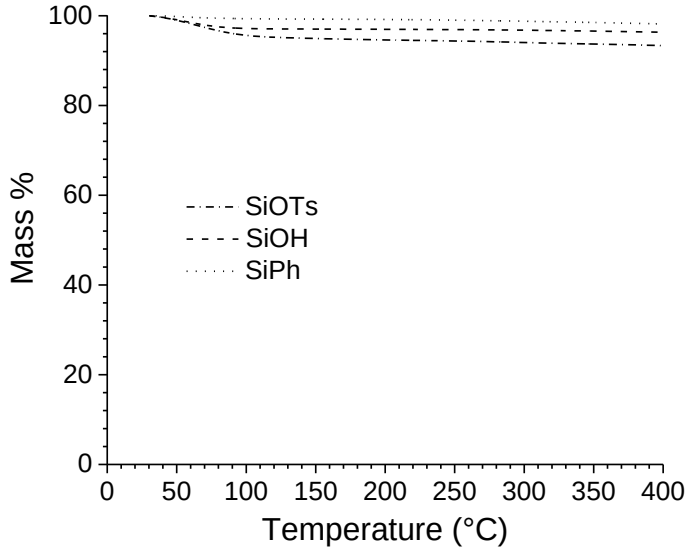

Figure B8. TGA scans of neat SiOH, SiOTs, and SiPh particles from 30-400 °C.

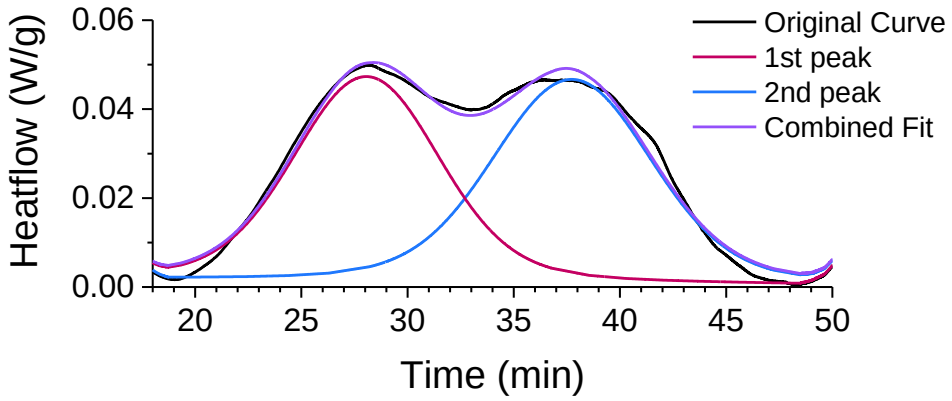

Figure B9. The exothermic peak from the DSC heat scan of the 60 wt % SiOTs blend and the fitted components of each peak as determined with CasaXPS.

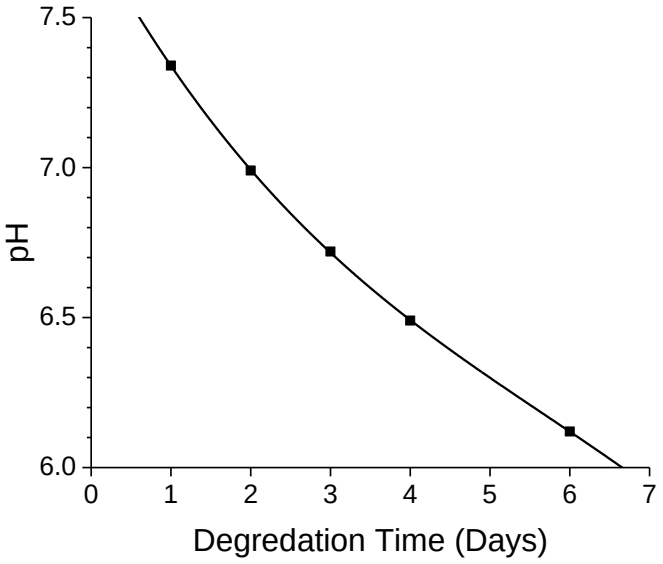

Figure B10. The pH change of solution as PLGA degrades in PBS at 37 °C over several days with an exponential fit.

Appendix C

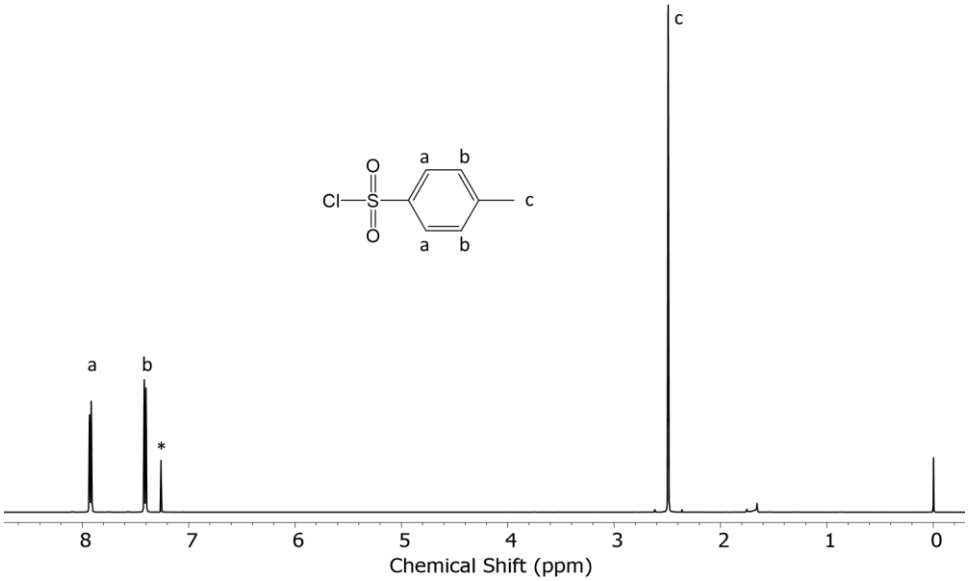

Figure C1. ^{1}H NMR spectrum (500 MHz, $CDCl_3$) of *p*-toluenesulfonyl chloride. **Chloroform*

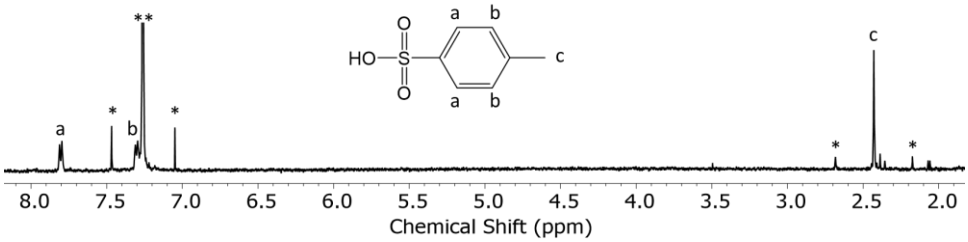

Figure C2. ^{1}H NMR spectrum (500 MHz, $CDCl_3$) of *p*-toluenesulfonic acid. **Satellite*, ***chloroform*

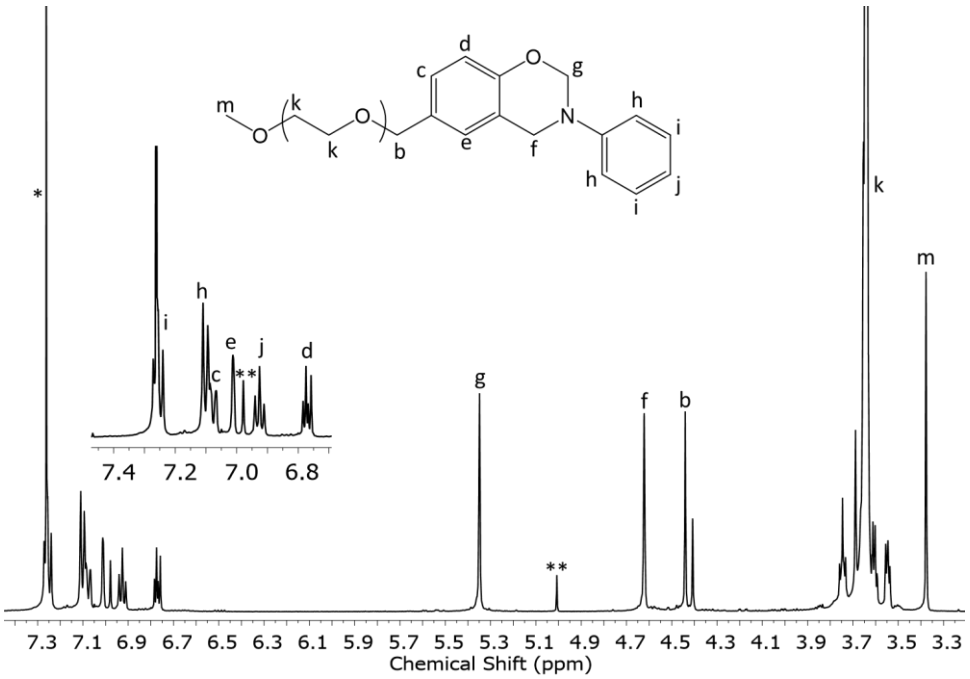

Figure C3. ^{1}H NMR spectrum (500 MHz, $CDCl_3$) of mPEGpHBA-a_{500}. **Chloroform*, ***butylated hydroxytoluene*

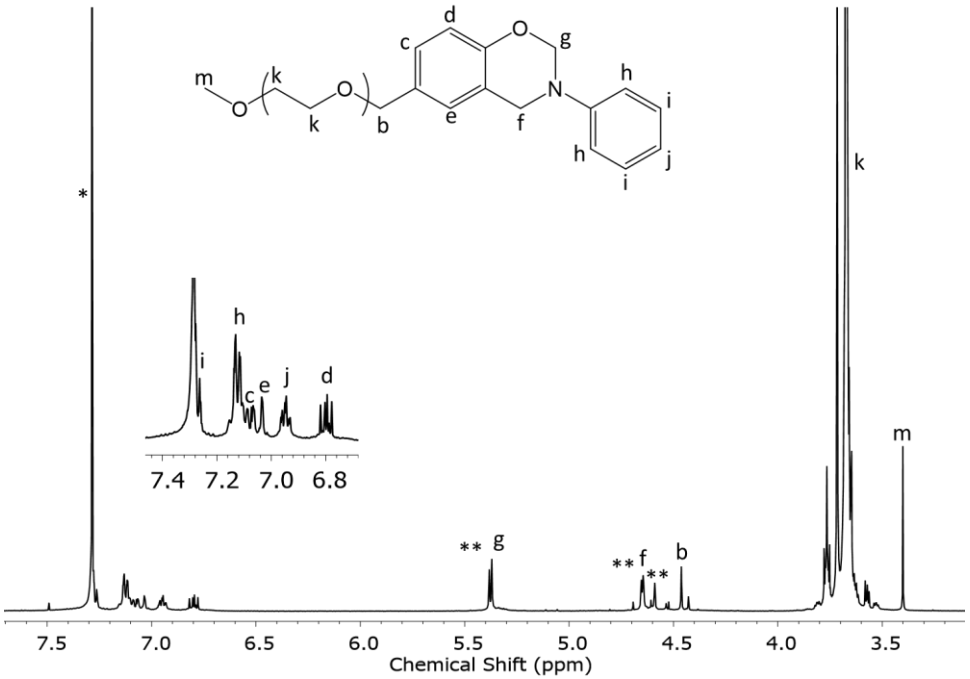

Figure C4. ^{1}H NMR spectrum (500 MHz, $CDCl_3$) of mPEGpHBA-a_{2000}. **Chloroform*, ***pHBA-a*

List of Abbreviations

Abbreviation	Definition
AGE	Allyl glycidyl ether
ATR	Attenuated total reflectance
BA	Benzoxazine
BA-a	Bisphenol A-based benzoxazine
CMC	Critical micelle concentration
CPP	Critical packing parameter
CTAB	Cetyltrimethylammonium bromide
CTAT	Cetyltrimethylammonium *p*-toluenesulfonate
DLS	Dynamic light scattering
DMA	Dynamic mechanical analysis
DMAP	Dimethylaminopyridine
DSC	Differential scanning calorimetry
FST	Flame, smoke, toxicity
FTIR	Fourier-transform infrared spectroscopy
GME	Glycidyl methyl ether
HOTs	*p*-Toluenesulfonic acid
MALDI-TOF	Matrix assisted laser desorption/ionization-time of flight
M_n	Number average molecular weight
mPEG	Methoxypoly(ethylene glycol)
mPEGOH	Methoxypoly(ethylene glycol)
$mPEGOH_{2000}$	Methoxypoly(ethylene glycol) M_n 2000
$mPEGOH_{500}$	Methoxypoly(ethylene glycol) M_n 500
$mPEGOH_{900}$	Methoxypoly(ethylene glycol) M_n 900
mPEGOTs	Methoxypoly(ethylene glycol) tosylate
$mPEGOTs_{2000}$	Methoxypoly(ethylene glycol) tosylate M_n 2000
$mPEGOTs_{500}$	Methoxypoly(ethylene glycol) tosylate M_n 500
$mPEGOTs_{900}$	Methoxypoly(ethylene glycol) tosylate M_n 900

mPEGpHBA-a	Benzoxazine terminated methoxypoly(ethylene glycol)
mPEGpHBA-a_{2000}	Benzoxazine terminated methoxypoly(ethylene glycol) M_n 2000
mPEGpHBA-a_{500}	Benzoxazine terminated methoxypoly(ethylene glycol) M_n 500
mPEGpHBA-a_{900}	Benzoxazine terminated methoxypoly(ethylene glycol) M_n 900
MS	Mass spectrometry
M_w	Weight average molecular weight
NMR	Nuclear Magnetic Resonance
P(BA-a)-*g*-mPEGOTs	P(BA-a)-*graft*-mPEGOTs
PAGE	Poly(allyl glycidyl ether)
PBA	Polybenzoxazine
PBA-a	Poly bisphenol A-based benzoxazine
PBS	Phosphate buffer solution
PCL	Poly(ε-caprolactone)
PDLLA	Poly(D,L-lactic acid)
PDLLAOH	Hydroxy terminated poly(D,L-lactic acid)
PDLLAOTs	Tosylate terminated poly(D,L-lactic acid)
PEG	Poly(ethylene glycol)
*p*HBA-a	*p*-Hydroxy methylbenzoxazine
PLA	Poly(lactic acid)
PLGA	Poly(lactic-*co*-glycolic acid)
PSU	Polysulfone
PSUOH	α,ω-Dihydroxy polysulfone
PSUOTs	α,ω-Bistosylate polysulfone
ROP	Ring opening polymerization
SDS	Sodium dodecyl sulfate
SEM	Scanning electron microscopy
SiOH	Silica
SiOTs	Tosylate functionalized silica
SiPh	Phenyl functionalized silica

$T_{d5\%}$	Temperature at 5 % mass loss
T_g	Glass transition temperature
TGA	Thermogravimetric analysis
TGA-FTIR	Thermogravimetric analysis-Fourier-transform infrared spectroscopy
TGA-MS	Thermogravimetric analysis-Mass spectrometry
T_m	Melt transition temperature
TsCl	*p*-Toluenesulfonyl chloride
wt %	Weight percent
XRD	X-ray diffraction
α,ω-HO-PEG-OH	α,ω-Dihydroxy poly(ethylene glycol)
ΔH_m	Enthalpy of melt